UNIVERSITÄT DUISBURG ESSEN

Open-Minded

Short and long term radiation effects after ionizing radiation and its dependence on chromatin modification and repair inhibition in human lung cell lines

Inaugural-Dissertation

zur

Erlangung des Doktorgrades

Dr. rer. nat.

der Fakultät für Biologie

an der

Universität Duisburg-Essen

vorgelegt von

Kristina Bannik

aus Moskau

September 2015

Die der vorliegenden Arbeit zugrunde liegenden Experimente wurden am Uniklinikum Essen durchgeführt.

1. Gutachter: Prof. Dr. Martin Stuschke

2. Gutachter: Prof. Dr. George Iliakis

Vorsitzender des Prüfungsausschusses: PD Dr. Jürgen Thomale

Tag der mündlichen Prüfung: 01.12.2015

“The important thing is to not stop questioning. Curiosity has its own reason for existing.”

Albert Einstein (quoted by William Miller in Life Magazine, May 2, 1955)

Table of Contents

List of abbreviations

%	Percentage
53BP1	p53-binding protein 1
aq.dest.	Aqua destillata
ATM	Ataxia telangiectasia mutated
ATR	Ataxia telangiectasia and Rad3 related kinase
BER	Base excision repair
B-NHEJ	Backup nonhomologous end joining
bp	Base pair
BRCA1, BRCA2	Breast cancer susceptibility genes 1 and 2
BSA	Bovine serum albumin
CCC	Condensed chromatin clustering
CICC	Chaetocin-induced chromatin clustering
DAPI	4′, 6- diamidino-2-phenyliodole
DDR	DNA damage response
Deq	Dose equivalent
dH_2O	Distilled water
DMEM	Dulbecco's modified eagle medium
DNA	Deoxyribonucleic Acid
DNA DSBs	DNA double strand breaks
DNA-PK	DNA-dependent protein kinase
$DNA\text{-}PK_{cs}$	DNA-dependent protein kinase catalytic subunit
DSB	DNA double strand break
DTT	Dithiothreitol
EDTA	Ethylene diamine tetraacetic acid
et al.	Et alii (and others)
FBS	Fetal bovine serum
FDR	Fraction of DNA released
g	Gravity
Gy	Gray - SI unit of absorbed radiation dose of ionizing radiation, and is defined as the absorption of one joule of ionizing radiation by one kilogram of matter

h	Hour
H1	Histone 1 – linker histone that binds to the DNA where it exits from nucleosome
H2A, H2B, H3, H4	Histone 2A, 2B, 3, 4 – core nucleosome histones – small positively charged, rich in arginine and lysine
H2AX	Histone H2AX variant
H_2O	Water
H_2O_2	Hydrogen peroxide
HEPES	4-(2-hydroxyl)-1-piperazineethanesulfonic acid
hFb	Human fibroblasts
HMT	Histone methyltransferase
HR	Homologous recombination
HRR	Homologous recombination repair
IC50	Respective half maximal inhibitory concentrations
i.e.	Id est
IF	Immunofluorescence
IR	Ionizing radiation
KAP-1	Kruppel-associated box (KRAB)-associated co-repressor
kDa	Kilodalton
Ku	Protein that binds to DNA double-strand break ends
LET	Linear energy transfer
MEM	Minimum essential media
mFbs	Mouse fibroblasts
NAC	N-acetyl-L-cysteine
NHEJ	Nonhomologous end joining
NSCLS	Non-small cell lung carcinoma
min	Minute
MRN	Mre11/Rad50/Nbs1
p	Phosphorylated
PARP1	Poly (ADP-ribose) polymerase 1
PBS	Phosphate buffered saline
PCNA	Proliferating cell nuclear antigen
PE	Plating efficiency
PFA	Paraformaldehyde

PFGE	Pulsed-field gel electrophoresis
PMSF	Phenylmethylsulfonyl fluoride
PVDF	Polyvinylidene difluoride
Rad51	Radiation protein 51
RNase	Ribonuclease
ROS	Reactive oxygen species
RPA	Replication protein A
RPMI	Roswell park memorial institute medium
RT	Room temperature
rpm	Revolutions per minute
s.d	Standard deviation
SEM	Standard error of mean
shRNA	Small hairpin RNA
siRNA	Small interfering RNA
SSB	Single strand break
Suv39h1	suppressor of variegation 3-9 homolog, gene
SUV39H1	suppressor of variegation 3-9 homolog, protein
TCD50	Tumour control dose 50%
TBS	Tris-buffered saline
Tris	Tris-(hydroxymetheyl)-aminomethane
γH2AX	Phosphorylated form of the histone H2AX
WB	Western blotting
WRN	Werner syndrome protein
wt	Wild type
XRCC1/4	X-ray repair cross-complementing protein group 1/4

List of figures

1 Introduction

1.1 Epigenetic regulations of cell

1.1.1 The importance of chromatin structure

Chromatin is a highly regulated nucleoprotein complex through which genetic material is structured and interfered to elicit cellular processes, including gene transcription, DNA replication, differentiation and DNA repair. Most of the epigenetic changes take place at the chromatin level, the higher order of DNA. Chromatin structure is built up by nucleosomes, which contain ± 146 bp of DNA wrapped around an octamer of four core histones (H2A, H2B, H3 and H4) (Figure 1.1). The chromatin structure is controlled by epigenetic mechanisms including DNA methylation, post-translational modifications of histones and nucleosome positioning. The dynamics of their modifications can define the accessibility of chromatin regions to the transcriptional machinery and thus alter gene expression (Maes *et al*., 2013). Moreover, chromatin structure and dynamics are supposed to be involved in the regulation and facilitation of DNA repair.

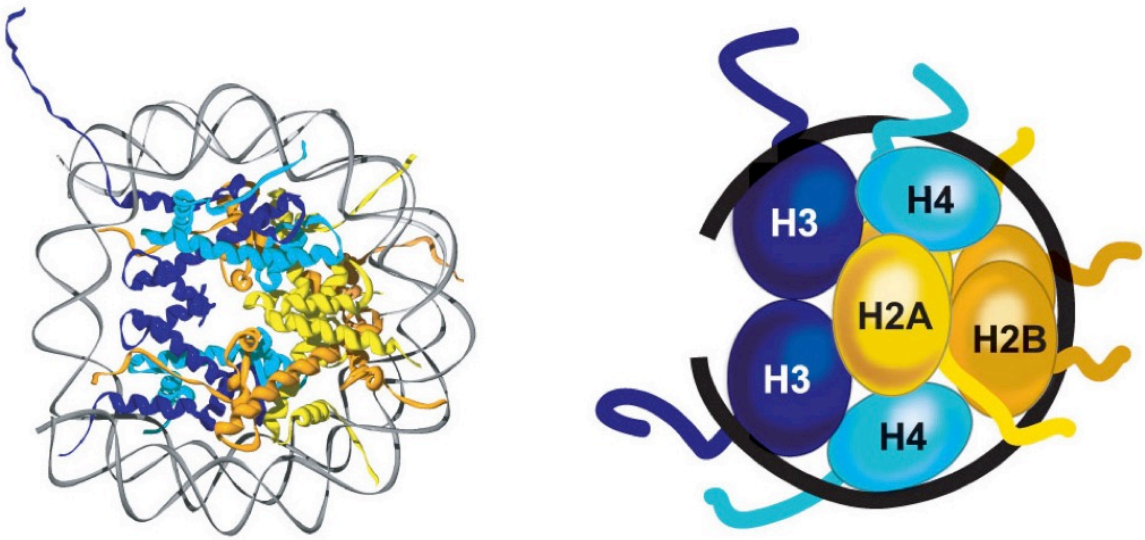

Figure 1.1: Nucleosome structure. A 2.8 Å model of a nucleosome *(left)*. A schematic representation of histone organization within the octamer core around which the DNA (*black line*) is wrapped *(right)*. Nucleosome formation occurs first through the disposition of an H3/H4 tetramer on the DNA, followed by two sets of H2A/H2B dimers. Unstructured amino terminal histone tails extrude from the nucleosome core, which consists of structured globular domains of the eight histone proteins. Picture from www.genesandsignals.org (Allis *et al*., 2006).

Historically, chromatin structure was divided into two main types: euchromatin, which is an open, gene-rich and transcriptionally active region of chromatin and heterochromatin,

which constitutes 15-30% of mammalian chromatin and represents condensed regions with low gene density but high level of repetitive sequences (Figure 1.2).

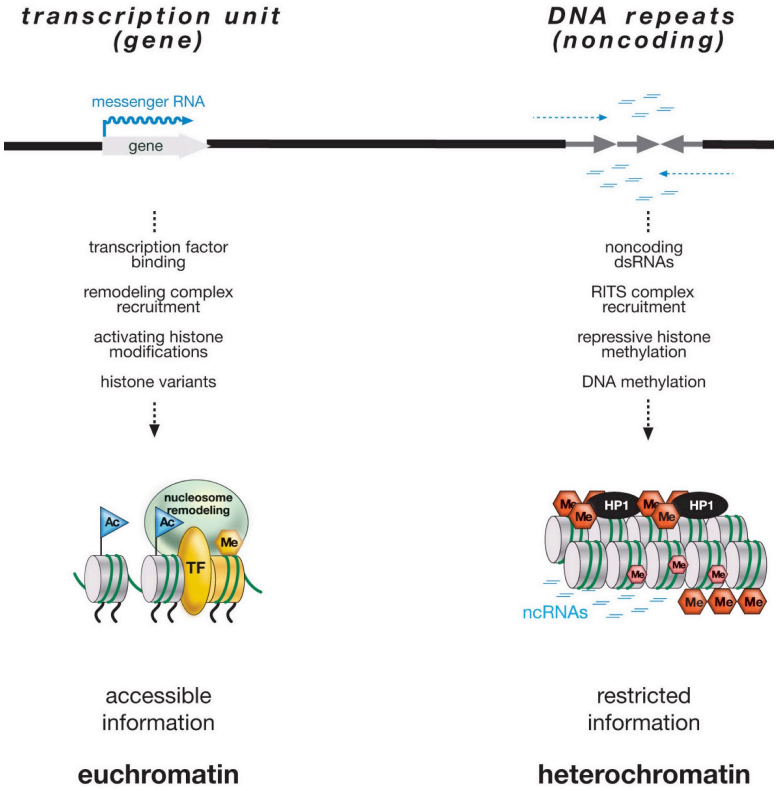

Figure 1.2: Distinction between euchromatin and heterochromatin. Summary of common differences between euchromatin and constitutive heterochromatin. This includes differences in the type of transcripts produced, recruitment of DNA-binding proteins, chromatin-associated proteins and complexes, covalent histone modifications, and histone variant composition. Picture from www.genesandsignals.org (Allis *et al*., 2006).

Histones within heterochromatin have low levels of acetylation, but high levels of histone H3 methylation on lysine 9 and 27 (Figure 1.3). In contrast, histones within euchromatin are highly acetylated and are methylated on lysine 4 and 36 of histone H3 (Barski *et al.,* 2007; Rice *et al*., 2003; Xu and Price, 2011). Heterochromatin mostly contains silent genes and compacted regions such as centromeres and telomeres. Typical marks include low levels of acetylation and methylation on H4K9, H3K27 and H4K20. In contrast, euchromatin is a less compacted region containing active genes, which contain high levels of acetylation, H3K4me3 and H3K36me3 (Maes *et al*., 2013).

Figure 1.3: Characterization of histone H3. The first 30 amino acids of histone H3 are shown. Human H3 lysine residues known to be posttranslational modified are depicted: red for methylation, green for acetylation, and yellow for both. Red lollipops indicate that H3 Lys9 can be mono-, di-, or trimethylated. The purple line from residues 5–16 denotes the branched synthetic peptide used for immunization. The shaded box reflects the epitope similarity between Lys9 and Lys27 (picture from Rice *et al*., 2003).

1.1.1.1 Chromatin and genome stability

Heterochromatin is important for maintaining genomic stability. It can be subdivided into facultative and constitutive heterochromatin. Facultative heterochromatin is composed of silent DNA, which can be transcriptionally activated under certain conditions, such as during cell development and differentiation. Constitutive heterochromatin contains repetitive DNA, which is not transcriptionally active, and is particularly prevalent at the centromeric, pericentric and telomeric regions. The difference in chromatin compaction between euchromatin and heterochromatin is determined by interaction of DNA with histones and other non-histone proteins.

Epigenetically heritable domains of heterochromatin control the structure and transcriptionally active domains and are required for proper chromosome segregation (Grewal and Moazed, 2003). The chromatin compaction of heterochromatin helps to protect DNA from damage. Interestingly, DNA damage in heterochromatin was shown to be refractory to repair and requires the surrounding chromatin structure to be decondensed (Cann and Dellaire, 2011; Cowell *et al*., 2007; Falk *et al*., 2008; Karagiannis *at al.*, 2007) . Thus, cells must maintain a delicate balance between allowing repair factors to access these regions and ensuring that these regions retain their organization to prevent increased DNA damage and chromosomal mutations (Cann and Dellaire, 2011).

1.1.1.2 Chromatin modification and the epigenetic control of gene expression

Epigenetics is defined as the sum of heritable and non-heritable changes in chromatin structure, which control gene expression, and is independent of changes in the primary DNA sequence. Histone modifications have the potential to affect many fundamental biological processes. Modification of chromatin structure and subsequent regulation of gene expression is controlled by direct DNA methylation by DNA methyltransferases (DNMTs) and/or structural modification of amino acid residues on the N-terminal tail of histone proteins by nuclear enzymes, including histone acetyltrasferases (HATs), histone deacetylases (HDACs), arginine methyltransferases (HRMTs), lysine methyltrasferases (HKMTs) and lysine demethylases (HKDMs). Alteration of the methylation, acetylation or phosphorylation state of the nucleosome unit influences chromatin condensation (Decarlo and Hadden, 2012).

Histones are modified at many sites with over 60 different residues where modification can be detected by specific antibodies. However, not all the modifications

appear on the same histone at the same time. Histone modifications are the result of complex interplay between different molecules referred to as chromatin remodelling proteins.

Methylation of histone residues represents an important modification that is involved in both activation and repression of transcription with three different forms: mono-, di-, or trimethyl (Kouzarides, 2007).

Histone phosphorylation is another major modification, which is highly dynamic. It may have important consequences for chromatin compaction via charge changes. Phosphorylation takes place mostly on serine or threonine residues on histone tails. The balance of phosphorylation is established by phosphatases and kinases, which remove and add phosphate groups, respectively. Histone phosphorylation regulates cell function including transcription, apoptosis, cell cycle, DNA repair and chromatin condensation (Maes *et al.*, 2013). Phosphorylation of the H2A variant H2AX for example plays an important role in DNA damage response of the cells.

1.1.2 The role of methylation in cancer: methyltrasferases

DNA methylation is an oldest epigenetic mechanism known to correlate with gene repression and thus plays a critical role in human carcinogenesis. There are at least two major processes by which methylation can contribute to the oncogenic phenotype: focal hypomethylation of promoter regions of oncogenes and hypermethylation of the promoters of tumour suppressor genes. Thus the indicated alterations in homeostasis of epigenetic mechanism are central regulations, which contribute to cancer initiation and progression (Baylin and Jones, 2006).

In addition, histone methylation is a key posttranscriptional modification known to play an important role in cell cycle regulation, development, DNA damage response. As shown in Figure 1.4 an abnormal histone methylation pattern can lead to cancer initiation or progression (Kouzarides and Berger, 2006). In contrast to acetylation, histone methylation does not alter the charge of arginine and lysine residues. Thus, methylation does not directly modulate the nucleosomal interactions required for chromatin restructuring (Hunt *et al.*, 2013). Two general classes of methylating enzymes have been described: the histone arginine methyltransferases (HRMTs) and histone lysine methyltransferases (HKMTs) (Allis *et al*., 2006; Lachner *et al*., 2003). Methylated lysine residues appear to be chemically more stable. All histone HKMTs and HRMTs require S-adenosylmethionine as a methyl group donor (Pachaiyappan and Woster, 2014).

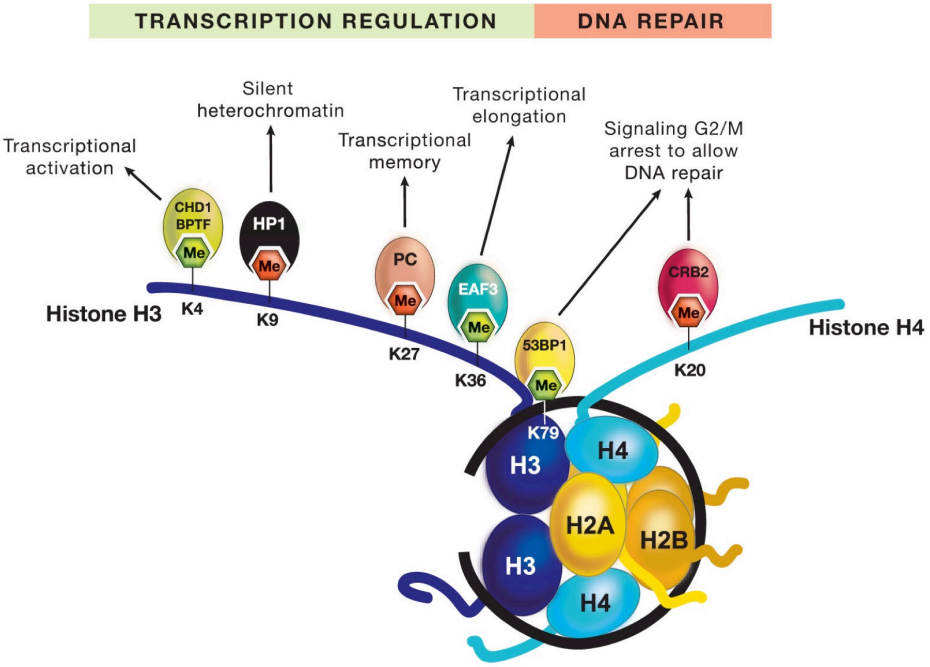

Figure 1.4: Sites of histone lysine methylation, their protein binders and functional role in genomic processes. Methylation of histones occurs at lysine residues in histone H3 and H4. Certain methylated lysine residues are associated with activating transcription (green Me flag), whereas other are involved in repressive processes (red Me flag). Proteins that bond particular methylated lysine residues are indicated. Source www.genesandsignals.org (Kouzarides and Berger, 2006).

HKMTs regulate transcriptional activity by writing epigenetic marks. The most widely studied HKMTs are G9a, SUV39H, EZH2 and DOT1L. Methylation of histone H3K9, a hallmark of silent chromatin, is regulated by two subgroups of HKMTs, G9a/G9a-like proteins that mainly induce mono- and di-methylation of histone H3K9 (H3K9me1, H3K9me2), whereas SUV39h1 contributes to tri-methylation of histone H3K9 (H3K9me3). Su(var)3-9 was initially identified as a suppressor of variegation and involves the spreading of heterochromatin into adjacent euchromatic regions (Elgin and Reuter, 2006). Methylation at histone H3K9 also increases DNA methylation and reduces the level of activating chromatin modifications at promoter regions of aberrantly silenced tumour suppressor, which can be often found in cancer cells (M. Takahashi *et al.,* 2012).

1.1.2.1. Chemical modulators of chromatin

Histone modifications play an important role in chromatin environment and their alterations can lead to tumorigenesis. The HMT SUV39h1 was described as the first SET domain-containing histone lysine methyltransferase (HKMT), which generates di- and trimethylation marks on H3K9 (Rea *et al*., 2000). Tachibana *et al*. (2001) reported HMT G9a as the second HKMT, which is primarily responsible for the dimethylation of lysine 9 on histone H3 (H3K9me2). The overexpression of G9a has been linked to several tumour types,

including the progression potential of metastatic lung cancer (Chen *et al*., 2010). The first reported G9a inhibitor BIX-01294, a diazepin-quinazolin-amine derivative, (Figure 1.5) showed good selectivity against other HMTs (Decarlo and Hadden, 2012).

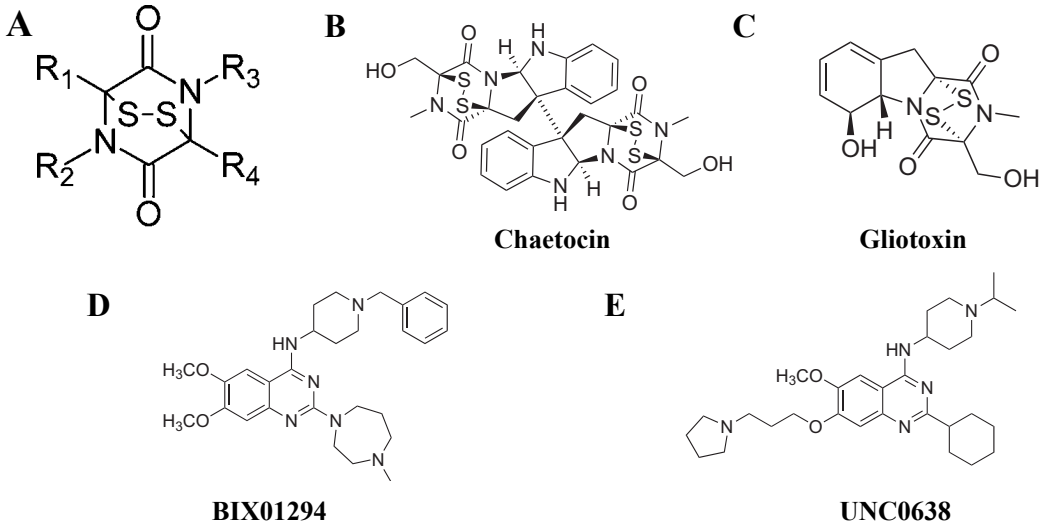

Figure 1.5: The chemical structure of small molecules inhibiting HMTs. A: Generic structure of an epidithiodioxopiperazine, the most common form of ETP. In some circumstances the sulphur bridge contains one, three or four sulphur atoms; these compounds are usually co-produced with those containing the disulphide. R=any atom or group; **B:** Structure based-design of Chaetocin; **C:** Structure-based design of gliotoxin; **D:** Quinazoline-based design of BIX-01294; **E:** Quinazoline-based design of UNC0638. (Modified picture from Decarlo and Hadden, 2012 and Gardiner *et al.*, 2005).

Chaetocin, Gliotoxin, UNC0638 and BIX01294 are small molecules described to inhibit histone H3K9 HMTs (Maleszewska *et al.*, 2014; M. Takahashi *et al.*, 2012; Vedadi *et al.*, 2012). Chaetocin and Gliotoxin, which possess more selective inhibiting activity against G9a and SUV39H1 belong to epipolythiodioxopiperazines (ETPs). ETPs, a class of fungal metabolites, are characterized by the presence of an internal disulphide bridge, which interact with thiol groups leading to the generation of reactive oxygen species by redox cycling and thereby can inactivate proteins. The diketopiperazine ring is derived from a cyclic dipeptide and its sulphur bridge imparts all known toxicity of these molecules. The toxicity of ETPs has made them the attractive potential therapeutic agents for cancer (Gardiner *et al*., 2005). Gliotoxin, another HKTs inhibitor, is one of the structurally simplest ETPs (M. Takahashi et al., 2012). It exerts an immunosuppressive effect and causes apoptotic and necrotic cell death *in vitro* (Vigushin et al., 2004). Chaetocin and Gliotoxin are conserved SAM-dependent-enzymes, which functions as a coactivator for HMTs to methylate proteins.

In contrast BIX01294 and UNC0638 inhibit G9a and GLP but not SUV39h1 (M. Takahashi *et al*., 2012). Both reduce the global H3K9me2 level in several cell lines (Vedadi *et al*., 2012).

1.2 Radiation and DNA repair

Tumour cells can be killed by radiation or chemotherapy via induction of damage in DNA. Ionizing radiation (IR) induces different biological effects, which depend on the type of radiation. Radiation effects are mostly classified by direct and indirect ionizing events to the target. The ionization events after exposure to IR cause DNA damage, either directly by occurring in the DNA molecule itself or indirectly through radicals produced by ionization of atoms or molecules in the vicinity of the DNA, which are not evenly distributed in space but localized along the tracks of the ionizing particles (Hall *et al*., 1993).

IR produces many hundreds of different simple chemical damages in DNA as well as their clustered combinations. The simple damage, including single-strand breaks (SSBs), tends to correlate poorly with biological effectiveness. In addition, DNA base damage, crosslinks of DNA-DNA as well as of DNA-protein and can also lead to significant biological effects (Tichý *et al*., 2010). However double-strand breaks (DSBs) are the most deleterious type of DNA damage with severe consequences for cell survival and maintenance of genomic stability (Ariyoshi *et al.*, 2007; Kinner *at el*., 2008; Mills *et al*., 2003). About 70% of the deposited energy from low LET induced isolated lesions and less complex DNA damage on short DNA sequences and only 30% of the energy causes clustered damage sites on DNA. In contrast, 90% of the deposited energy from high LET results in clustered damage sites on longer DNA sequences (Lavelle and Foray, 2014; Leatherbarrow *et al*., 2006; Qiu, 2015). Thus, both the direct and indirect effects may damage genomic DNA after IR. DNA damage effects by IR are dependent on the local architecture of the DNA sequence, such as naked DNA, chromosomal territory, open euchromatin and densely compacted chromatin. In this respect, it was shown that genomic DNA in central euchromatin regions is affected with less energy and radicals than that of peripheral heterochtomatin, and most of energy and radicals are partially and/or completely lost in peripheral heterochromatin (Qiu, 2015).

The DNA DSBs are considered to be the most relevant damage for the deleterious effects of IR. Thus, the DNA damage response (DDR) pathway, especially of DSBs, is essential for the maintenance of genomic stability. DDR is a network of signalling pathways, which responds to DNA damage and activates cell cycle checkpoints, DNA repair and cell death pathways, e.g. apoptosis (Lou *et al*., 2006).

1.2.1 Double strand breaks and its repair

Double strand breaks (DSBs) can be formed by a single ionizing event by the coincidence of SSB on the complementary strands. DNA DSBs are the main cause of

genotoxic effects, such as chromosomal breaks and exchanges and can thus lead to cell death (Christmann *at al*., 2003; Iliakis *et al*., 2007; Lips and Kaina, 2001). Posttranslational modifications (PTMs) including phosphorylation, acetylation, methylation and ubiquitylation play an important role in the signalling of DNA repair processes. It has been shown that histone modifications play a primary role in DNA damage repair by facilitating the access of repair proteins to DNA breaks (Hunt *et al*., 2013).

There are two main repair pathways for DSBs: nonhomologous end joining (NHEJ) and homologous recombination (HR). The NHEJ is active in all cell cycle phases, but appears to play a major role during the G1 phase of the cell cycle. NHEJ is characterized as "quick and dirty" process and thus is a highly error prone process, because of the generation of new sequence combinations in the genome via deletions or additions of nucleotides, which can lead to mutations.

NHEJ directly re-joins two broken ends and it generally leads to deletions of DNA sequence (Figure 1.6). It mainly requires DNA-PK, which is composed of Ku70, Ku80 and DNA-PKcs, the catalytic subunit. DNA-PKcs is activated by interaction with a single-strand DNA at the site of DSB (Christmann *et al.*, 2003). DNA-PK-dependent non-homologous end joining is also termed as D-NHEJ. This active kinase complex causes the phosphorylation of other proteins, which are involved in DSB repair mechanisms, such as PRA2, WRN (Werner syndrome protein), XLF/Cernunnos, XRCC4 and DNA ligase IV. The latter then joins DSB ends together by ligation (Jackson, 2002; Mladenov and Iliakis, 2011). Inactivation of the genes involved in NHEJ repair in cells leads to radiation sensitivity of the cells.

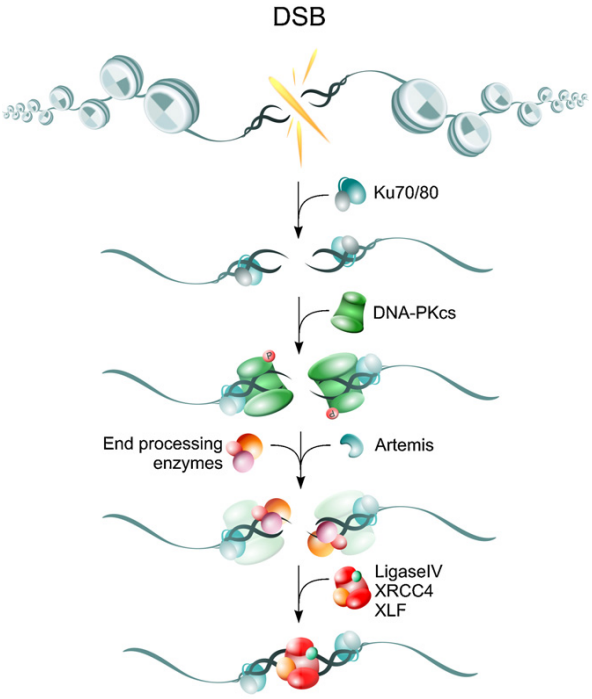

Figure 1.6: Mechanism of classical nonhomologous end joining (D-NHEJ) pathway. See text for details. (The picture from Mladenov and Iliakis, 2011).

Recruitment of DNA repair factors and spreading of signalling around the damage initiate the DDR and result in the formation of discrete repair foci (Bekker-Jensen *et al*., 2006; Ziv *et al*., 2006). One of the first histone modification events linked with the DDR is phosphorylation of H2AX variant on residue serine 139 in cells, when DNA DSBs are induced by ionizing radiation. The γ-component is a form of H2AX phosphorylated in the C-terminal region (Figure 1.7) (Fernandez-Capetillo *et al*., 2004; Kinner *et al*., 2008; Paull *et al*., 2000; Rothkamm and Löbrich, 2003). DSBs cause chromatin remodelling and formation of so-called ionizing radiation-induced foci, where during the first minutes after irradiation proteins involved in DNA repair are attracted to the DSB (Tichý *et al*., 2010). Foci formation of γH2AX, which is an important signalling molecule of DSBs and that of 53BP1 (p53-bilding protein1), are widely used for visualization of DSBs (Nagy and Soutoglou, 2009; Panier and Durocher, 2013). Both of them are markers for DSBs and a hallmark for the activation of NHEJ repair pathway.

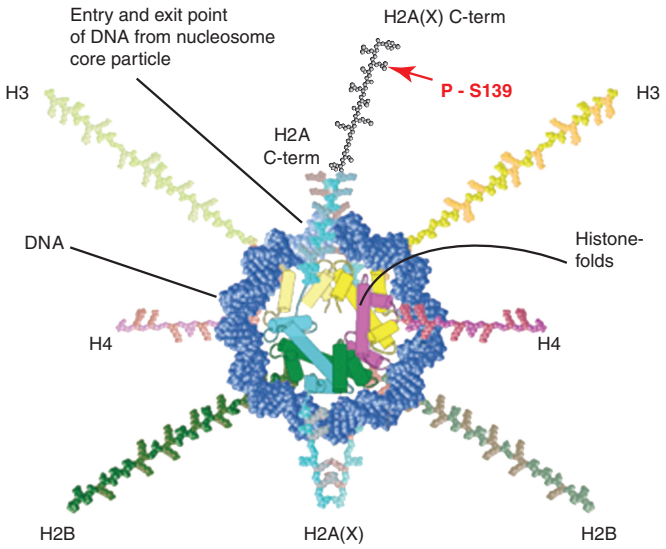

Figure 1.7: A model of the nucleosome core particle showing DNA interactions with core histone. The DNA entry and exit points are localized at the H2A/H2B dimer. The H2AX C-terminus, which is 14 amino acids longer than that of H2A, is drawn here in black with a red arrow marking the phosphorylation site within the SQEY motif (Kinner *et al*., 2008).

An important regulator of DSB signalling is 53BP1, which was described two decades ago. It is a large protein of 1972 amino acids, that has no apparent enzymatic activity but contains interaction surface for numerous DSB-responsive proteins (Panier and Boulton, 2014). The current model of 53BP1 recruitment to DSB sites proposes that H4K20 methylation is also induced and becomes available for 53BP1 after DNA damage (Figure 1.8). Therefore, 53BP1 is a bivalent histone modification reader that can recognize a histone code produced by DSB signalling (Fradet-Turcotte *et al*., 2013). However these histone modifications are normally present on chromatin and do not change after IR-induced DNA damage. 53BP1 also promotes ATM-dependent checkpoint signalling, especially at low levels of DNA damage. It is a key protein for DSB repair pathway choice and promotes the synapsis of distal DNA ends during NHEJ (Panier and Boulton, 2014).

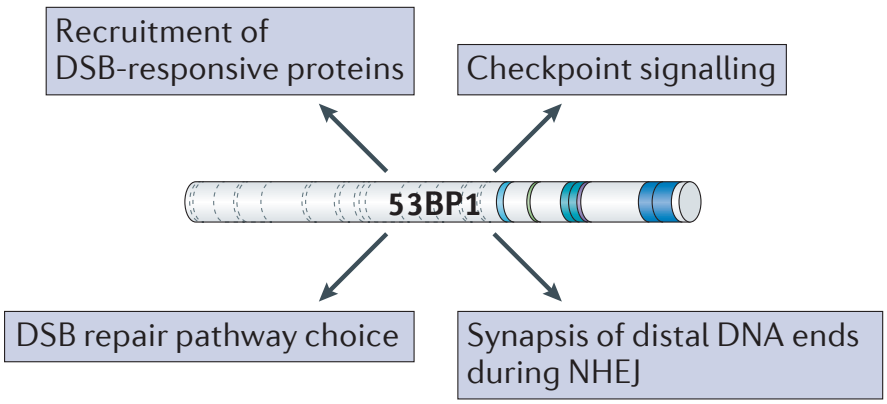

Figure 1.8: Summarize of 53BP1 functions in the DNA damage response. (Panier and Boulton, 2014).

At present, immunostaining of γH2AX and also of 53BP1 is the most sensitive method for monitoring DSB induction (with IR doses in the order of mGy) and repair (Falk *et al.,* 2010). Loss of H2AX increases genomic instability, supporting the critical role of γH2AX in DDR (Fernandez-Capetillo *et al*., 2004).

1.2.1.1. Backup pathways of nonhomologous end joining

Several studies have shown that human tumour cells deficient in DNA-PKcs re-join DSBs with a similar fast and a slow component. Complete re-joining of DSBs was observed in cells deficient in Ku or DNA ligase IV. Results suggest that if D-NHEJ is genetically or chemically downregulated and at the same time HR somehow fails, then DNA DSBs could be repaired by backup NHEJ (Dibiase *et al*., 2000, Wang *et al*. 2001a, Wang *et al*., 2001b, Iliakis et al., 2007). The repair by the backup pathway (B-NHEJ) is slower, less efficient and more error prone than the DNA-PK dependent pathway (D-NHEJ) because of changing alterations in nucleotide sequence or the joining of unrelated ends. It can lead to a higher frequency of chromosomal translocations than other DNA repair pathways (Iliakis *et al*., 2007). B-NHEJ operates throughout the cell cycle (Iliakis, 2009), but its activity also shows cell cycle-dependent fluctuations with an increased activity in G2 and a reduced one in G1 phase (Singh *et al*., 2011).

Although the mechanism of B-NHEJ is still not fully understood, some of the putative components, which act in B-NHEJ, are already described. When essential components of D-NHEJ are absent, PARP-1 is recruited for DSB repair. PARP-1 binds to the end of the DNA. Usually PARP-1 acts in SSB and base excision repair (BER), where it works as a sensor for DNA damage (Caldecott, 2001), but it is also involved in B-NHEJ (Figure 1.9A). Moreover, the histone H1 has similar functions as Ku in D-NHEJ (Figure 1.9B). The ligation during B-NHEJ is carried out by DNA ligase III (Wang *et al*., 2005) or ligase I, which is regulated in complex with XRCC1 by PARP-1, instead of ligase IV in D-NHEJ (Wang *et al*., 2006). Evidence shows that histone H1, the MRN complex and Werner syndrome protein (Wrn) are involved in B-NHEJ (Mladenov and Iliakis, 2011).

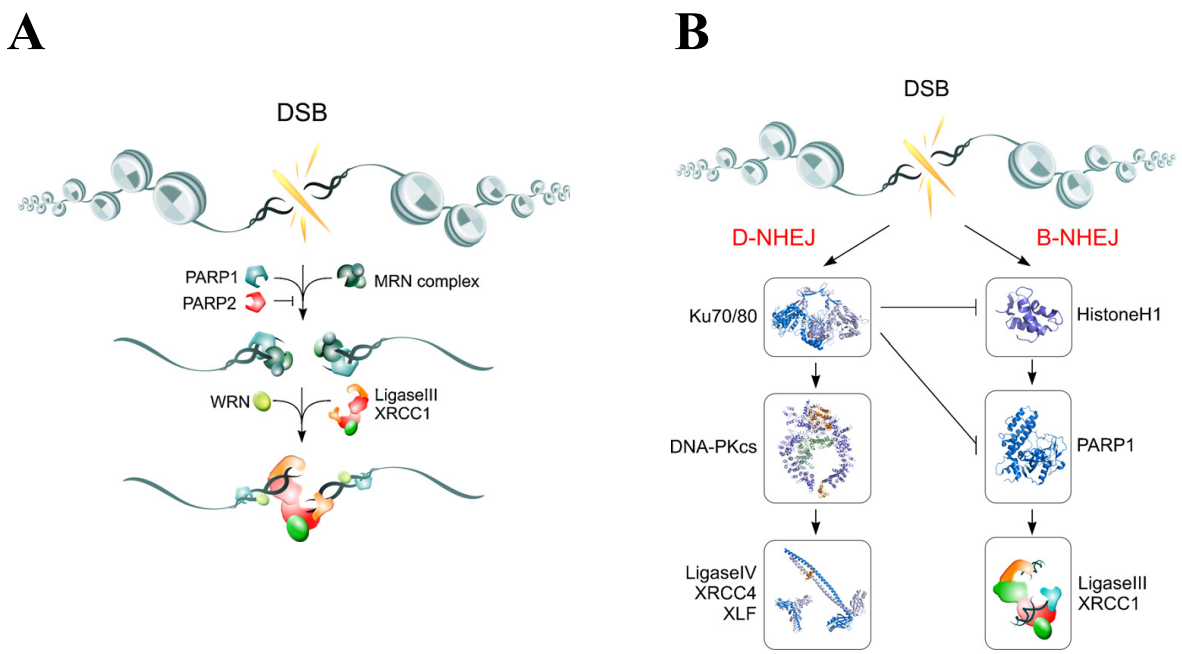

Figure 1.9: Mechanism of B-NHEJ pathway. A: Outline of the main players in B-NHEJ pathway; **B:** Outline of possible interactions between D-NHEJ and B-NHEJ (Mladenov and Iliakis, 2011).

1.2.1.2. Homologous recombination repair

Homologous recombination repair (HRR) functions only in late S and G2 phases of the cell cycle when the DNA is replicated. HRR is, in contrast to D-NHEJ and B-NHEJ, an error-free repair process. During HRR the damaged DNA enters into physical contact with undamaged DNA of the homologues chromosome and shares sequence homology, which is used as template for repair.

HRR is initiated by a nucleolytic resection of DSB by the MRE11-RAD50-NBS1 (MRN) complex. Resulting DNA tails are coated with replication protein A (RPA) forming a nucleoprotein (Takahashi *et al*., 2014). Rad52 protein, which protects against exonucleolytic activity, forms a heptameric ring complex with single-stranded DNA. Rad52 interacts with Rad51 and RPA, stimulating DNA strand exchange activity of Rad51. Thereafter, Rad51 catalyses the strand-exchange events with a complementary strand in which the damaged DNA molecule invades the undamaged DNA duplex and displaces one strand as D-loop (Christmann *et al*., 2003). Assembly of the Rad51 is facilitated by different Rad51 paralogues (Rad51B, Rad51C, Rad51D and XRCC2 with XRCC3). After DSB recognition, DNA synthesis, ligation and branch migration, the resulting structure becomes resolved (Figure 1.10).

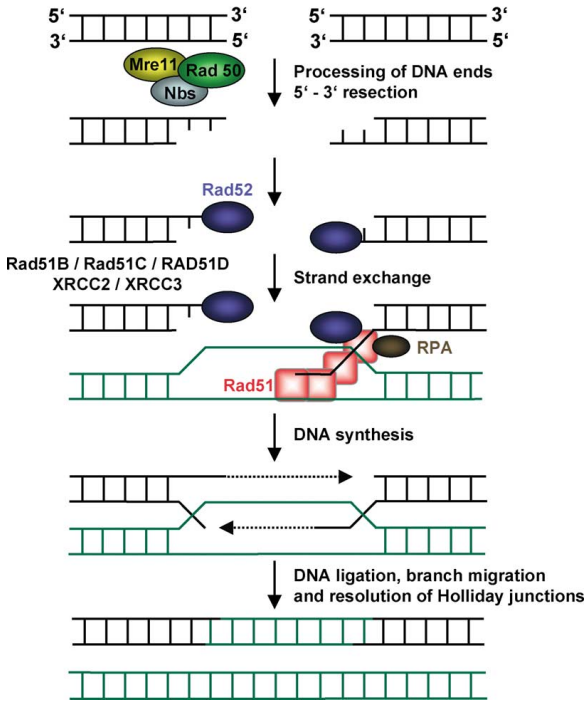

Figure 1.10: Mechanism of homologous recombination repair (HRR). Homologous recombination starts with nucleolytic resection of the DSB in the $5' \rightarrow 3'$ direction by the MRE11–Rad50–NBS1 complex, forming a $3'$ single-stranded DNA fragment to which Rad52 binds. Rad52 interacts with Rad51, provoking a DNA strand exchange with the undamaged, homologous DNA molecule. Assembly of the Rad51 nucleoprotein filament is facilitated by different Rad51 paralogues (such as Rad51B, Rad51C and Rad51D, XRCC2 and XRCC3). After DNA synthesis, ligation and branch migration, the resulting structure is resolved (Christmann *et al*., 2003).

1.2.2 Epigenetic modification and DNA damage response

DNA DSBs are the most toxic form of DNA damages that offer a potential risk both to genetic and epigenetic integrity. Mutations and perturbed epigenetic regulations both are essential characteristics of cancer. Severe disruptions of chromatin configuration in heterochromatin, like those caused by radiation-induced DSBs, can lead to incomplete or incorrect restoration of chromatin structure, leaving a DSB induced epigenetic memory of damage (Lorat *et al*., 2012). Hence, to understand how cells repair DSB damage in the context of the nuclear architecture and condensed chromatin structure is an important aim of currently radiology.

Several studies showed that the chromatin structure has an influence on cell survival and the efficiency of DSB repair after irradiation (Falk *et al*., 2008). In this respect, Karagiannis *at al*., (2007) reposted that cells treated with Trichostatin, an inhibitor of histone deacetylases, accumulates γH2AX foci, which then leads to the radiation sensitivity of tumour cells. There was also an effect on the spatial distribution of γH2AX foci with significantly higher foci number in heterochromatin compared to that in euchromatin. It has been shown

that a decrease in H3K9 trimethylation in heterochromatin, which results in a relaxation of heterochromatin structure, is important for DNA damage response (Wang *et al*., 2013). In addition, perturbation of histone methyltransferase SUV39H1 and demethylase JMJD2b was shown to have a significant impact on DSB repair. Depletion of JMJD2b or sustained expression of SUV39H1 delay the repair of heterochromatic DNA and reduces clonogenic survival after IR, as described by Zheng *et al*., (2014).

Falk *et al*., (2010) reported that artificial chromatin hypercondensation inhibited the repair process, but did not decrease chromatin sensitivity as measured by γH2AX induction. They also could not find accumulation of the repressive mark H3K9me2 at damage sites.

Additionally, heterochromatin and euchromatin exert different DNA damage sensitivity and repair process (Falk *et al*., 2014; Jeggo *et al*., 2011; Murray *et al*., 2012; Sak *et al*., 2015). The explanation for the heterogeneity in the damage response in eu- and heterochromatin may be that the majority of DSBs are caused by indirect effect mediated by reactive free radicals, with only about 20% of DSBs generated by direct ionisation effect of IR on DNA (Falk *et al*., 2014). More radicals are produced in decondensed chromatin due to its high hydratation. In addition, DNA in dense heterochromatin is better shielded against the harmful radicals due to higher fraction of proteins associated with the chromatin (Figure 1.11). According to bodyguard hypothesis, the compacted heterochromatin helps to protect DNA from damage and to block the expansion of H2AX phosphorylation (Hsu, 1975; Qiu, 2015). However, the molecular mechanism for the higher resistance of heterochromatin to DSB induction by sparsely ionizing radiation is still unclear.

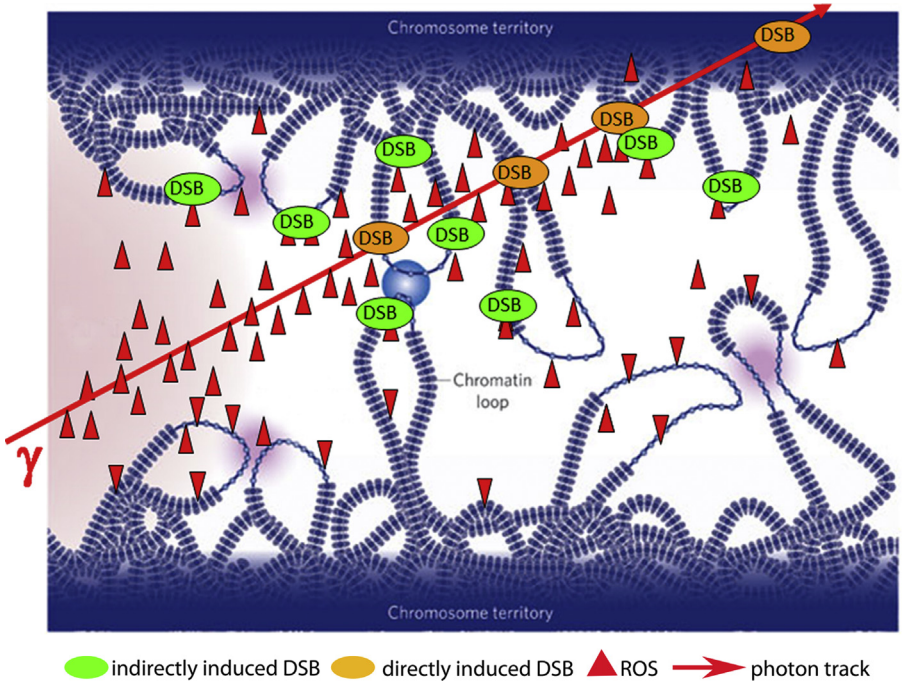

Figure 1.11: A possible explanation of the higher sensitivity of the decondensed eurochromatin to the DSB induction by low-LET γ-rays. (Details see in text, the picture from Falk *et al*., 2014).

Goodarzi *et al*., (2010) reported that heterochromatic DSBs compared to that of euchromatin are repaired at a later times after DNA DSB induction. DSB repair in heterochromatin is mainly dependent on the HR pathway with the formation of foci at sites of heterochromatic DSBs proceeding with slower kinetics compared to that of euchromatic regions (Chiolo *et al*., 2011). Furthermore it was shown that the local decondensation of heterochromatin at the sites of DSBs leads to the movement of DSBs to the heterochromatin periphery where repair may take place (Falk *et al*., 2014; Falk *et al*., 2007; Jakob *et al*., 2011; Zhang *et al*., 2015). These data implicate that the highly compacted chromatin structure could be a physical barrier to the detection of DSB and signalling of its repair (Goodarzi and Jeggo 2012; Lorat *et al*., 2012). It has been proposed that ATM is essential for repair of the DSBs in heterochromatin, because it was shown to be required for DSB repair in heterochromatin, but was dispensable for the relocalization within heterochromatin (Figure 1.12). Thus, ATM signalling enhances heterochromatin relaxation in the DSB vicinity and therefore it could be a prerequisite for DSB repair in heterochromatin. In other words, the heterochromatin superstructure confers a barrier to DSB repair, which can be relieved by loss of the proteins that contribute to the heterochromatin structure.

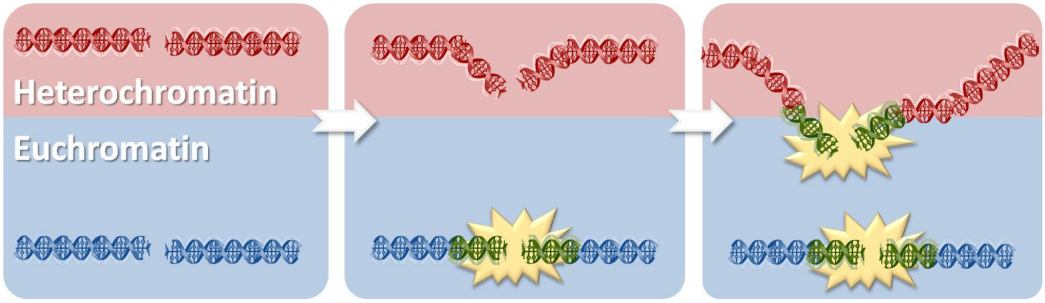

1. DNA double strand breaks (DSBs) form in heterochromatin (HC) and euchromatin (EC).

2. In EC, the DSB elicits rapid IRIF formation. The DSB in HC migrates away from HC core to periphery with EC.

3. Once at the HC:EC border, the DSB within HC elicits IRIF, which expands away from HC core into EC.

Figure 1.12: Differential irradiation induced foci (IRIF) formation between euchromatin and heterochromatin. (1) DNA double strand breaks (DSBs) form within either heterochromatin (red) or euchromatin (blue); (2) γH2AX occurs on chromatin at the DSB site (green) enabling the formation of the larger IRIF (yellow star) comprised of proteins such as Mre11, Rad50, NBS1, MDC1, RNF8, RNF168 and 53BP1. In heterochromatin IRIF fail to form to a similar extent (or at all) at the same time point. Rather, the heterochromatic DSB relocates from the heterochromatic core to the peripheral zone bordering on euchromatin; (3) Once relocated to the heterochromatin: euchromatin border, the heterochromatic DSB elicits IRIF formation which expands into the surrounding euchromatic space (Goodarzi and Jeggo, 2012).

1.3 Non-small cell lung cancer (NSCLC)

Lung cancer is a worldwide problem because of its poor prognosis. There are two major forms of lung cancer: small cell lung cancer (SCLC), representing approximately 20%, and non-small cell lung cancer (NSCLC), which accounts for the remaining 80% of lung cancers. Histologically, NSCLC can be classified into adenocarcinoma, which is the most prevalent form (40% prevalence), followed by squamous cell carcinoma (25% prevalence), and large cell carcinoma, which represents only 10% of the cases (Mehta *et al*., 2015). Most of the clinical studies in lung cancer are focused on NSCLC, because it is the predominant histological type of lung cancer and accounts for approximately 75% of lung cancers. In Germany patients with lung cancer have a poor prognosis with a 5 years survival of about 15% (Robert Koch Institute, 2014).

Initiation and progression of lung carcinoma is the result of the interaction between genetic, epigenetic and environmental factors. In lung cancer, accumulation of genetic alterations, including point mutations, deletions, translocation, and/or amplifications, is a common event (Balgkouranidou *et al*., 2013). Genome analysis of lung cancer cells shows that genetic and also epigenetic events are involved in tumorigenesis (Fontanière *et al*., 2006; Helman *et al*., 2012). Global DNA hypomethylation is frequent in NSCLC and is associated with genomic instability (Daskalos *et al*., 2011).

One of the major epigenetic changes is DNA hypermethylation in the promoter region of tumour suppressor genes. Silencing of these genes can promote tumorigenesis by several mechanisms, including increasing the cell proliferation rate or suppressing DNA repair and apoptosis (Liu *et al.*, 2013). Due to the reversibility of epigenetic modifications, chromatin modifiers are potential targets for the development of more effective therapeutic strategies against cancer. Thus, the epigenetic regulation by methylation plays an important role in tumorigenesis.

1.4 Aims of this study

Epigenetic modification plays a critical role in gene regulation during differentiation, cellular survival, and apoptosis, as well as in many types of human cancer. In the present study, we focused on histone methylation, which is correlated with transcriptional repression. Methylation of histones by specific histone methyl transferases (HMT) are key events in the regulation of epigenetic modification. However, the exact role of epigenetic chromatin modification in cellular processes has not yet been established. The HMT SUV39H1 was shown to be implicated in different types of cancers, including lung cancer (Barh *et al*., 2013; Yost, 2011). Cells lacking SUV39H1 show deregulated cell proliferation (Wang *et al*. 2013), mammalian development (Peters *et al*., 2001) and have increased radiation sensitivity (Ayrapetov *et al*., 2014).

So far, most of the research groups focused on the role of SUV39H1 in gene expression or genomic instability regards it as a potential target for epigenetic cancer therapy (Chiba *et al*., 2014; Sidler *et al*., 2014). Sidler provided evidences that downregulation of SUV39H1 in human fetal lung fibroblasts in response to DNA-damaging agent was associated with induction of apoptosis, DNA repair and senescence.

However, SUV39H1 was also shown to be recruited to DNA double strand breaks and thus implicated in the heterochromatic DSB repair mechanisms (Ayrapetov *et al*., 2014). Thus, the aim of the present work was to study several aspects of epigenetic modulations by Suv39h1 and its effect on the radiation response. For this purpose several endpoints were addressed by studying (i) methylation pattern, (ii) global condensation status of chromatin structure, i.e. condensed versus open (iii) DNA DSB repair pathways (NHEJ and HR), (iv) apoptosis and (v) clonogenic survival. These questions were addressed using different experimental strategies: (a) by genetic model of Suv39h1 knockout mouse fibroblast, (b) by siRNA mediated Suv39h1 knockdown in NSCLC cell lines and (iii) by using specific HMT inhibitors.

2 Material and Methods

2.1 Material

2.1.1 Technical devices

Description	Supplier
CO_2 Incubator	Thermo scientific
Centrifuge	Universal 32R, Hettich zentrifugen Rotina 380R, Hettich zentrifugen Mikro 200, Hettich zentrifugen
ChemiDOC, Imaging System	Bio RAD
FluorImager	Typhoon 9400, Molecular Dynamics, Germany
Novex Mini-cell	Invitrogen
Light Microscopy	LEITZ DM IL, Leica, Germany
Florescence Microscopy	Imager.Z1, Zeizz, Germany
Confocal Microscopy	TCS SP5 Leica Microsystems, Wetzlar, Germany
Flow cytometry system, Galaxy	DAKO
iBlot® Dry Blotting System	Introgen, Life Technologies, Germany
Odyssey® infrared imaging system	LI-COR Biosciences, Germany
Multiskan Ascent	Thermo Electron Corporation

2.1.2 Chemical and biological materials

β-Mercaptoethanol	Sigma-Aldrich
Agarose	Bio-Rad
Amphidicolin	Sigma
Apocynin	Sigma
BSA	Sigma
Crystal violet	Merck

DMEM	Gibco™
DMSO	Sigma
DTT	Roth
FBS	Gibco™
Ethanol	Sigma-Aldrich
Formaldehyde 37%	Sigma
Glycerol	Calbiochem
HCl	Roth
H_2O_2	Merck
Leibowitz L-15	Gibco™
MEM	Gibco™
Membrane blocking agent	GE Healthcare UK
Methanol	J.T. Beker
NaCl	Sigma
NaF	Merck
NaN_3	Merck
Phenylmethylsulfonyl fluoride (PMSF)	Life Technology
Phospatase inhibitor	Thermo Scientific
PRMI	Gibco™
Protease inhibitor cocktail tablets	Roche
RIPA	Sigma
RNAse	Roth
Sheath Fluid for Flow System	PARTEC
Tiron	Sigma
Tris	Roth
Triton X100	Sigma
Trypan Blue stain 0.4%	Biozym
Trypcin/EDTA	Gibco™
Trichostatin A TSA	Sigma
TWEEN20	Sigma-Aldrich
Zeocin™	Invitrogen

2.1.2.1 Small molecules inhibiting HMTs

BIX0194	Selleckchem, USA

Chaetocin	Cayman chemical, USA
Gliotoxin	Cayman chemical, USA
Triptolide	Sigma, USA
UNC0638	Sigma, USA

2.1.3 Plasmids and siRNA

psiRNA-hSUV39H1	#psirna42-hsuv39h1	Invivogen
EHMT2	ID s21468	Ambion
SUV39H1	ID s13658	Ambion
SUV39H1	ID s13659	Ambion
SUV39H1	ID s13660	Ambion

2.1.4 Antibodies and dyes

2.1.4.1 Primary antibodies

Antibody	Company	Host species	Catalog no.	Dilution used
53BP1	abcam	rabbit	Ab21083	IF 1:500
pH2AX	Millipore	mouse	05-636	IF 1:500
	abcam	rabbit	ab2893	WB 1:1000
pH2AX	abcam	mouse	Ab22551	IF 1:500
pATM	abcam	rabbit	Ab81292	WB/IF 1:500
pKAP-1	abcam	rabbit	Ab70369	WB 1:1000
SUV39H1	abcam	rabbit	ab155164	WB 1:1000
G9a	abcam	rabbit	Ab134062	WB 1:500
Rad51	CALBIOCHEM	rabbit	PC130	IF 1:500
H3K9me1	abcam	rabbit	ab9045	WB 1:1000
H3K9me2	abcam	mouse	ab1220-100	WB 1:1000
H3K9me3	abcam	rabbit	ab8898	IF 1:500
				WB 1:1000
H3K27me3	abcam	mouse	ab6002	IF 1:500

H3K4me3	abcam	rabitt	ab8580	IF 1:500
HP1alpha	abcam	rabbit	Ab50514-100	IF 1:500
	upstate	mouse	05-689	IF 1:500
CyclinE1	Cell Signaling	mouse	4129S	IF 1:500
Cyclin A	Santa Cruz	rabbit	Sc-596	IF 1:500
Cyclin B1	Upstate	mouse	05-373	IF 1:500
PCNA	abcam	rabbit	ab18197	IF 1:500

2.1.4.2 Secondary antibodies and dyes

Antibody	**Company**	**Host species**	**Catalog no.**	**Dilution used**
actin	Santa Cruz	rabbit	sc-1616	WB 1:500
Alexa488	Molecular probes	mouse	A11017	IF 1:500
Cy3	Immune Research Jackson	rabitt	800-367-52	IF 1:500
GAPDH	abcam	mouse	ab8245	WB 1:3000
H3	abcam	rabbit	ab1791	IF 1:500
				WB 1:3000
Hoechst 33342	Sigma			WB 1:3000
DAPI	Sigma-Aldrich			1mg/ml

2.1.5 Software

Partec FloMax ver. 2.4.7	Partec, Muenster, Germany
MultiCycle for windows ver.3.0	University of Washington, USA
Axiovision ver. 4.8.2.	Zeiss
Image Lab ver, 4.1	BIO RAD
LAS-AF	Leica Microsystems

Imaris v.7.7	Bitplane, Zurich, Switzerland
Image Quant ver. 5.2	GE Healthcare Life Sciences, USA

2.1.6 Buffer and solutions

Crystal violet in 500 mL:

3.75 g Crystal violet

1.75 g NaCl

161.5 ml Ethanol

35.5 ml Formaldehyde 37%

rest dH2O

Tris-buffered saline (TBS)

50 mM Tris-Cl, pH 7.5

150 mM NaCl

Triton Extraction Buffer

0.5% Triton X

2 mM phenylmethylsulfonyl fluoride (PMSF)

0.02% (3 mM) NaN_3

in PBS

Extraction buffer (E-buffer (-))

50 mM NaF

20 mM Hepes pH 7.6

450 mM NaCl

25% Glycerol

0.2 mM EDTA

in dH_2O

E-Buffer (+)

In 1 mL:

950 µl E-Buffer (-)

37.5 µl Protease inhibitor

2.5 µl DTT

10 µl PMSF

P-buffer

100 mM Tris Cl pH 7.4

50 nM EDTA

0.5% Trition100

Blocking Buffer

3% BSA

0.1% Tween 20

4xSSC

7.7 mM NaN_3

in dH_2O

10 x TBE

890 mM Tris

890 mM boric acid

200 mL EDTA stock solution 0.5 M EDTA pH 8

0.5% Agarose in 0.5 x TBE

in 250 ml solution add 1.25 g Agarose

Lysis solution

10 mM Tris

100 mM EDTA

50 mM NaCl

2% w/v NLS

0.2 mg/ml Protease (only before using), stored in cold room

Washing solution

10 mM Tris

100 mM EDTA

50 mM NaCl

0.1 mg/ml RNAse (only before using) stored in cold room

Low melt Agarose 1%

For 50 ml 0.5 g Agarose in Serum free HEPE's bufferes medium

2.2 Methods

2.2.1 Cell lines and cell culture

The human primary fibroblasts (hFbs) from a skin biopsy were grown in Minimum essential media medium (MEM) supplemented with 15% fetal bovine serum. Prof. T. Jenuwein (Max-Plank Institute, Freiburg) donated us with the SUV39h1/2 knock-out mouse fibroblast cells. The murine fibroblasts (mFbs) **W8** (wt) and **D5** (Suv39h1/2$^{-/-}$) were grown in Dulbecco's modified eagle medium (DMEM) supplemented with 10% fetal bovine serum, 2 mM glutaMax, 1x non-essential amino acids, 1 mM Na-pyruvate and 0.1 mM β-mercaptoethanol.

H460 (non-small cell lung carcinoma (NSCLC), p53 wild type) and **H1299** (NSCLC, p53 mutant) were obtained from American Type Culture Collection (ATCC, Rockville, MD, USA) and were maintained in Roswell park memorial institute medium (RPMI 1640) with 10% fetal calf serum (FBS). MEMS, RPMI, DMEM were supplemented with penecillin/streptomycin (100 units ml^{-1}, all Gibco-BRL, Paisley, UK). Cells were grown in T-75 flaks with 15 ml growth medium and maintained in the logarithmic phase of growth through routine passaging by dilution with fresh medium.

2.2.2 Irradiation

Cells were irradiated using either a ^{60}Co source (Philips) at dose-rate of 0.7 Gy/min. For some experiments as indicated in the results section, irradiation was done with different doses of X-rays as required by the experimental protocol using a Seifert/Pantak X-ray machine (Siemens, USA) operated at 320 keV, 10 mA with a 1.65 mm Al filter (effective photon energy approximately 90 keV), at a distance of 750 mm for 100 mm dishes and 500 mm for 60 mm dishes, and a dose rate of 1.3 – 3 Gy/min. The dosimetry was performed with a PTB dosimeter (Physikalisch-Technische Bundesanstalt, Braunschweig, Germany) and Frick`s chemical dosimetry, which was used to calibrate an in-field ionization monitor. The distribution of dose was ensured by rotating the radiation table. Cells were returned to the incubator immediately after exposure to IR.

2.2.3 Proliferation assay

To determine the respective half maximal inhibitory concentrations (IC50), plateau-phase H1299 and H460 cells were harvested and plated into 6-well (9.6 cm^2/well) tissue

culture plates (Falcon) $0.2x10^6$ cells per well. Drugs were added into the culture plates to a final concentrations of 0, 10, 25, 50, 100, 200 nM for **Chaetocin**; 0, 10, 25, 50, 100, 200 nM for **Triptolide**; 0, 5, 10, 20, 50 100 nM for **Gliotoxin**; 0, 0.1, 0.5, 1, 2, 5 μM for **BIX01294**; 0, 1, 5, 10, 20, 50 μM for **UNC0638** 24 h after plating. Cells were incubated at 37°C in 5% CO_2 for 72 h. Then the cell number was counted by Neubauer chamber. The IC50 was calculated by statistic program R.

Logarithm of calculation for R:

concentration <- c(X_1,X_2,…,X_n)
perc.cells <- c(Y_1,Y2,…,Y_n)
z.dat <- cbind(concentration,perc.cells)

mean.perc.cells=as.vector(by(z.dat[,2],factor(z.dat[,1]),mean,na.rm=T))

IC50=approx(y=unique(z.dat[,1]),x=mean.perc.cells,xout=.5)$y

IC50
Where X_n is a number of concentrations,
Y_n is a percentage of cells.

2.2.4 Life cell imaging

For Life cell imaging, plateau-phase cells H1299 were harvested and plated into 4-well (1.7 cm^2/chamber) chamber on cover glass (SARSTEDT, Nuebrecht) 150.000 cells per chamber. After 24 h the cell culture was treated with Chaetocin at 30 nM (IC50) and incubated at 37°C in 5% CO_2 for 24 h. After 24 h Chaetocin was washed out and Hoechst 33342 was added to the culture medium after 6 h at final concentration of 120 μg/ml. After 1 h incubation the medium was changed to Leibowitz L-15. The live cell imaging was made during next 17 h at 37°C by confocal microscopy. Immunofluorescence images of live cells were captured on a Leica TCS SP5 laser scanning confocal microscope using the LAS-AF software and were further processed using the Imaris software.

2.2.5 Clonogenic survival assay

The cells were trypsinized and plated into T25 flasks (Nunclon™) or 6-well tissue plates (Falcon). Cells were irradiated after 4 h and incubated at 37°C in 5% CO_2 for 10 days for 6-well tissue or 14 days for T25 flask. D5 cells were plated into T25 flasks with feeder cells to form colonies.

Chaetocin treatment

For clonogenic survival assay, plateau-phase H1299 and H460 cells were harvested and plated into T25 flasks with a density of $0.5x10^6$ cells/flask. After 4 h Chaetocin was added to the culture medium and the cells were incubated at 37°C in 5% CO_2 24 h. After Chaetocin incubation cell were irradiated with doses at 2, 4, 6, 8 Gy. At 24 h after IR the cells were plated into 6-wells plates for 10 days.

To determine clonogenic survival after fractionated IR, cell lines H1299 and H460 were plated into T25 flasks with a density of $0.5x10^6$ cells/flask. After 4 h Chaetocin was added to the culture medium and the cells were incubated at 37°C in 5% CO_2. The cell culture was irradiated for 3 times with 2 Gy every 24 h after Chaetocin treatment. 24 h after the last IR cells were plated into 6-wells (control (non-irradiated cells) – 200 cells/well; control (Chaetocin- untreated cells), ¼ IC50 and ½ IC50 – 400cells/well; IC50 – 600 cells/well) and then incubated for 10 days. Cells were fixed and stained with crystal violet, washed with water. Colonies (more than 50 cells) were counted manually.

2.2.6 Aphidicolin treatment

2.2.6.1 Proliferation with Aphidicolin and Chaetocin treatment

H1299 cells were harvested and plated into 6-well plates with a density of $0.4x10^6$ cells/well. After 4 h the cells were treated with Chaetocin and Aphidicolin (2 μM) either in a combined or single treatment schedule for 18-20 h and the cells were incubated at 37°C in 5% CO_2. Chaetocin was washed out and Aphidicolin was continued for 24, 48 and 72 h. The cells were incubated at 37°C in 5% CO_2. Then the medium was removed; cells were washed once with PBS, trypsinized and were counted by Neubauer chamber.

2.2.6.2 Cell cycle after Aphidicolin treatment

Cells were harvested and plated into T25 flasks with a density of $0.5x10^6$ cells. After 4 h incubation the cells were treated with Aphidicolin (2 μM) for 4 and 20 h. The probes were trypsinized and collected into tubes, washed with PBS, fixed with 80% of ethanol overnight at 4^0C. For the cell cycle analysis the samples were washed with PBS and stained with DAPI (1 μg/mL) overnight. The samples were measured by Flow Cytometry. The results were analysed by software FloMax and MultiCycle ver.3.0.

2.2.7 Transfection with siRNA

One day before transfection, cells were plated into 8-well (0.69 cm^2) chamber slides ($0.015x10^6$ cells/chamber) for immunofluorescence analysis or 6 well culture plates ($0.4x10^6$ cells/well) with the respective growth medium for western blotting assay. Optimal cell density was optimized to reach 60-80% at the time of transfection.

For each transfection sample, Lipofectamine® RNAiMAX reagent was prepared, a transfection kit (Invitrogen), complexes as follow:

Solution A: Depending on the experimental contitions siRNA, negative siRNA control and dH_2O were separately diluted in Opti-MEM® (Gibco) without serum and antibiotics and antimycotics and mixed gently.

Solution B: 6 µl of RNAiMAX® regent (Invitrogen) was diluted in Opti-MEM®. The diluted transfection reagent (solution B) was added directly to the siRNA solution (solution A). The tubes with solutions were mixed gently and incubated for 20 minutes at RT. The cells were washed once with Hank's Buffer and Opti-MEM®. The cells were incubated at 37^0C for 20 min. For each transfection 250 µl of transfection mix solution was added to each of the 8-well chambers and 1 ml for 6 well tissue culture plates. Then the cells were incubated at 37^0C for 4 h. After 4 h incubation equal volume of growth medium with 20% FBS was added to 8-well chamber (250 µl) and 1ml for 6 well tissue culture plates. The cells were incubated for 48 h at 37^0C in 5% CO_2.

2.2.8 Transfection with shRNA

The cells were plated into 24-well tissue culture plates ($0.1x10^6$ cells). Optimal cell density was optimized to reach 60-80% at the time of transfection. The cells were transfected according to supplier's protocol (Lipofectamine® 3000 (Life Technologies). Two days after transfection Zeocin™ (200 µg/ml) was added. The selection was performed for 2 weeks.

2.2.9 Histone extraction

The cells were harvested and washed twice with ice-cold PBS. Then the cells were centrifuged at 300 g for 5 min. Resuspended cells were transferred into the Triton Extraction Buffer (TEB) with 1/25 protease inhibitor cocktail and 1/100 phosphatase inhibitor. The cells were lysed on ice for 10 min by gentle stirring and centrifuged at 600 g for 10 min at 4^0C to spin down the nuclei and the supernatant was removed. Nuclei were washed in TBE (100 µl). After centrifugation cells were suspended in 50 µl cold 0.2N HCl and histone proteins were

extracted over night at 4^0C. Next day the samples were centrifuged again at 600 g for 10 min at 4^0C. The supernatant, which contains the histone proteins, was collected and the protein concentration was determined by using the Bradford assay and aliquots were stored at -20^0C.

2.2.10 Protein extraction

The cells were harvested and washed twice with ice-cold PBS and centrifuged at 300 g for 5 min. Approximately 3-5x10^6 cells were resuspended with 50 µl E-buffer (+). Cells were frozen for 1 min in N_2, and then were put into warm bath at $30C^0$ for 1 min. This procedure was repeated four times. Thereafter the cells were centrifuged at 15.000 g for 10 min at $4C^0$.

For higher molecular weight proteins extraction method with RIPA buffer was used. The cells were harvested, centrifuged twice at 2500 g for 5 min, and then 100 µl of RIPA buffer containing with 1/100 phosphatase and 1/25 protease inhibitor cocktail was added. The cells were incubated on ice for 15 min by gentle stirring and centrifuged at 15000 g for 15 min at $4C^0$.

2.2.11 Protein quantification

Protein concentrations were determined using the BioRad Protein Assay according to the manufacture`s instruction. Protein concentration was measured by colorimetric Bradford method.

2.2.12 Western blotting

Protein samples were mixed with 4x sample buffer and boiled at 95^0C for 5 min, centrifuged and loaded onto the gel. Pre-cast acrylamide gels 4-12% NuPAGE® Bis-Tris Gels (Invitrogen) for high molecular weight proteins and 12% NuPAGE® Bis-Tris Gels for histone proteins were loaded with the respective samples. The proteins were separated by gel electrophoresis with running buffer MOPS SDS Running Buffer (Life technologies).

The gel was running for 15 min at 90 V, and then the voltage was increased up to 180 V and continued for further 30-60 min, depending on the experimental conditions. Proteins were transferred with 1x transfer buffer (Life technologies) containing 10% Methanol onto Immun-Blot® LF PDVF membrane (BIO-RAD); 30 min for histones and 45 min for heavy proteins at 45 V. For the blotting procedure filter pads was soaked in 1x blotting buffer with 10% methanol. The PDVF membrane was firstly soaked in methanol for 30 seconds until it becomes transparent. The proteins were transferred to PVDF membrane with 40 V for 45 min. Then the membrane was blocked for 30 min in TBST containing 5% dry milk powder,

0.5% Tween20 and then incubated with the respective primary antibodies over night at 4^0C. The antibody was diluted in lowCross-buffer® (Candor bioscience GmbH). The membrane was washed 3x 10 min with washing buffer (TBS, 0.5% Tween20). The secondary antibody was diluted in block buffer (TBS, 5% dry milk powder, 0.1% Tween20) and the membrane incubated for 90 min at RT. Before detection, the membrane was washed for 3x 10 min in wash buffer.

For detection of the signal, Lumigen™ TMA-6 (GE Healthcare UK) solution A and B were diluted (1:4) with TBS; for detection of strong signal the WesternBright™ ECL with WesternBright™ Peroxide (1:1) was used. Imaging system with chemiluminiscence and fluorescence (Alexa488) filters was used for signal detection. Images were analysed by Image Lab (BIO-RAD). After detection the membrane was washed in dH_2O. For reblotting, re-blot plus mild solution (Millipore) was used and the membrane was incubated for 30 min at RT. Afterwards the membrane was blocked again and incubated with the respective antibodies as before.

2.2.13 Immunofluorescence

Cells were seeded onto the 4- or 8-wells chamber slides. For immunofluorescence, cells were fixed in 4% paraformaldehyde (PFA) for 15 min, washed twice with PBS for 10 min, permeabilised with P-buffer for 15 min at RT and washed twice with PBS for 10 min. The slides were put into the blocking solution over night at 4^0C. For immunostaining, slides were washed with PBS + 1% FBS solution for 3x 10 min. Primary antibody was diluted in buffer (1% BSA, 0.1% tween20 in PBS) and 300 µl was added onto the slides. The samples were incubated in a wet chamber over night at 4^0C. Slides were washed in PBS 3x 10 min and incubated with secondary antibodies and DAPI (1 µg/ml) for 90 min at room temperature. Cells were washed in PBS three times and dried on air. For mounting, aqua immu-mount (Thermo Scientific) was used.

EdU assay

Cells were seed into 4-chamber slides with $0.1x10^6$ cell/well. After 24 h incubation cells were treated with Chaetocin for 24 h at $37C^0$. The cells were stained according to supplier's protocol (Click-iT® EdU Alexa Flour® 488 Imaging kit, Molecular Probes™).

Cells were incubated for 1 h at $37C^0$. After incubation, the medium was removed and the slides were fixed in 4% formaldehyde for 15 min. After fixation the slides were washed

twice with 3% BSA in PBS and further incubated with 0.5% Triton-100X in PBS for 20 min at RT. The Click-iT solution was added onto the slide and incubated for 30 min at RT in darkness. Hoechst 33342 was added onto the slides and incubated for 30 min at RT in darkness. The slides was washed twice in PBS and prepared for IF microscopy.

2.2.14 Pulsed-field gel electrophoresis (PFGE)

PFGE is a technique used for the separation of large DNA molecules by applying to an agarose gel an electric field that periodically changes direction. The advantage of this method is that fragmentation of chromosomal DNA with radiation leads to a linear dose-dependent increase in the fraction of DNA that enters the gel, whereas intact mammalian chromosomes are unable to migrate into the gel. PFGE resolves DNA fragments ranging in size from 0.2 – 6 Mbp, whereas gel electrophoresis with a constant electric field cannot resolve DNA fragments above 50 Kbp. This enables the measure of induction and repair of DSBs. Cells were seeded into 60 mm petri dishes with $0.5x10^6$ cells per dish one day before irradiation.

2.2.14.1 Dose response of DSB induction

Cells were trypsinized, centrifuged and washed with PBS and counted. After washing agarose plugs containing the cells were prepared as described. After cutting, plugs were placed into 3 ml serum free HEPES buffered medium and irradiated on ice. Three plugs for each treatment conditions 0, 10, 20, 30 Gy were prepared.

2.2.14.2 Repair kinetics

Cells were irradiated in petri dishes on ice at 20 Gy. After irradiation the cells were replaced into the incubator for ½ h, 1 h, 2 h, 4 h and 8 h. At about 5 min before collecting the cells, the dishes were removed from the incubator, trypsinized and collected in a falcon tube and resuspended with 3 ml ice cold medium. Cells were washed twice on a shaking platform with 1500 rpm at 4^0C. Control cells (non-irradiated cells) were typsinized and collected at 4 h and 8 h time point after IR. Plugs were prepared (4 plugs for each time point) as described.

2.2.14.3 Preparation of plugs

The freshly prepared low melting agarose was warmed up at 300 W in the microwave for 2 min and put into the water bath at 50^0C. Cells at a concentration of about $6x10^6$ cell/ml in 1% low melting agarose were mixed. The solution was put into the glass tubes and left on

ice for 5 min or longer. Agarose plugs containing the cells mix were removed from the glass tube and cut to 0.5 cm pieces. After cutting the plugs they were put in the 3 ml lysis solution (3-4 plugs) for 16 h at 50^0C with about $0.15x10^6$ cells/plug. Then the lysis solution was removed and washed with 3 ml wash buffer per 3-4 plugs and incubated at 37^0C for 1 h. After incubation at 37^0C the washing solution was removed and RNAse solution was added and incubated at 37^0C for 2 h and stored at 4^0C until used.

2.2.14.4 Preparing and running of agarose gel electropharesis

For each gel 250 ml of 0.5% agarose in 0.5xTBE was prepared. The solution was warmed up in the microwave for 5 min and put into waterbath at 50^0C. After preparation the chamber for electrophoresis and the respective agarose gel, plugs containing the naked DNA were loaded into wells and sealed with 1% Agarose three times. Electrophoresis was performed for 40 h at 8^0C in 0.5x TBE using alternating cycles of 50 V in the direction of the DNA migration for 900 s and 200 V for 75 s in the reverse direction. After 40 h the gel was stained with 5 mg/ml EtBr in 0.5x TBE solution. The gel was stained for 4 h at RT by shaking and distained with water overnight.

2.2.14.5 Scanning and analysis

Gels were scanned in the Typhoon and analysed using the Image Quant and Excel software. The fluorescence settings were 200 microns, 3 mm focal plane. Setup emission filter 610 BP SPYRO RyPy EtBr; PMT470 Green.

2.2.15 Minimonolayer

Cells were trypsinized, counted and recovered from trypsin for 2 h in PRMI medium with 10% FBS. Cells were seeded as a small plaque of higher density, with 80-95% of the cells having cell-cell contacts. Approximately 1500 cells in 5 ml medium were seeded as a 3 mm spot into each well of 24-well culture plates, resulting in a cell density of approximately $2x\ 10^4$ cells/cm^2 in the plaque monolayer. The plates were incubated for 20-40 min until the cells were attached to the surface. Then 0.5 ml of PRMI medium with 10% of FBS was added into the wells and the cells were incubated for 24 h at 37^0C. The medium was removed, 1 ml of medium with drugs was added and the cells were incubated for 4-6 h before irradiation. The final concentration of Chaetocin was 0 nM, 10 nM and 15 nM. Thereafter, cells were irradiated with the respective single irradiation doses of 0, 2, 4, 8, 12, 16, 18, 20 up to 25 Gy.

For the fractionated irradiation experiments with 2 Gy/day per fraction mini-monolayer were irradiated until reaching the respective overall radiation doses. For all

treatment conditions, Chaetocin-containing medium was removed at about 6 h after the last irradiation (14x 2 Gy). Two 2 ml growth medium was added and the samples were incubated at 37^0C, 5% CO_2 for up to 6 weeks. A plaque monolayer was designated as surviving if cells reached >50% confluence in the well and cell number increased >10-fold (Sak *et al*., 2012).

2.2.16 Co-localization DNA repair foci in CICC

For the detection of colocalised γH2AX foci with CICC phenotype cells, we used the ApoTome fluorescence microscope with Plan-APOCHROMAT 63x/1.4 oil DC objective. The software Axiovision ver 4.8.2 was used for analysis. We selected the cells manually and every cell was separately semiautomaticly analyzed. The region of DAPI, which represented the nucleus with the CICC structure, was determined by mask (sky blue) (Figure 2.1). Then the green mask visualized the region of γH2AX foci in nucleus (Figure 2.2). The colocalization of CICC region versus γH2AX was identified by pink mask (Figure 2.3).

All foci per nucleus were counted and separated into two groups: “Foci in” group, which identified more than 50% of localization region (mask pink); “Foci out” group, which indentified less than 50% of localization region.

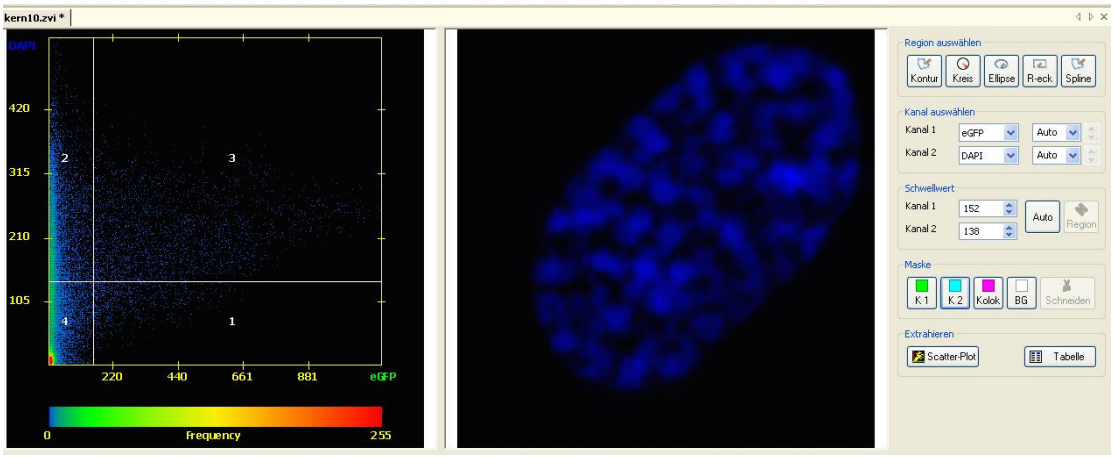

Figure 2.1: The representative picture of the nucleus. The nucleus was stained with DAPI (deep blue), the picture was made by using the Axiovision programm.

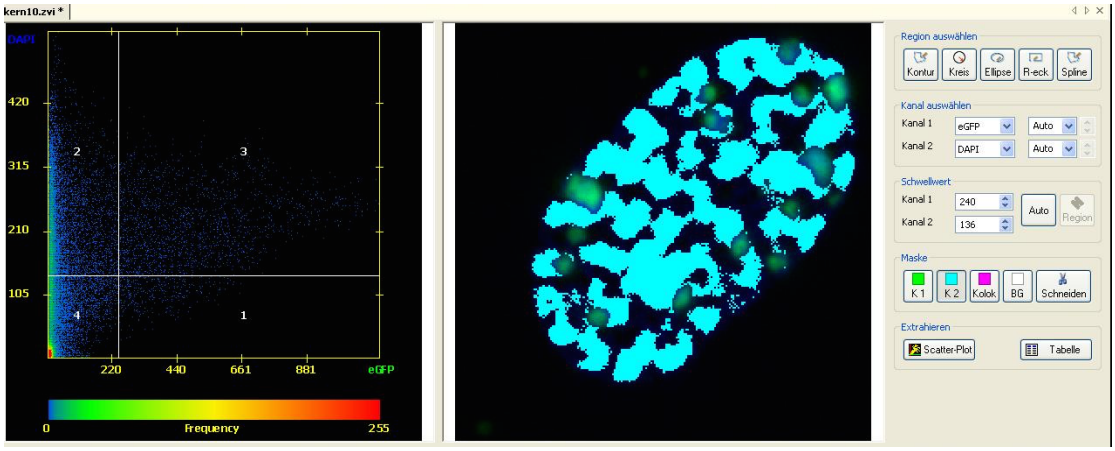

Figure 2.2: The representative picture of DAPI mask. DAPI mask (deep blue) show chromatin neriched regions within the nuclei.

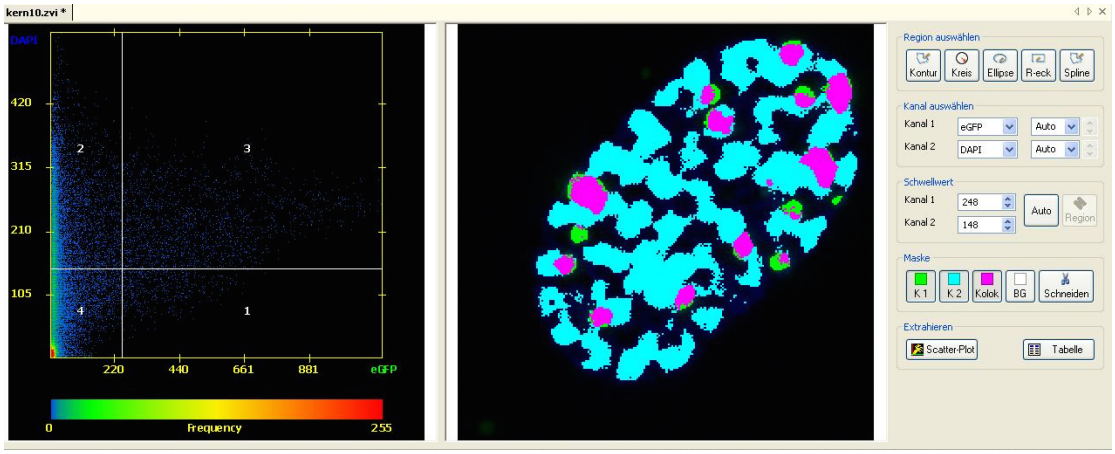

Figure 2.3: The representative picture of the colocolization of DAPI enriched CICC regions versus γH2AX foci. The nucleus was stained with DAPI (deep blue) versus γH2AX foci (green) in H1299 cells and analyzed by using the Axiovision program. Colocalization is represented by pink marks.

2.2.17 Statistical analysis

Data analysis and the graphs were done using Prism software and R environment free program (section 2.1).

3. Results

In this study, we focused on histone methylation, which plays an important role in the regulation of chromatin structure. We hypothesized that the histone methyltrasferase (HMT) suppressor of variegation 3-9 homolog 1 (Suv39h1), which is involved in the spreading of heterochromatin into adjacent euchromatin genes, may also regulate the radiation response of the cells. To investigate the influence of Suv39h1 on radiation response, i.e. cell proliferation, induction and repair of DNA DSBs and cell death in fibroblasts and tumour cell lines, we decided to modulate the activity of Suv39h1. To do this, different models were used: (i) knockout mouse Fbs (wild type (W8) and knockout Suv39h1 (D5)), (ii) knockdown of Suv39h1 by siRNA and shRNA in NSCLC cell lines (H1299, H460) and (iii) small molecule inhibitors of SUV39H1.

3.1 Increasing radiation sensitivity in HMT SUV39H1 deficient cells

3.1.1 Decreased the cell survival in Suv39h1 knockout mFb

Several studies demonstrated that overexpression of HMT SUV39H1 induced altered proliferation and differentiation of cells (Czvitkovich *et al*., 2001; Spyropoulou *et al*., 2014). To analyse the cell's ability to proliferate and to form colonies after IR in HMT SUV39H1 deficient cells, we used mFbs (Suv39h1$^{-/-}$ D5 and the respective wild type cells, W8). Our results demonstrate that D5 cells proliferate slower as compared with W8 cells (Figure 3.1A). Comparable level of cell proliferation was achieved in both cell lines by mixing the medium with 0.1 mM β-mercaptoethanol, which reduced reactive oxygen species in cells. Thus, in all experimental settings β-mercaptoethanol was in the growth medium of both mouse cell lines. In addition, the plating efficiency and the consistency of D5 cells to form colonies in comparison to that of W8 cells were also low (Figure 3.1B). Thus, D5 cells have to be seeded out with feeder cells, which increased plating efficiency of D5 cells to that of the wt W8 cells.

Surviving fractions were measured in both cell lines under these condition after irradiation with 0 Gy, 2 Gy, 4 Gy and 6 Gy. The results show, that the surviving fraction after 2 Gy (SF2) significantly decreased from 0.71 to 0.49 in D5 compared with that of W8. The difference in surviving fraction was even higher at higher irradiation doses (Figure 3.1C).

A

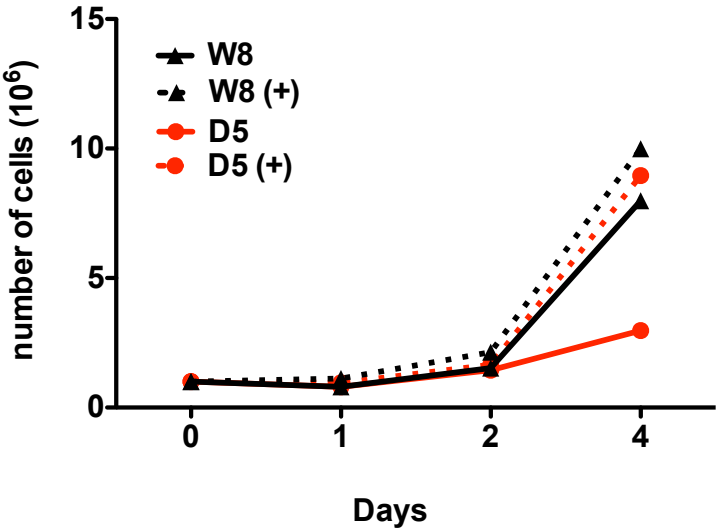

B

	W8	D5	D5 + feeder cells
PE (%)	24.3 ± 10.8	10.6 ± 4.1	26.2 ± 6.7

C

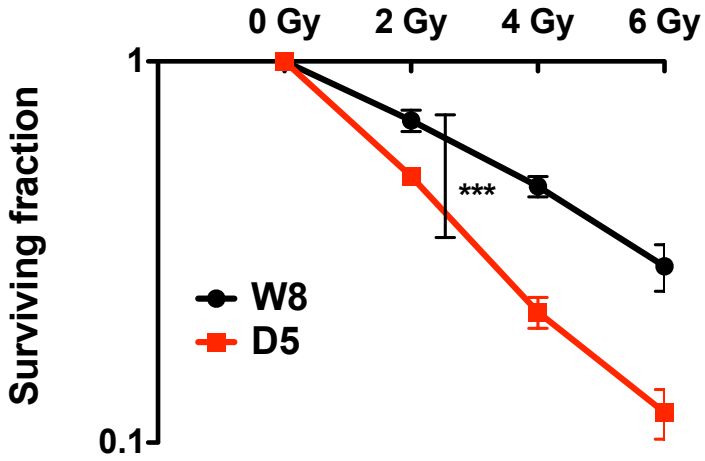

Figure 3.1: Role of HMT SUV39H1 in cell proliferation and cell survival in mFbs. A: The graph shows the proliferation with β-mecaptoethanol (+) in mFB (n=1); **B:** The table of the plating efficiency in mFbs. Results represent the mean ± s.d of 4 experiments; **C:** The graph represents the radiation sensitivity in D5 mFbs compared with W8 after exposure to IR. Representative results from at least four independent experiments are shown. Bars represent the mean ± SEM. Statistical analyses: 2-way ANOVA with Borferroni posttest for mFbs, $p < 0.001$ (***).

3.1.2 Radiation sensitivity in SUV39H1 knockdown tumour cells

Epigenetic regulation plays an important role for the radiation sensitivity of lung cancer cell lines (Kim *et al*., 2010). To validate this hypothesis, we used two human NSCLC cell lines, H460 and H1299, with different responses to IR (Jeong *et al*., 2009). In order to explore the radiation sensitivity of both NSCLC cell lines, cells were irradiated with 0, 2, 4, 6, 8 Gy and incubated for 14 days. The results show significantly higher radiation sensitivity of H460 compared to the H1299 cell line (Figure 3.2).

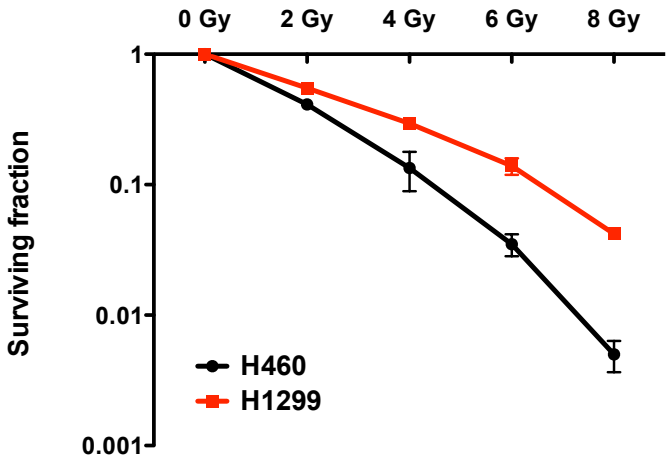

Figure 3.2: The radiation sensitivity of NSCLC cell lines. H460 and H1299 cells were irradiated at 0, 2, 4, 6, 8 Gy and incubated for 14 days. Representative results from five independent experiments are shown. Bars represent the mean ± s.d.

In order to examine the effect of Suv39h1 on the radiation sensitivity of NSCLC cell lines, 48 h before the cells were irradiated, we have knocked down the expression of HMT SUV39H1 by using shRNA approach. The results show that there is significant difference ($p < 0.05$) in the ability of the cells to form colonies after irradiation with 6 Gy in the transfected H1299 as compared with the non-transfected cells (Figure 3.3). However, over all irradiation doses, there was no significant effect of Suv39h1 knockdown on the surviving fraction in both cell lines.

A

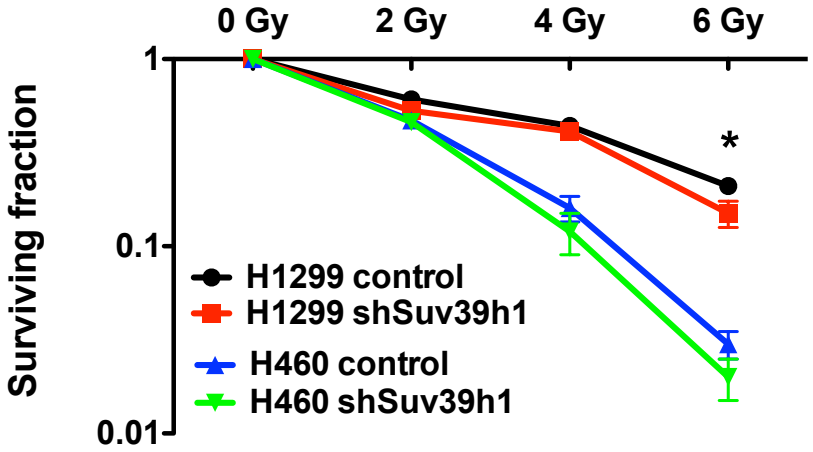

B

	control	shSuv39h1
H460	72.3 ± 7 %	54.4 ± 14.4 %
H1299	38.5 ± 9 %	31.4 ± 12 %

Figure 3.3: Effect of Suv39h1 on cell survival in NSCLC. A: The graph represents the cell survival in the transfected H1299 and H460 by shRNA targeting Suv39h1; **B:** The table shows PE in Control and Suv39h1 siRNA-treated cells. Representative results from at least six independent experiments are shown. Bars represent the mean ± SEM. Statistical analyses: trend by t-test, $p < 0.05$ (*).

To sum it up, lack of SUV39H1 affects the cell proliferation in mFbs and their colony formation capacity in mFb as well as in NSCLC.

3.2 The role of HMT SUV39H1 in DNA repair

3.2.1 The enhancement of DNA repair in tumour cells after HMT SUV39H1 knockdown

To evaluate the effect of HMT SUV39H1 on DNA repair mechanisms, we initially inhibited the expression of SUV39H1 protein by using siRNA approach. Successful reduction of protein expression of SUV39H1 and G9a to about 50% of that of the non-transfected cells after transfection with siRNA by western blotting was shown (Figure 3.4).

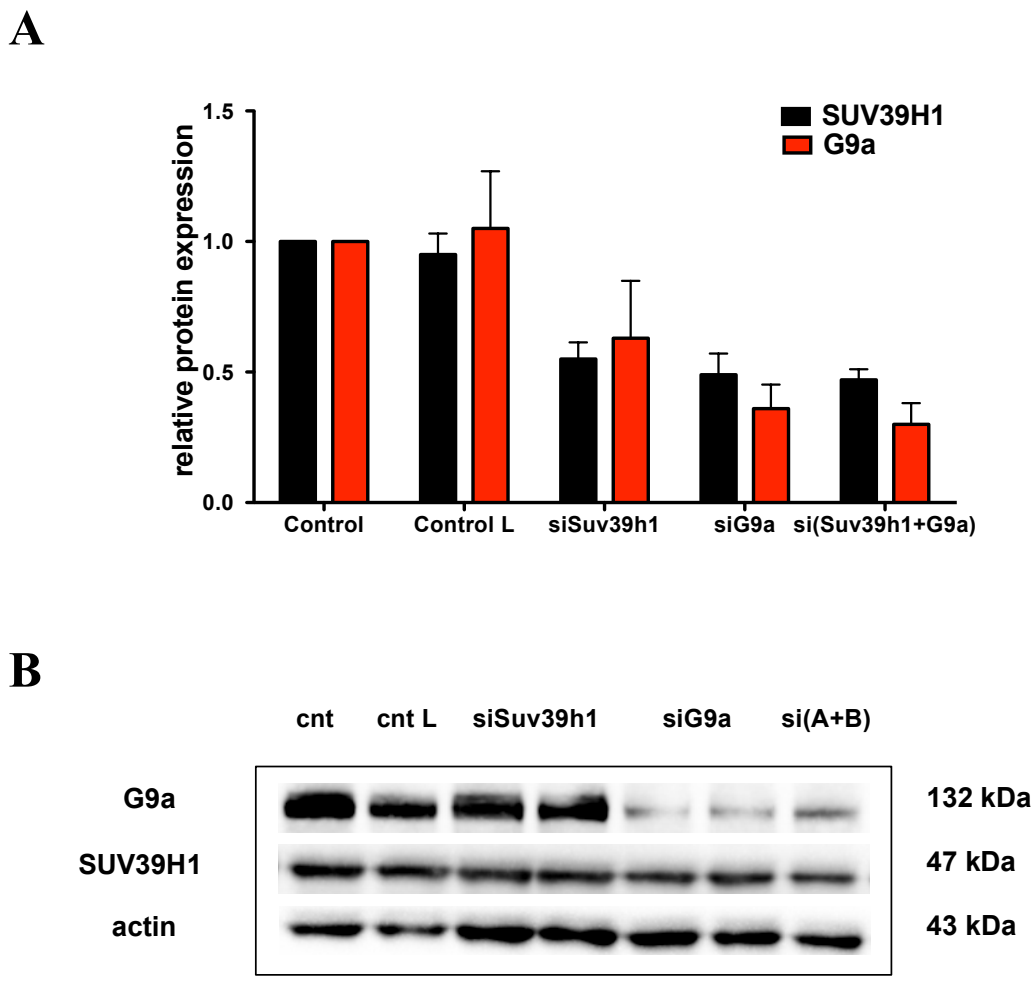

Figure 3.4: Reduction of SUV39H1 and G9a protein expression by siRNA. H1299 cells were transfected by siRNA targeting Suv39h1 and/or G9a for 48 h. L is the respective lipofectamine control. **A:** Results from three independent experiments are shown. Bars represent the mean ± SEM; **B:** Representative western blot showing G9a and actin as internal control. si(A + B) is defined as si(SUV39H1 + G9a).

The H1299 cells were transfected by siRNA targeting Suv39h1 and/or G9a for 48 h, and irradiated with 0.5 Gy and 10 Gy for the measurement of initial and residual damage. The respective cells were fixed at 1 h, 4 h and 24 h after IR and stained for γH2AX and 53BP1 as

a measure for the activity of the NHEJ pathway. The data showed that there was no difference in the initial number of DSBs after IR (0.5 Gy) in cell lines transfected with the specific siRNA for Suv39h1 (Figure 3.5) and G9a (Figure 3.6). However, downregulation of SUV39H1 expression significantly reduced the numbers of the residual γH2AX and 53BP1 foci 24 h after IR in H1299 cells.

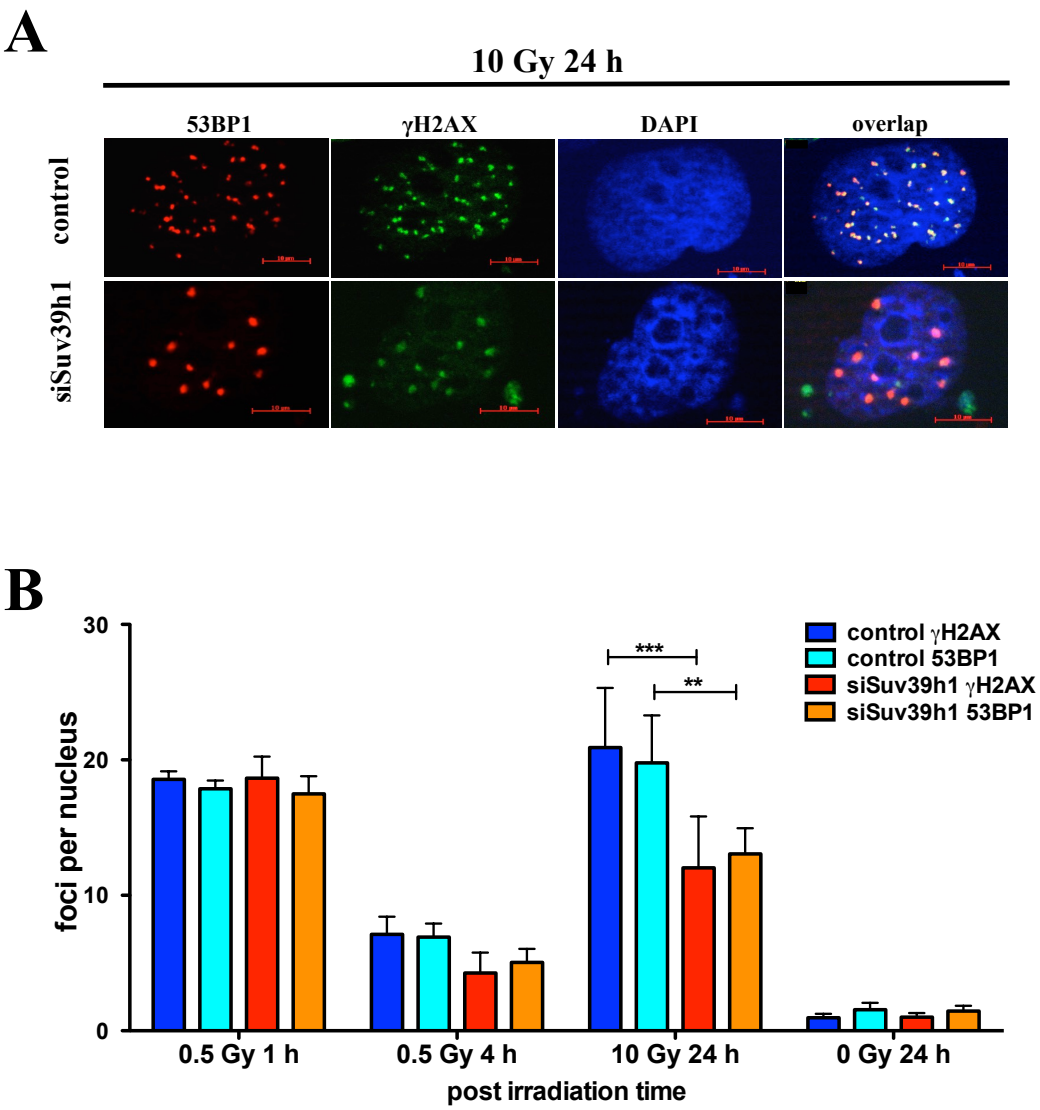

Figure 3.5: Downregulation of HMT SUV39H1 affects NHEJ repair mechanism in H1299. Cells were transfected with siRNA targeting Suv39h1 for 48 h, then exposited to IR at 0.5 Gy, 10 Gy and fixed at 1 h, 4 h and 24 h post irradiation. The samples were stained with γH2AX and 53BP1. **A:** The immunofluorescence images of γH2AX (green) and 53BP1 foci (red) in 24 h after IR at 10 Gy; **B:** The quantification of the DNA repair kinetics after IR by visible γH2AX and 53BP1 foci. Representative results from four independent experiments are shown. Bars represent the mean ± s.d. Statistical analysis: 2-way ANOVA analysis with Bonferroni posttest, $p < 0.01$ (**), $p < 0.001$ (***). Scale bar = 10 μm.

Overall, our results show that downregulation of SUV39H1 affected NHEJ repair mechanism, i.e. decreased number of residual foci at 24 h after IR in the radioresistant H1299. In comparison, downregulation of the HMT G9a showed no significant effect on γH2AX and

53BP1 foci and thus seems to be not involved in the signalling of NHEJ.

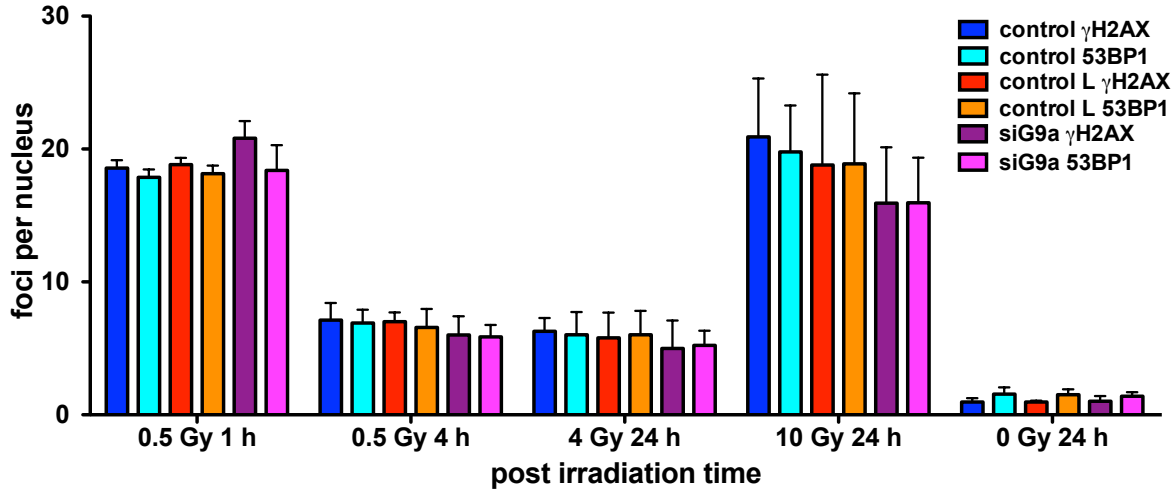

Figure 3.6: Downregulation of HMT G9a and its effect on NHEJ repair. H1299 cells were transferred for 48 h by using siRNA G9a, exposited to IR at 0.5 Gy and 10 Gy and fixed in 1 h, 4 h and 24 h post irradiation time. The samples were stained with γH2AX and 53BP1, a hallmark of NHEJ repair. Representative results from four independent experiments are shown. Control L is a lipofectamine control. Representative results from at least three independent experiments are shown. Bars represent the mean ± s.d.

It is possible that siRNA mediated downregulation of SUV39H1 protein level to about 50% was not sufficient to affect initial repair signalling. Thus, we decided to investigate the influence of SUV39H1 on NHEJ and HR repair in H1299 cells by using shRNA, which allow more stable downregulation of SUV39H1. The kinetic of DSB repair was evaluated in H1299 cells transfected with Suv39h1 shRNA and compared this to the non-transfected wild type cells. The respective cells were irradiated with 0 Gy, 0.5 Gy, 4 Gy and 10 Gy and fixed at 1 h, 4 h and 24 h after IR. For the analysis of NHEJ repair, cells were stained with γH2AX and 53BP1 antibodies as a measure for NHEJ and Rad51 as a measure for HR. To control the level of SUV39H1 protein expression for each experiment, nuclear extracts were prepared and analysed by Western blotting (Figure 3.7). The downregulation of SUV39H1 protein level was not higher than 50% from that of the control cells and significantly reduced H3K9me2 and H3K9me3 as well as an increased H3K9me1 level, which was used as a functional read-out for SUV39H1 activity and a measure for reduced heterochromatic fraction of the respective cells (Figure 3.8).

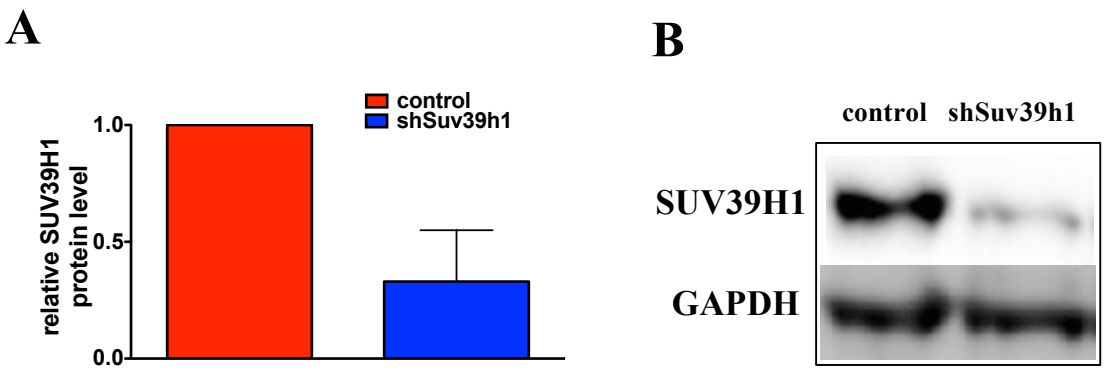

Figure 3.7: SUV39H1 protein expression after transfection with shSuv39h1. A: Reduction of SUV39H1 protein expression; **B:** Representative western blot showing SUV39H1 and GAPDH as internal control. Results from three independent experiments are shown. Bars represent the mean ± s.d.

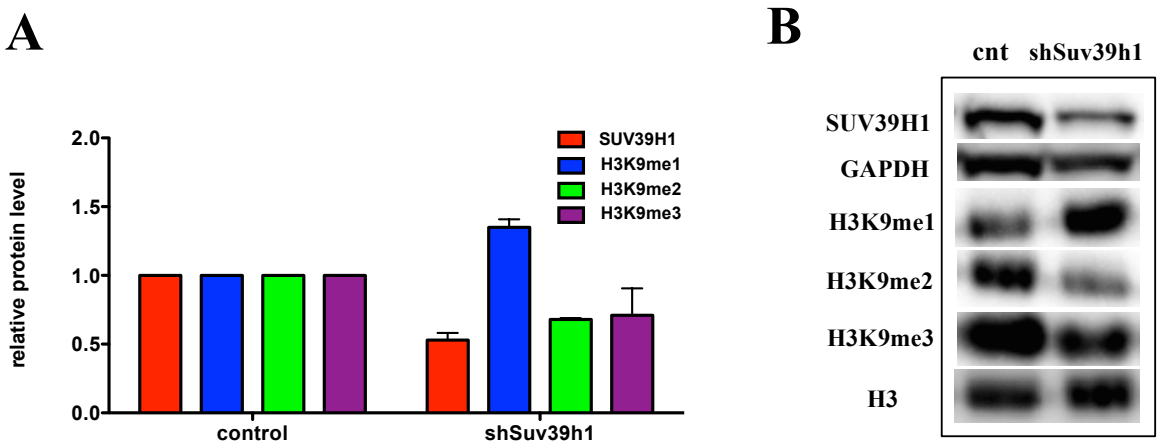

Figure 3.8: The histone level expression in shSuv39h1 cells. A: The histogram represents the relative histone level expression in H1299 cells, which were transferred with shSuv39h1. Protein was isolated from passage 2, 4, 6. Representative results from at least three independent experiments are shown. Bars represent the mean ± s.d; **B:** Representative western blot shows SUV39H1, H3K9me1, H3K9me2, H3K9me3 and GAPDH, H3 as internal control.

The results show that downregulation of SUV39H1 leads to significantly lower initial number of γH2AX and Rad51 compared to non-transfected H1299 cells and thus affects initial signalling of NHEJ (Figure 3.9) and HR repair (Figure 3.10). In addition, residual number of γH2AX and 53BP1 foci also significantly decreases in cells lacking SUV39H1 after IR with 4 Gy and 10 Gy.

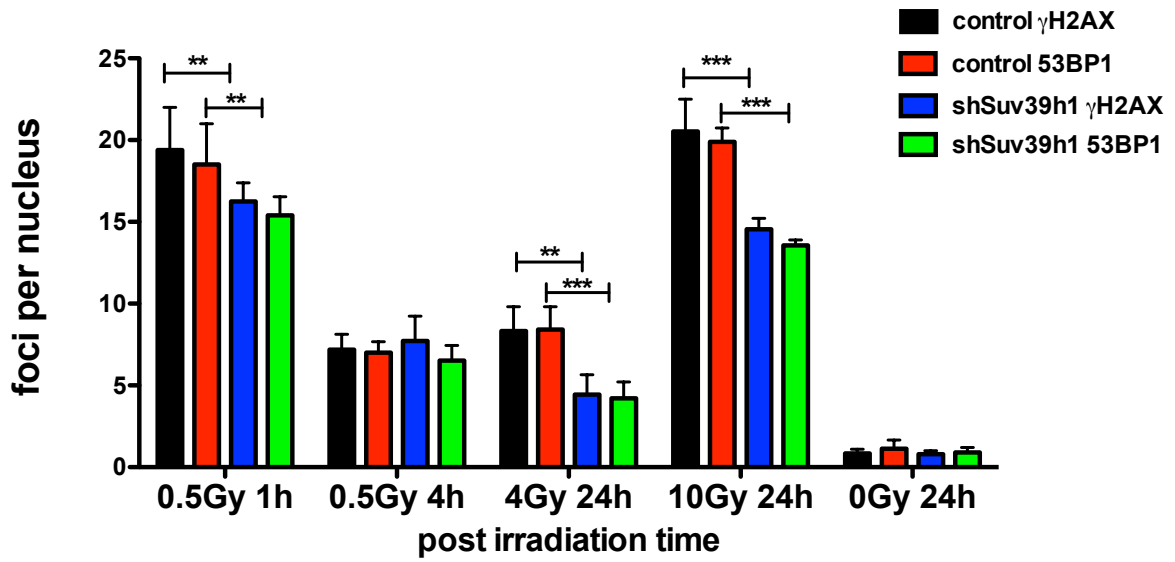

Figure 3.9: Downregulation of SUV39H1 and its effect on NHEJ in H1299. Non-transfected and shSuv39h1 transfected cells were irradiated (0, 0.5, 4, 10 Gy), allowed to recover for 1 h, 4 h and 24 h; stained with antibodies targeting γH2AX and 53BP1. Representative results from at least three independent experiments are shown. Bars represent the mean ± s.d. Statistical analysis: 2-way ANOVA analysis with Bonferroni posttest, $p < 0.01$ (**), $p < 0.001$ (***).

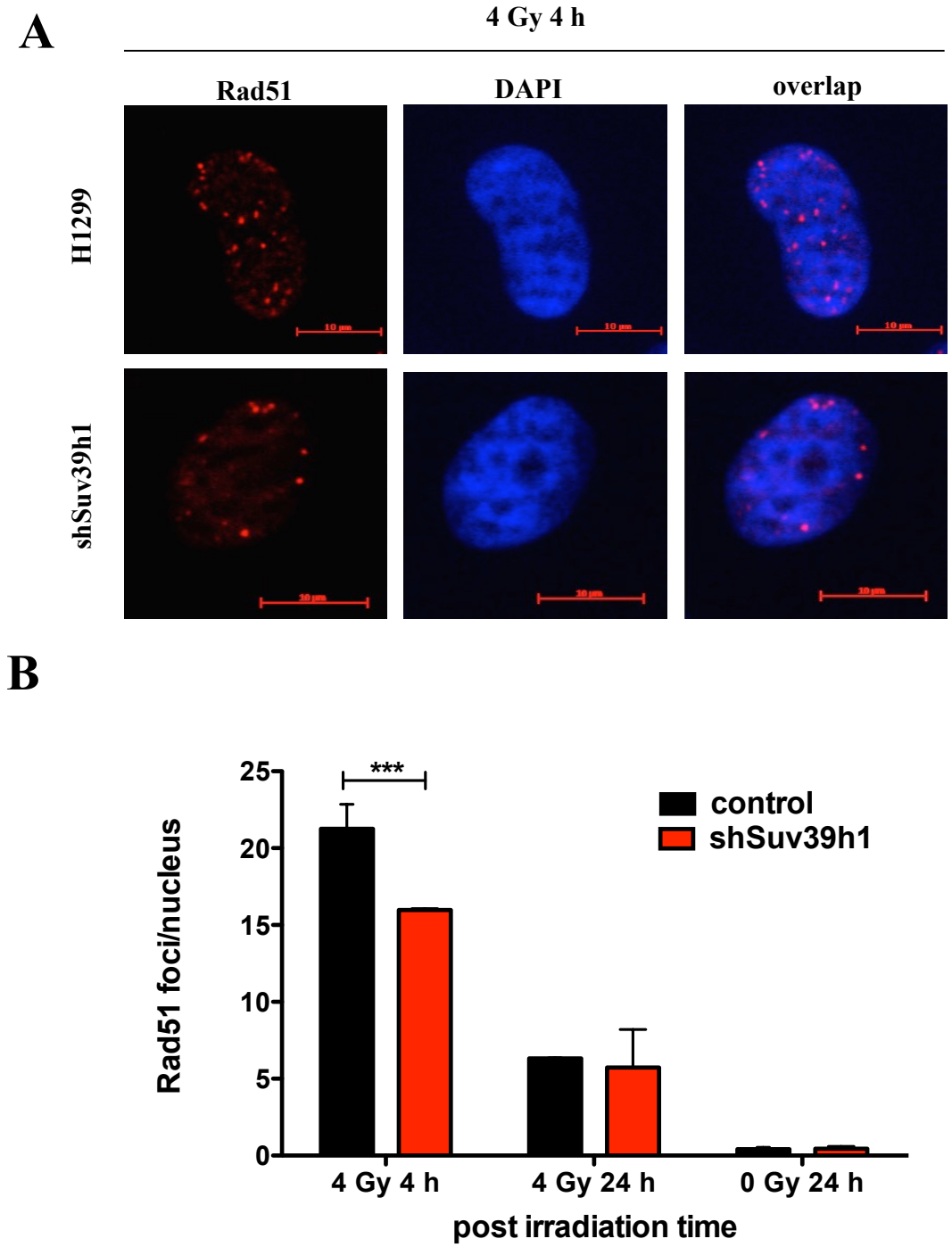

Figure 3.10: Role of HMT SUV39H1 downregulation in homologues recombination repair in H1299. Non-transfected and shSuv39h1 transfected cells were irradiated with 0 Gy and 4 Gy allowed to recover for 4 h and 24 h and stained with antibody Rad51. **A:** The immunofluorescence images from experiment (B). Staining for Rad51 (red) and DAPI (blue) is as indicated. Scale bar = 10 µm; **B:** The quantification of the DNA repair kinetics after IR by visible Rad51 foci. Representative results from at least three independent experiments are shown. Bars represent the mean ± s.d. Statistical analysis: 2way ANOVA analysis with Bonferroni posttes, $p < 0.001$ (***).

Overall, by using the shSuv39h1 approach we were able to demonstrate that downregulation of SUV39H1 affects both NHEJ and HR signalling by reduced initial foci

formation measured at 1 h after 0.5 Gy for the NHEJ and 4 h for the HR as well as residual damage for NHEJ.

3.2.2 The role of HMT SUV39H1 on DNA repair in mFb

In order to confirm the effect of HMT SUV39H1 for DNA damage signalling by NHEJ and HR in NSCLC cells, we also explored the effect of Suv39h1 for repair signalling used the Suv39h1 knockout mFbs. The damage induction and repair kinetics of DNA DSBs in mFbs (wt W8 and Suv39h1$^{-/-}$ D5) after irradiation was studied. Cells were irradiated with 0 Gy and 0.5 Gy; the repair foci were counted per nucleus at 1 h, 4 h and 24 h post irradiation. For the analysis, cells were stained for 53BP1 and for the analysis of NHEJ and HR repair.

The results showed that the number of initial number of 53BP1 foci at 1 h after irradiation with 0.5 Gy was significantly decreased in the knockout (D5) compared with the wild type (W8) cells (Figure 3.11). In comparison, the number of residual 53BP1 foci was significantly higher in cell lacking Suv39h1 compared to wt. These results indicate slower repair signalling in D5 as compared to W8. With respect to HR, no significant effect on the number of initial and residual number of Rad51 foci in D5 and W8 cells was found (Figure 3.12).

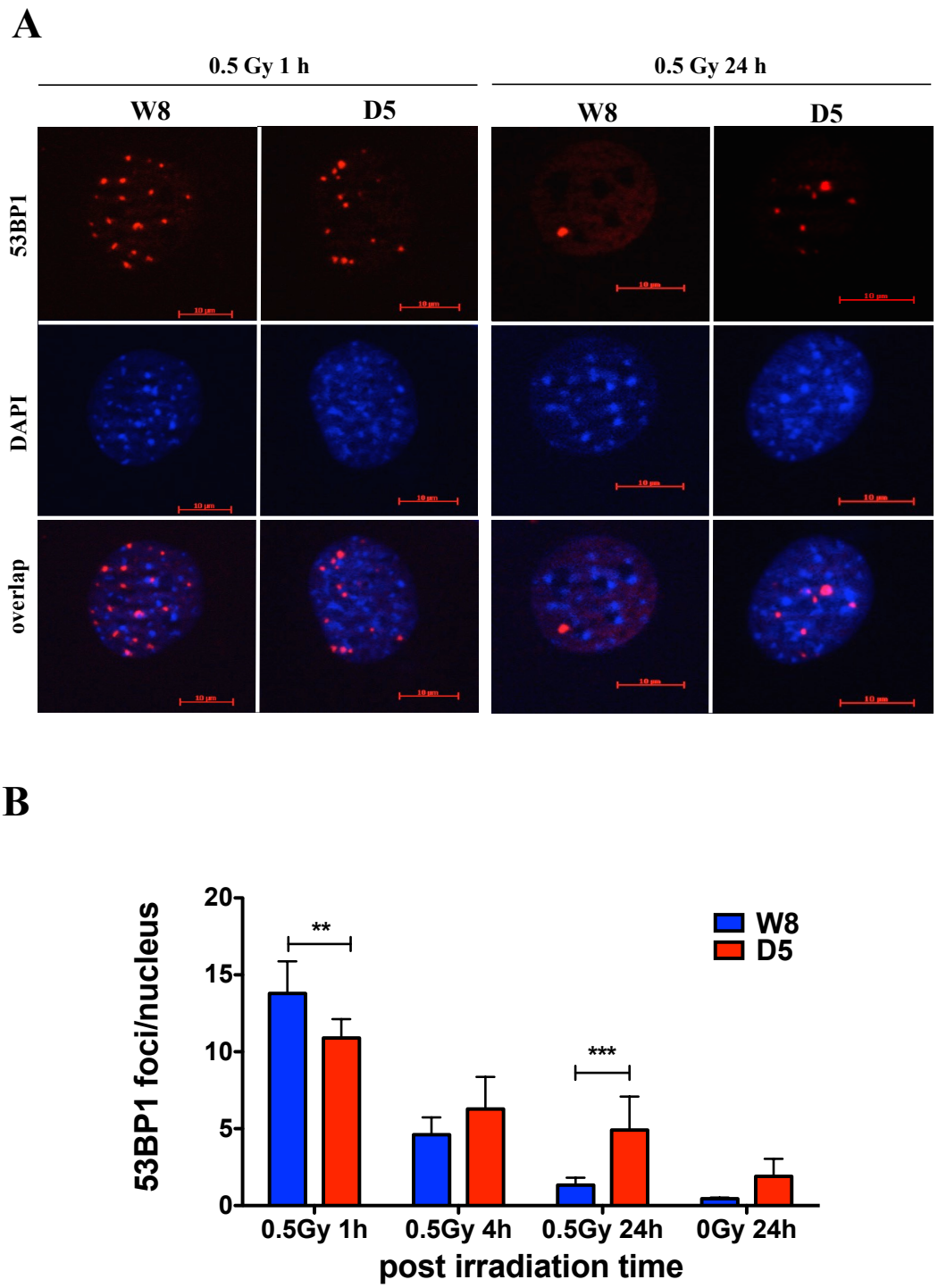

Figure 3.11: Role of HMT SUV39H1 for nonhomologous end joining. Mouse cell lines, wild type (W8) and Suv39h1 knockout (D5) cells were irradiated with 0 Gy and 0.5 Gy, allowed to recover for 1 h to measure initial damage or 4 h and 24 h for residual damage and stained with 53BP1 antibody. **A:** Examples of immunofluorescence images. Staining for 53BP1 (red) and DAPI is as indicated. Scale bar = 10 µm; **B:** Quantification of the 53BP1 foci kinetics after IR. Representative results from five independent experiments are shown. Bars represent the mean ± s.d. Statistical analysis: 2-way ANOVA analysis with Bonferroni posttest, $p < 0.01$ (**), $p < 0.001$ (***).

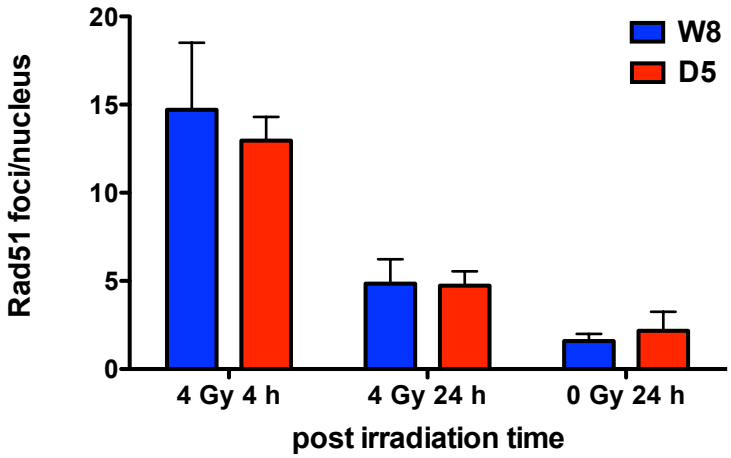

Figure 3.12: Role of HMT SUV39H1 for homologous recombination repair. mFbs W8 and D5 were irradiated with 4 Gy, allowed to recover for 4 h (initial damage) and 24 h (residual damage) and stained with Rad51 antibody. Representative results from five independent experiments are shown. Bars represent the mean ± s.d.

In summary, lack of HMT SUV39H1 influenced NHEJ repair mechanisms in NSCLC as well as in mFbs by decreasing the number of initial foci and has an opposite effect on the number of residual foci in H1299 cells and in mFbs. It also affects HR in NSCLC, but not in mFbs. These data confirm our previous results that the number of initial 53BP1 foci is significantly decreased in NSCLC cells with reduced expression of SUV39H1.

3.2.3 The role of HMT SUV39H1 on DNA DSB induction and rejoining

As was described above, we initially used the number of radiation induced γH2AX foci as a measure for DSB. γH2AX foci are commonly used as markers for DSBs and it has been reported that the number of γH2AX foci correlates with the number of DSBs present, and that it increases linearly with radiation dose (Rothkamm and Löbrich, 2003). However, the kinetics of γH2AX foci formation that visualized DSB related signalling and those of the removal of physical breaks measured by pulsed-field gel electrophoresis (PFGE) are widely different (Kinner *et al*., 2008). PFGE is a reliable method for determination of the induction of DSBs and their physical rejoining. However, due to its insensitivity experiments have to be done after irradiation with relatively high radiation doses. Nevertheless, a γH2AX foci scoring was thought to represent an acceptable surrogate for physical DSB determination (Kinner *et al*., 2008; Löbrich *et al*., 2005)

Thus, in order to analyse the direct induction and rejoining of DNA DSBs after IR, the PFGE technique was used. In this technique, the number of DSBs present in the cells is

measured by the fraction of DNA released (FDR). To obtain an adequate dose response effect, the fraction of DNA released (FDR) was plotted against the applied radiation doses up to 30 Gy. The dose response curves were used to estimate the dose equivalent (Deq) values from each FDR value.

The mFbs W8 and D5, with wild type and Suv39h1$^{-/-}$ genotypes, were initially used to determine DNA DSB dose response curves. The results from PFGE analysis after lysing cells at high temperature (50°C) lysis demonstrate that DNA dose response damage is increased in Suv39h1$^{-/-}$ cells compared to that of the wt cells (Figure 3.13).

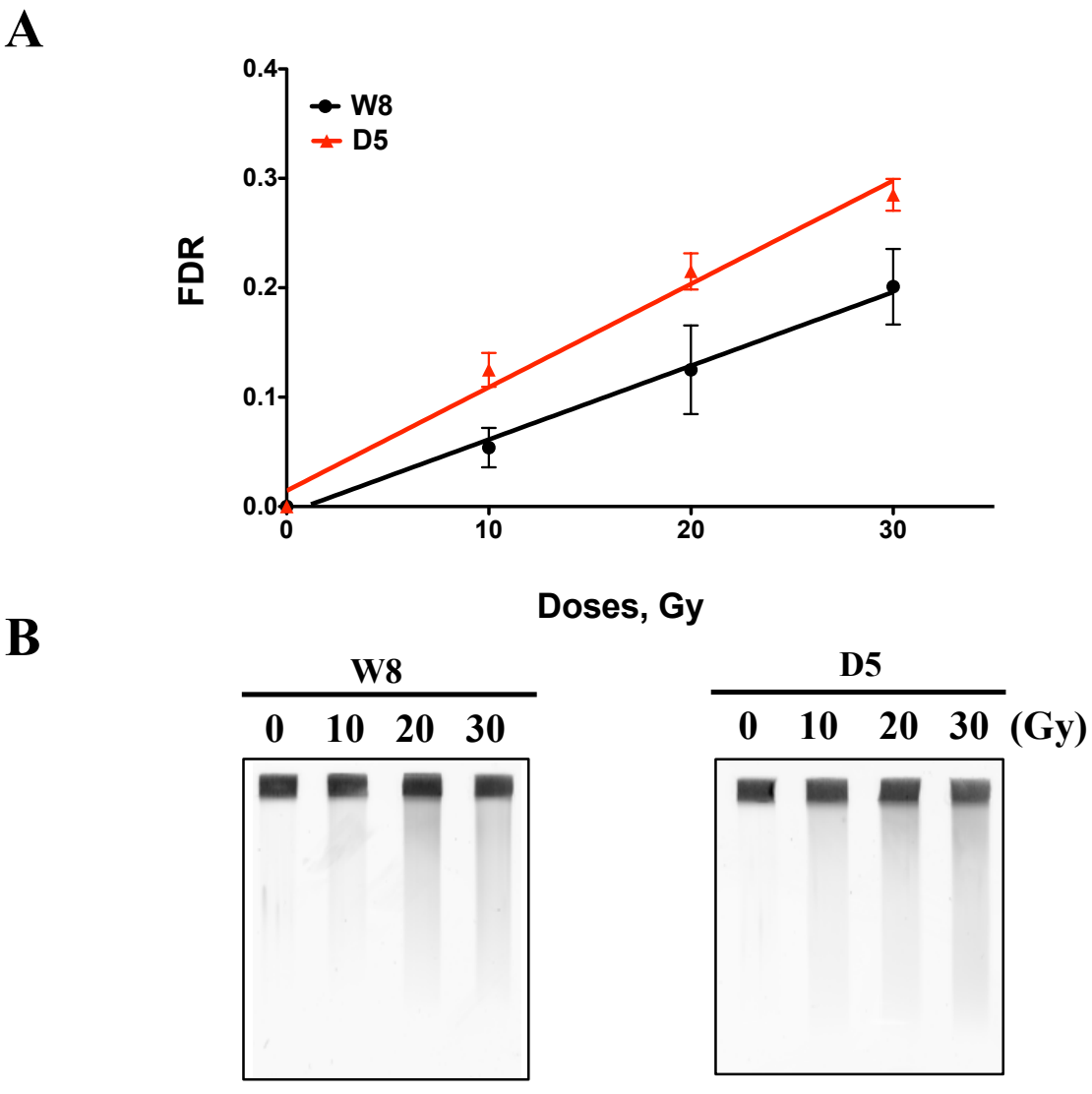

Figure 3.13: Role of HMT SUV39H1 DSB yield in mFbs as measured by PFGE. A: The respective dose response curves. The lines show linear regressions through the measured points of each data set; **B:** Representative gels from three independent experiments with identical results are shown. Bars represent the mean ± SEM from 3 determinations of independent 4 experiments.

The results from PFGE demonstrate that Suv39h1$^{-/-}$ cells (D5) repaired damages slightly slower with increased residual damage than the respective wt (W8) cells (Figure 3.14). Although these results from PFGE did not reach statistical significance, they share similarity with results from immunofluorescence foci assay, indicating slight repair deficiency in D5 cells.

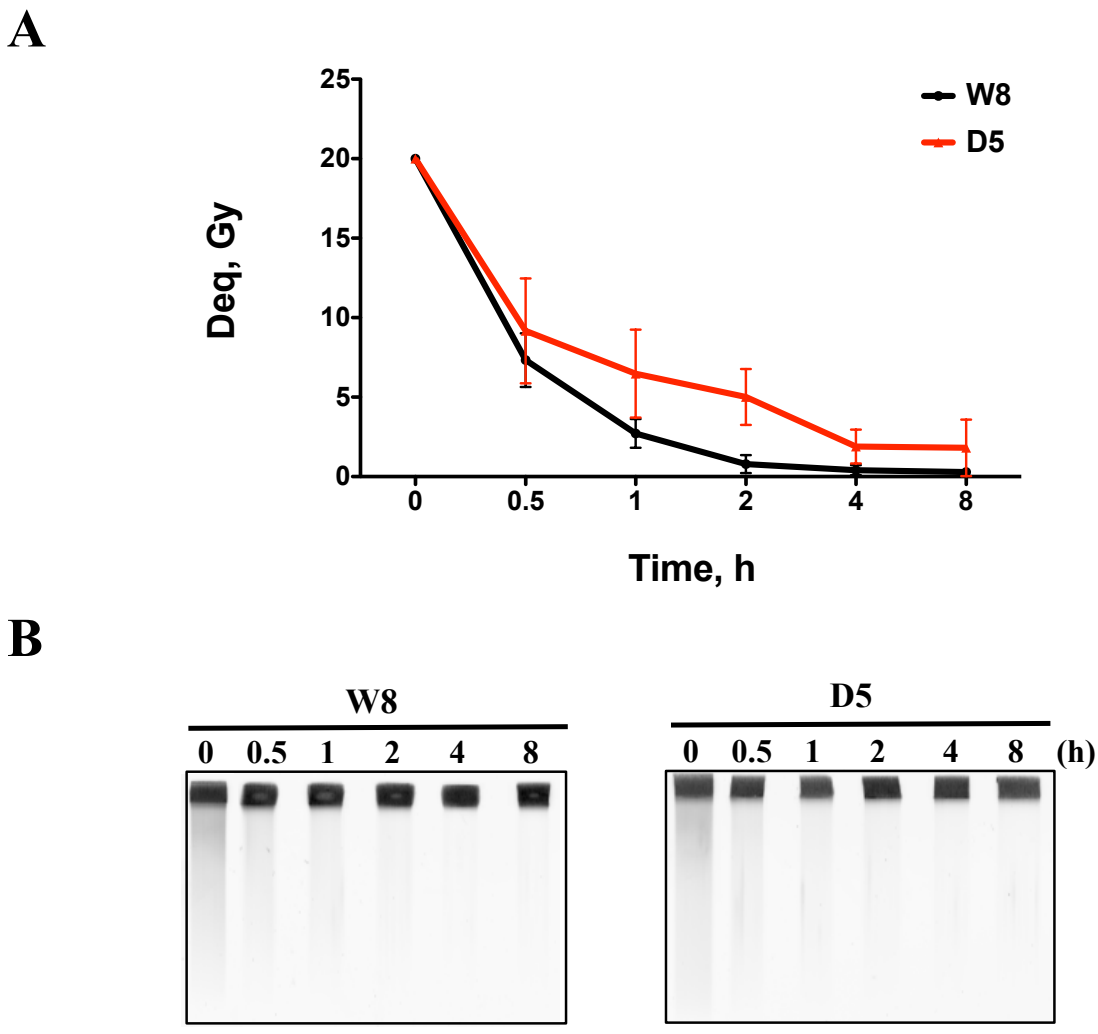

Figure 3.14: DNA repair kinetics in HMT SUV39H1 deficient mFbs as measured by PFGE. A: Results show the DNA repair kinetics after IR at 20 Gy with or without Chaetocin treatment; **B:** the representative gels from three independent experiments with identical results are shown. Bars represent the mean ± SEM from 3 determinations in 3 experiments.

The next step was to investigate the role of HMT SUV39H1 in the direct DSB dose response damage and DSB rejoining kinetics in knockdown NSCLC cells lines. The results demonstrate that there is no difference in the DSB dose response damage between the radiosensitive H460 and radioresistant H1299 cell lines. In addition, knockdown of

shSuv39h1 by shRNA also have no effect on the initial number of DSB induced after IR (Figure 3.15A). However, slower DNA repair kinetics in H460 compared with that of H1299 (Figure 3.15B) is evident. Moreover, DNA repair kinetics was slightly steeper in both Suv39h1 knockdown cells compared to the wild type H460 and H1299 cells. However, the difference does not reach statistical significance in our experiments.

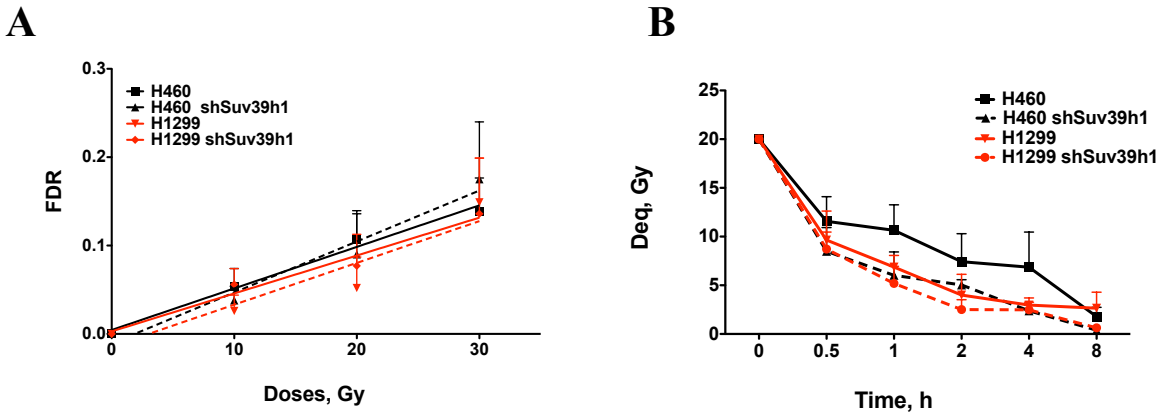

Figure 3.15: The yield of DSBs and DNA repair kinetics in shSuv39h1-treated NSCLC cells. A: The respective dose response relation for DSBs in the respective cell lines. The lines shown are linear regressions through the measured points of each data set; **B:** DNA repair kinetics as measured by PFGE. The respective (H460 and H1299) cell lines with and without shSuv39h1. Bars represent the mean ± SEM from 3 determinations of at least in 3 independent experiments.

Overall, the results suggest that HMT SUV39H1 affects DNA repair kinetics more efficiently in knockout mFbs compared to that of knockdown NSCLC cell lines.

3.3 Modulation of chromatin structure by small molecules targeting HMTs and its effect on the radiation response

The results with the HMT SUV39H1 show that radiation response of cells might be modulated by decreasing the activity of this enzyme. Thus, we were further interested in how modulation of HMT SUV39H1 with small molecules (Chaetocin and Triptolide) and thus of the chromatin structure regulates proliferation, activation of cell cycle checkpoints after IR, DNA repair mechanisms (NHEJ and HR) and cell survival.

3.3.1 Effect of modulators of chromatin structure on cell proliferation

Initially, we examined the effect of the modulators on proliferation of the NSCLC cell lines H460 and H1299 (Figure 3.16A). The data show that growth rate of the H460 cell line is

higher compared to that of the H1299 cell line, with an increase of the initial number of cells by a factor of 16 and 36, respectively. Next, the respective half maximal inhibitory concentration (IC50) was determined for each modulator. Cells were treated with different concentrations of the HMT inhibitors for 96 h. The IC50 values were calculated by the R environment software. The respective IC50 values for cell proliferation were 1.5 nM and 2.9 nM for Triptolide in H460 and H1299, respectively (Figure 3.16B). The respective values for Chaetocin were 37 nM and 29 nM (Figure 3.16C). Overall, the present results show that all modifiers of chromatin used in the present study inhibit proliferation of the NSCLC cell lines.

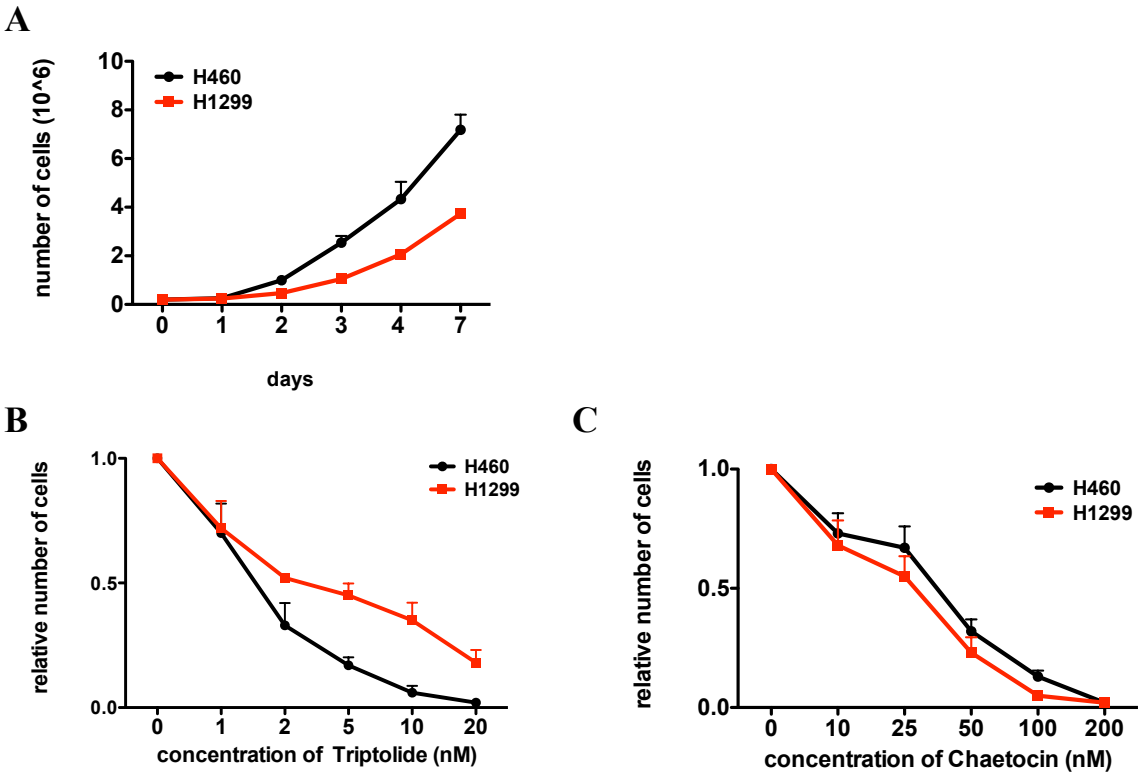

Figure 3.16: Effect of chromatin modulation on the proliferation of NSCLC cell lines. H460 and H1299 cells were treated for 96 h inhibitors Chaetocin and Triptolide. The relative number of cells at the end of the treatment with respect to the untreated cells was calculated. **A:** Comparison of the proliferation of H460 and H1299 without treatment. B and C: Effect of chromatin modulators on proliferation for Triptolide **(B)**, Chaetocin **(C)** treatment. Representative results from at least three independent experiments are shown. Bars represent the mean ± SEM.

3.3.2 Effect of Chaetocin on cell cycle progression and apoptosis

To analyse the effect of Chaetocin, which inhibits the activity of the HMTs SUV39H1 and G9a on cell cycle progression, H460 and H1299 cells were treated with different concentrations of Chaetocin, fixed at 72 h and stained with DAPI for cell cycle analysis. Treatment of cells with 75 nM Chaetocin for 72 h significantly decreased the fraction of cells in G1 phase from 63.8 ± 1.3% to 53.5 ± 2.6% ($p < 0.001$) in H460 cells and significantly

increased the fraction of cells in G2 from 7.42 ± 1.3% to 17.0 ± 1.4% ($p < 0.001$) (Figure 3.17A). In H1299 cells, 75 nM had no effect, but higher concentration of Chaetocin (150 nM) significantly decreased the fraction of cells in G1 phase from 59.1 ± 11.4% to 40.63 ± 14.2% ($p < 0.05$) and increased the fraction of cells in G2 from 10.6 ± 3.3% to 31.8 ± 13.7% ($p < 0.05$) (Figure 3.17B).

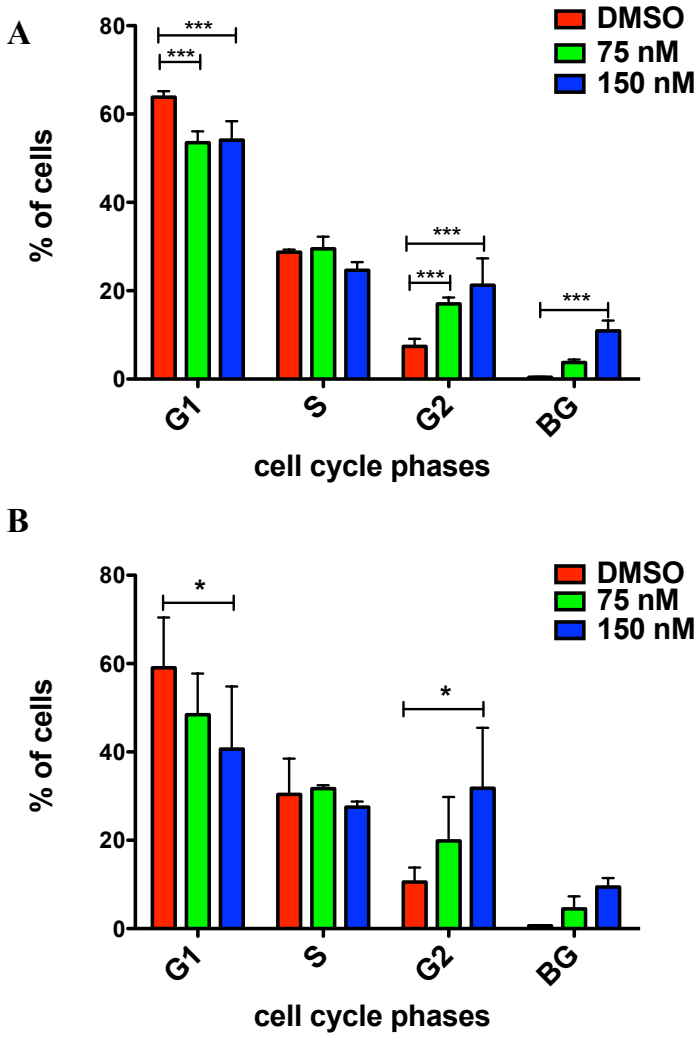

Figure 3.17: Influence of Chaetocin on cell cycle progression. H460 and H1299 cells were treated with different concentrations of Chaetocin for 72 h. Flow cytometry data showing cell cycle distribution of H460 **(A)** and H1299 cells **(B)**. Representative results of three independent experiments are shown. "BG" is a background signal from apoptotic and degraded cells. Bars represent means ± s.d. Statistical analysis: 2-way ANOVA analysis with Bonferroni posttest, $p < 0.05$ (*), $p < 0.001$ (***).

In conclusion, the results show that Chaetocin reduces the fraction of cells in the G1-phase and accumulates cells in G2-phase of the cell cycle in a concentration-dependent manner in both cell lines.

To study the effect of Chaetocin on apoptotic cell death, we treated the cells with increasing concentrations of Chaetocin and irradiated them with 10 Gy at 4 h after beginning

of Chaetocin treatment. Cells were fixed at 48 h thereafter. The fraction of detached cells was used as a measure for apoptosis, which was previously shown to be an appropriate measure for apoptosis in NSCLC cell lines (Stuschke *et al*., 2002). Chaetocin increases apoptosis in a concentration-dependent manner in both cell lines (Figure 3.18). We also observed that IR slightly increased the percentage of apoptotic cells in combination with Chaetocin in H1299, but not in H460.

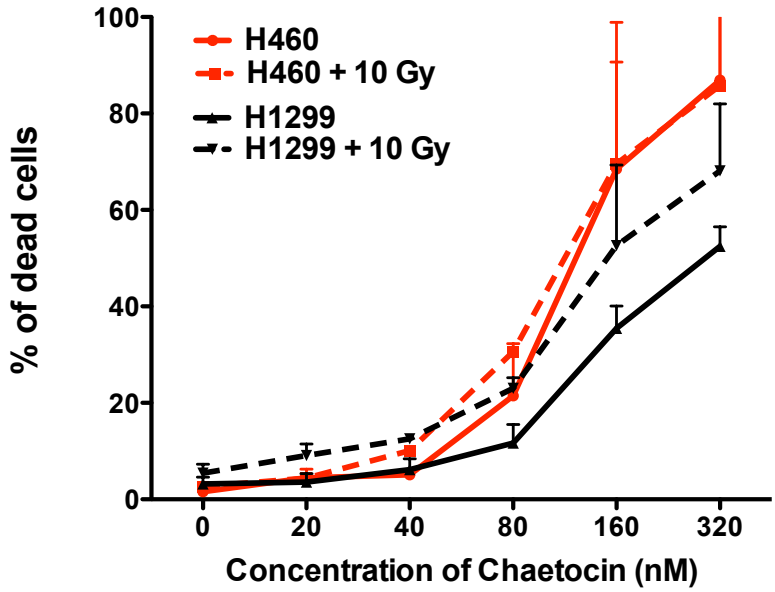

Figure 3.18: Effect of Chaetocin on radiation-induced apoptosis in NSCLC cell lines. Cells were treated with different concentrations of Chaetocin for 4 h, irradiated with 10 Gy after 24 h Chaetocin treatment and continued the treatment for further 48 h. The fraction of detached cells as a measure for apoptotic, cells were collected and counted. Representative results from two independent experiments are shown. Bars represent the mean ± s.d.

3.3.3 Effect of HMT inhibitors on DNA DSB repair in tumour cell lines

Based on the hypothesis that abnormal histone methylation and chromatin remodelling may lead to deficient DNA repair signalling, we previously showed that genetic modulation of the HMT SUV39h1 impairs repair signalling in Suv39h1 knockdown NSCLC as well as in knockout Suv39h1 mFb cells. Here, we extended these studies and evaluated the effect of small molecule HMT inhibitors on DNA repair pathways (NHEJ and HR). For this purpose, the NSCLC cell lines H460 and H1299 were treated with Chaetocin and Triptolide for 4 h, irradiated thereafter with 0.5 Gy and 4 Gy for NHEJ and HR pathways, respectively and fixed at 1 h, 4 h and 24 h after IR.

In order to examine the effect of Chaetocin and Triptolide on NHEJ repair pathway cell lines were stained with 53BP1. The results show that Triptolide has no significant effect on DNA repair signalling in both cell lines (Figure 3.19). However, the number of residual 53BP1 foci at 4 h post irradiation time is significantly higher ($p < 0.01$) in H1299 cell line as compared to untreated cells (Figure 3.19B).

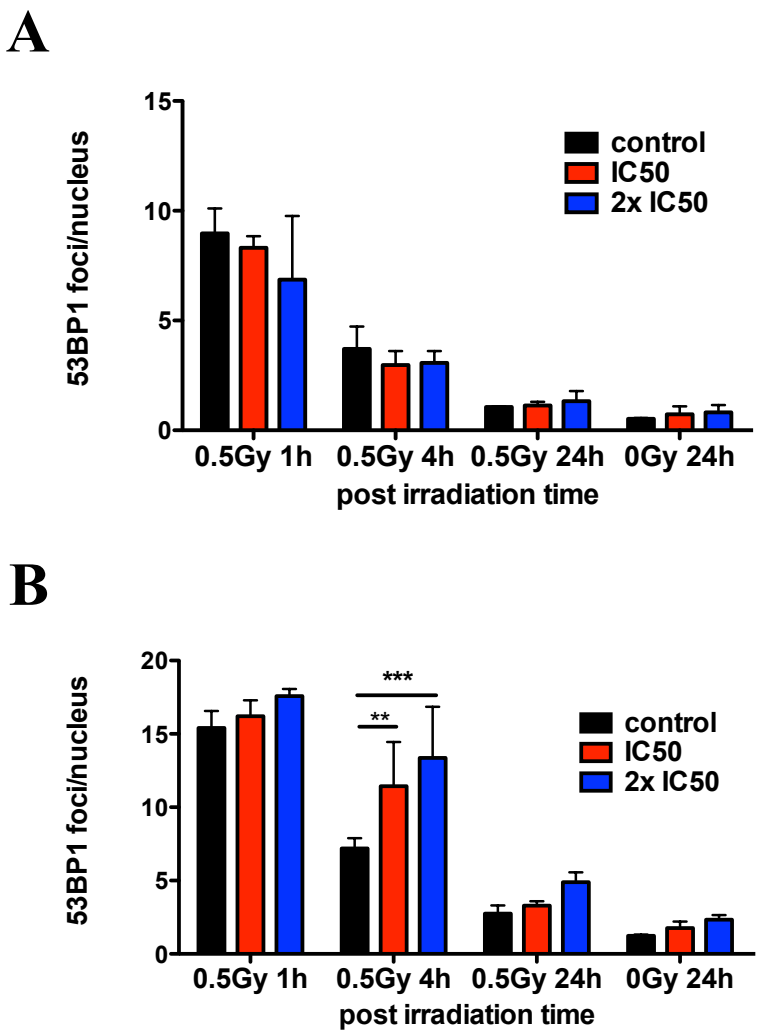

Figure 3.19: Effect of Triptolide on NHEJ repair in NSCLC cell lines after IR. The cells were treated for 4 h with and without Triptolide in combination with IR and stained with 53BP1 antibody. Graphs show the DNA repair kinetics after IR at 0.5 Gy in H460 **(A)** and in H1299 **(B)** cell line. Representative results from three independent experiments are shown. Bars represent the mean ± s.d. Statistical analysis: 2-way ANOVA analysis with Bonferroni posttest, $p < 0.01$ (**), $p < 0.001$ (***).

Short time incubation with Chaetocin for 4 h before irradiation increased the initial as well as residual number of 53BP1 foci in H1299 (Figure 3.20B), but only residual number of foci in H460 (Figure 3.20A). Moreover, Chaetocin delays the foci kinetics in H1299 at 4 h after combined treatment with IR and Chaetocin at the respective IC50 (29 nM). Interestingly, if H1299 cells were treated with higher concentration of Chaetocin (300 nM), corresponding to

about 10x IC50, the initial 53BP1 foci were completely diminished as compared to the untreated cells.

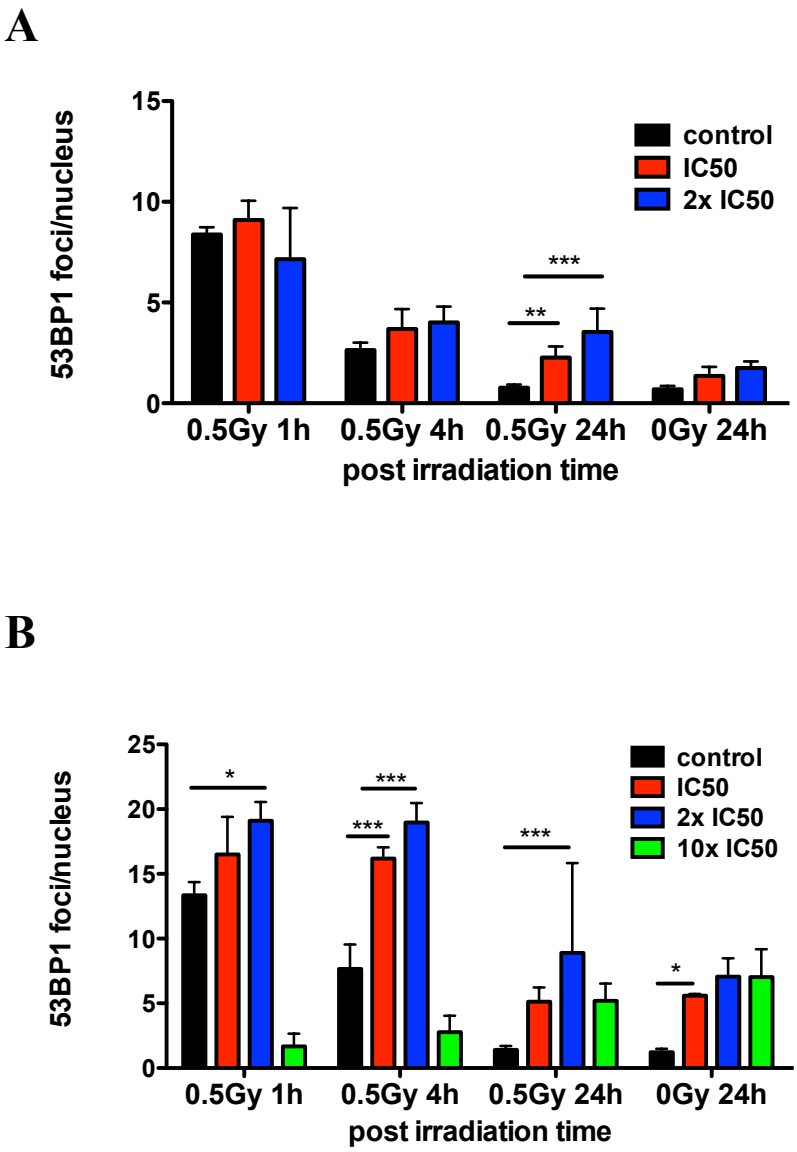

Figure 3.20: Effect of Chaetocin on NHEJ repair in NSCLC cell lines after IR. H460 and H1299 cells were treated with and without Chaetocin (with the respective IC50 (29 nM) for H1299 and H460 (37 nM)) for 4 h and then irradiated with 0 Gy and 0.5 Gy. The cells were stained with 53BP1 antibody and the number of foci was determined in H460 **(A)** and H1299 **(B)**. Results from three independent experiments are shown. Bars represent the mean ± s.d. Statistical analysis: 2-way ANOVA analysis with Bonferroni posttest, $p < 0.05$ (*), $p < 0.01$ (**), $p < 0.001$ (***).

To examine the effect of Chaetocin and Triptolide on homologous recombination repair in NSCLC cell lines, H460 and H1299 cells were pre-treated with the respective drugs for 4 h and then irradiated with 4 Gy. The number of Rad51 foci was determined at 4 h and 24 h after IR, as a measure for initial and residual damage. The results show that Triptolide had no effect on HR in H460 (Figure 3.21A) but it strongly decreased the number of initial and increased the number of residual Rad51 foci in H1299 in a concentration-dependent manner

(Figure 3.21B). In comparison, Chaetocin decreases the initial number of Rad51 foci and increased the residual number of Rad51 foci in both cell lines (Figure 3.22).

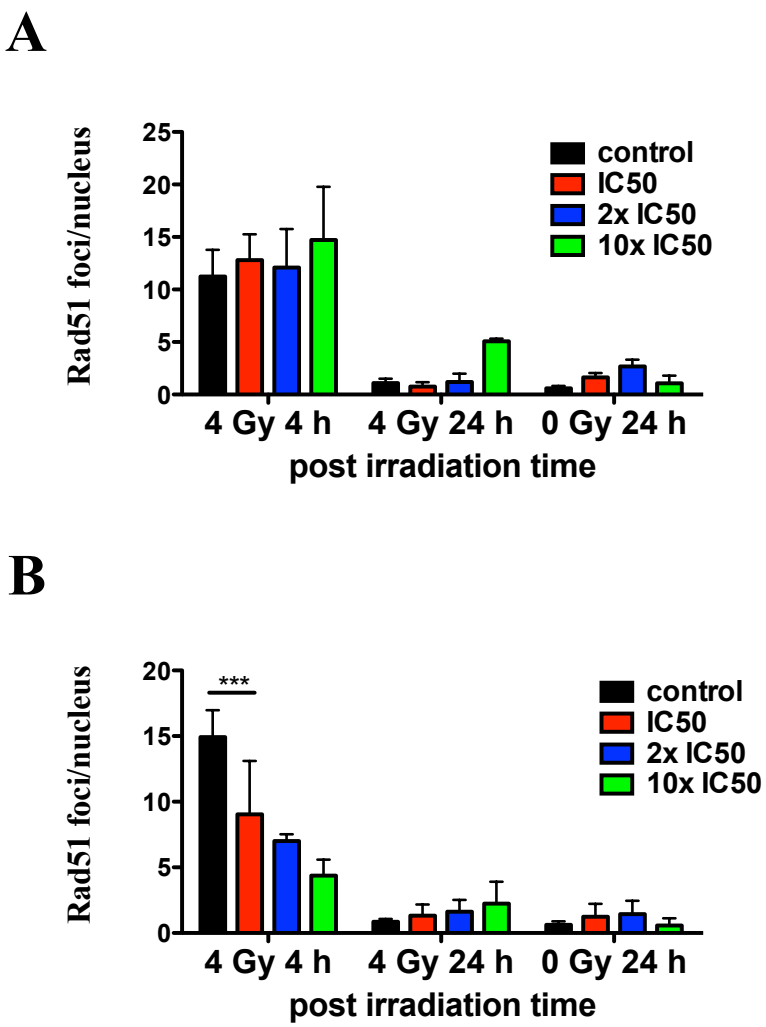

Figure 3.21: Effect of Triptolide on HR repair in NSCLC cell lines after IR. The cells were treated for 4 h with and without Chaetocin in combination with IR and stained with Rad51 antibody, a hallmark of HR repair pathway. Graphs show the DNA repair kinetics after IR at 0.5 Gy in H460 **(A)** and in H1299 **(B)** cell line. Representative results from three independent experiments are shown. Bars represent the mean ± s.d. Statistical analysis: 2-way ANOVA analysis with Borferroni posttest, $p < 0.001$ (***).

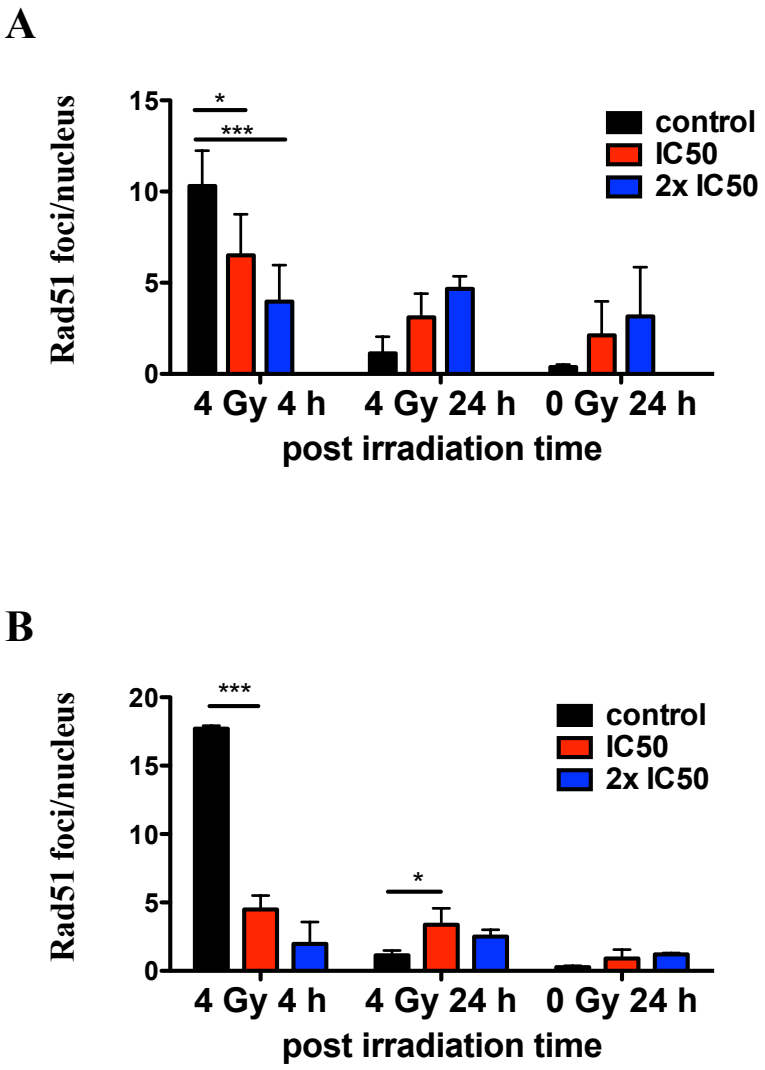

Figure 3.22: Effect of Chaetocin on HR repair in NSCLC cell lines after IR. Cells were treated with and without Chaetocin at the respective IC50 (29 nM) for H1299 and H460 (37 nM) for 4 h and then irradiated with 0 Gy and 4 Gy. Cells were stained with Rad51 antibody and the number of Rad51 foci determined at 4 h and 24 h after IR in H460 **(A)** and H1299 **(B)**. Representative results from three independent experiments are shown. Bars represent the mean ± s.d. Statistical analysis: 2-way ANOVA analysis with Bonferroni posttest, $p < 0.05$ (*), $p < 0.001$ (***).

In the next step, pre-treatment with Chaetocin was extended from 4 h to 24 h before cells were irradiated and its effect on repair signalling was determined by using the 53BP1 foci assay. Cells were pre-treated for 24 h with Chaetocin at 2x IC50 (60 nM), irradiated with 0.5 Gy, fixed at 1 h, 4 h and 24 h thereafter and stained with γH2AX antibody. As expected, Chaetocin significantly increases the number of initial as well as of residual γH2AX foci compared with untreated control group (Figure 3.23).

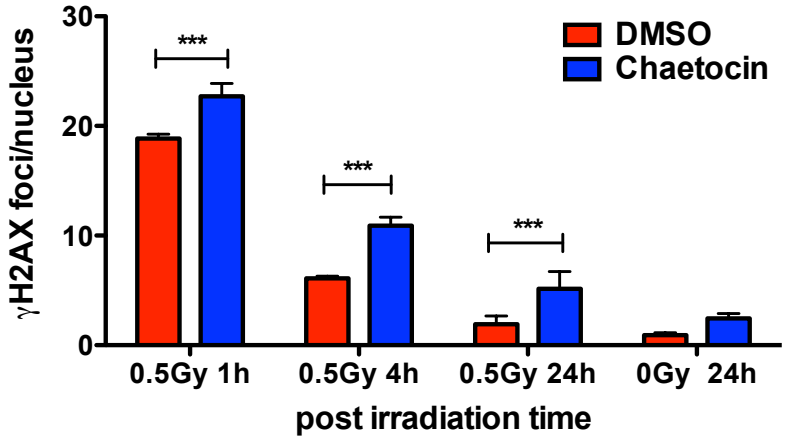

Figure 3.23: Effect of Chaetocin on NHEJ repair after extended pre-treatment. H1299 cells were pre-treated with Chaetocin (60 nM) for 24 h, irradiated with 0.5 Gy, allowed to recover for 1 h, 4 h and 24 h and stained with γH2AX. Representative results from three independent experiments are shown. Bars represent the mean ± s.d. Statistical analysis: 2-way ANOVA analysis with Bonferroni posttest, $p < 0.001$ (***).

To analyse the effect of Chaetocin on HR repair after extended pre-treatment, cells were treated with Chaetocin (30 nM and 60 nM) for 24 h, irradiated with 4 Gy, fixed at 4 h and 24 h after IR and stained with Rad51 as well as with cyclin B1, which identifies cells in the G2-phase. Positive cells for cyclin B1 were scored for the number of Rad51 foci. In comparison with the previous results of shorter pre-treatment of only 4 h, these results from extended treatment show significant increase in the number of initial and residual Rad51 foci (Figure 3.24).

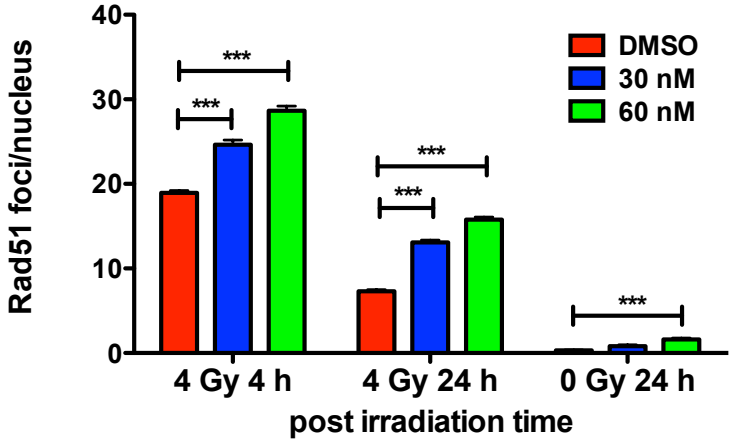

Figure 3.24: Effect of Chaetocin on HR repair after extended pre-treatment. H1299 cells were pre-treated with Chaetocin (30 nM and 60 nM) for 24 h, irradiated with 0.5 Gy, allowed to recover for 1 h, 4 h and 24 h and; stained with Rad51 and Cyclin B1. Rad51 foci were scored only in Cyclin B1 positive cells. Representative results from three independent experiments are shown. Bars represent the mean ± s.d. Statistical analysis: 2-way ANOVA analysis with Bonferroni posttest, $p < 0.001$ (***).

Additionally, Chaetocin and Triptolide were reported as potential inhibitors of H3K9me3. Unexpectedly, that we could not detect any effect of Chaetocin on H3K9me3 in both cell lines at low concentrations (< 300 nM) of Chaetocin (Figure 3.25).

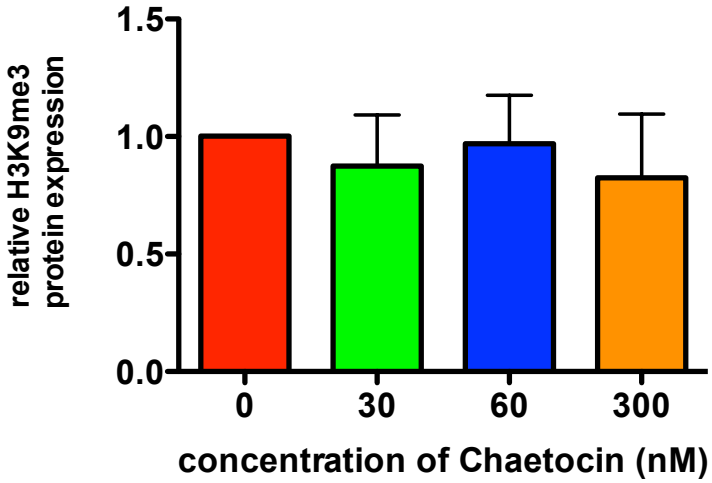

Figure 3.25: Chaetocin does not affect H3K9me3 protein expression in H1299 cell line. Graph shows the relative H3K9me3 histone expression in H1299 after Chaetocin treatment. Representative results from at least three independent experiments are shown. Bars represent mean ± s.d.

Taking together, although Chaetocin regulated NHEJ and HR repair pathway, we did not detect significant reduction of H3K9me3 on protein expression level.

3.3.4 Effect of Chaetocin on cell survival

In order to investigate the effect of Chaetocin on clonogenic survival of H460 and H1299, cells were treated with Chaetocin with the respective concentrations of 1x IC50 (29 nM for H1299 and 37 nM for H460), 2x IC50 and 10x IC50 for 24 h, irradiated thereafter with 0, 2, 4, 6 Gy and incubated for further 24 h. Single cell suspensions were plated out for colony formation at 24 h after irradiation, after cells completed repair processes and incubated for further 10 days for colony formation.

Chaetocin treatment at concentrations of about 1x IC50 and 2x IC50 had no effect on the surviving fraction after irradiation up to 6 Gy. Only at higher concentration surviving fraction was significantly ($p < 0.05$) reduced after irradiation with 2 Gy and 6 Gy (Figure 3.26B). In comparison, no effect of Chaetocin at all was evident in H460.

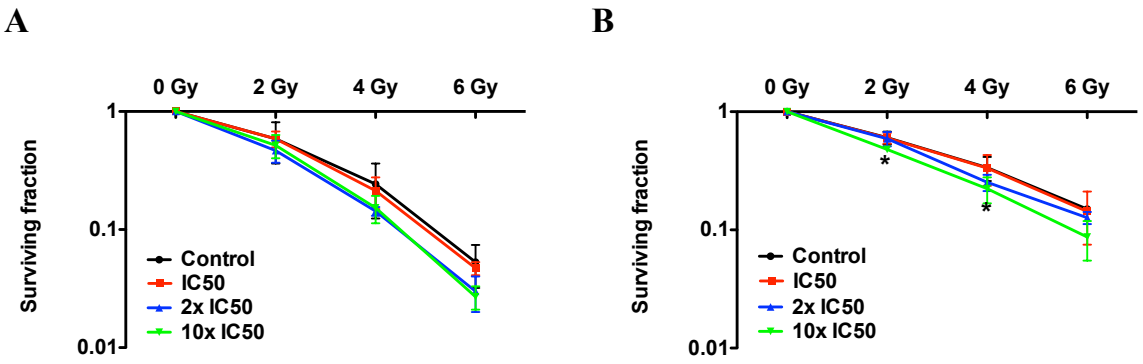

Figure 3.26: Effect of Chaetocin on the radiation sensitivity of NSCLC cell lines. Cells were treated with different concentration of Chaetocin with 1x IC50 (37 nM for H460 and 29 nM for H1299), 2x IC50 and 10x IC50, irradiated with 0, 2, 4, 6, 8 Gy and incubated for 10 days. **A:** Cell survival curves of H460; **B:** Survival curves of H1299. Representative results from three independent experiments are shown. Bars represent the mean ± s.d. Statistical analysis: 2-way ANOVA analysis with Bonferroni posttest, $p < 0.05$ (*).

Overall, surviving fraction after irradiation was significantly reduced only at high concentration of Chaetocin (290 nM) in H1299.

3.3.5 Combined effect of Chaetocin and fractionated irradiation on cell survival

As was described above, there was no significant effect of Chaetocin at low concentrations on the surviving fraction after combined single radiation schedules. As shown in paragraph 3.3.3, Chaetocin increased residual number of γH2AX at 24 h after irradiation. Thus, we hypothesized that the fraction of these sublethal damages may increase during protracted radiation exposure. In order to evaluate the impact the residual DSBs on cell survival, fractionated radiation with daily fractions of 2 Gy was used.

For this purpose, H1299 cells were pre-treated with low doses of Chaetocin (0, 7.5, 15, 30 nM) for 4 h and irradiated thereafter with daily 2 Gy fractions up to a total dose of 6 Gy. The highest concentration of 30 nM Chaetocin used in this set of experiments correspond to 1x IC50 values in H1299. The initial number of γH2AX foci at 1h after irradiation with 2 Gy as well as residual number at 4 h and 24 h after irradiation were determined. In addition, the number of γH2AX after 3x 2 Gy was determined at 24 h after the last fraction. As shown in Figure 3.27 the initial as well as residual number of γH2AX at 1 h and 4 h after IR significantly increased with increasing concentrations of Chaetocin. An increase of the residual number of foci with increasing Chaetocin concentrations at 24 h after single irradiation with 2 Gy was evident, but not significant. However, fractionated irradiation

significantly increased the residual number of γH2AX foci with increasing Chaetocin concentrations.

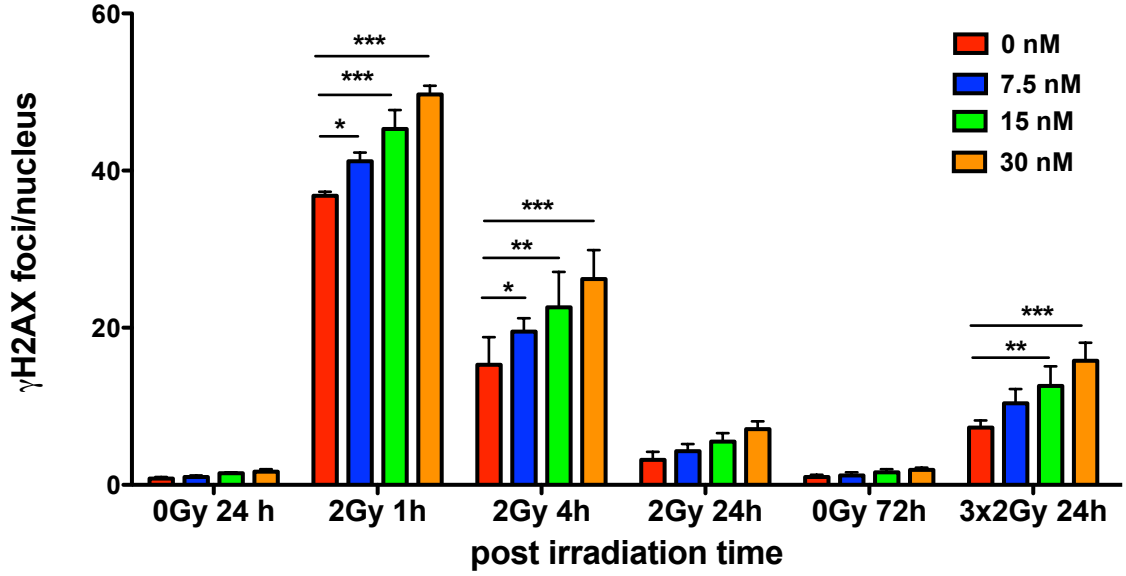

Figure 3.27: Effect of Chaetocin on radiation induced γH2AX after fractionated irradiation. H1299 cells were treated with different concentrations of Chaetocin (0, 7.5, 15, 30 nM) for 4 h and irradiated 3 times with 2 Gy every 24 h. Cells were fixed and stained with γH2AX at 24 h after the last radiation fraction. For initial foci detection, cells were fixed after first irradiation treatment at 1 h, 4 h and 24 h. Results from three independent experiments are shown. Bars represent the mean ± s.d. Statistical analysis: 2-way ANOVA analysis with Bonferroni posttest, $p < 0.05$ (*), $p < 0.01$(**), $p < 0.001$(***).

In order to evaluate the effect of fractionated irradiation, i.e. the accumulation of residual damage on the surviving fraction cells were plated for colony formation at 24 h after the last fraction and continued incubation for further 10 days without Chaetocin. As shown in Figure 3.28, Chaetocin gradually reduced the surviving fraction after fractionated irradiation. However, the effect was significant ($p < 0.05$) only at the highest concentration of 30 nM, corresponding to the respective 1x IC50 value in H1299 cells. We could not detect significant reduction of cell survival at lower doses of Chaetocin by clonogenical assay.

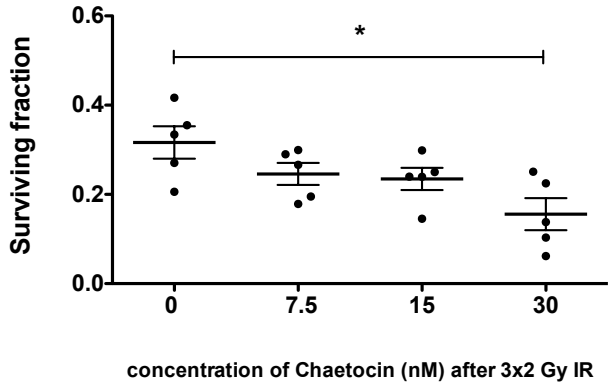

Figure 3.28: Effect of Chaetocin on cell survival by fractionated irradiation. H1299 cells were treated with different concentrations of Chaetocin (0, 7.5, 15, 30 nM) for 4 h and irradiated 3 times with 2 Gy every 24 h. At 24 h after last radiation treatment the cells were seeded for colony formation without Chaetocin and incubated for further 10 days. Results from five independent experiments are shown. Bars represent the mean ± SEM. Statistical analysis: Paired t-test ($p < 0.05$).

In conclusion, Chaetocin gradually increased the fraction of residual number of γH2AX foci and decreased surviving fraction after fractionated irradiation schedules.

3.3.6 Effect of Chaetocin on tumour control

As a long term survival control assay the plaque-monolayer assay was performed. It is a sensitive and quantitative procedure for evaluating cell proliferation for extended periods of time (Sak *et al.*, 2012).

The H460 and H1299 cells with a cell number of 1500 cells were seeded into 24 well tissue plates and treated 24 h later with Chaetocin concentrations of 0, 10, 15 nM for H1299 and 0, 7.5, 10, 15, 20 nM for H1460. At about 4 h after treatment, cells were irradiated with single doses of 0, 2, 4, 8, 12, 15, 16, 17, 19, 20, 21, 23, 25 Gy. In a parallel assay, cells were irradiated with fractionated doses with 2 Gy per fraction every 6 h. After the last fraction Chaetocin was washed out and the cells were incubated for 6 weeks at all. The overall time for Chaetocin treatment was the same for the single schedule and fractionated irradiation group.

After single irradiation, Chaetocin significantly reduced the dose to control growth of 50% of the H1299 plague-monolayer (TCD50) from 19.5 Gy to 9.9 Gy and 3.2 Gy for 0 nM, 10 nM and 15 nM, respectively (Figure 3.29A). In comparison, fractionated irradiation reduced TCD50 from 25.0 Gy in the untreated cells to 14.7 Gy and 9.8 Gy after 10 nM and 15 nM Chaetocin, respectively (Figure 3.29B).

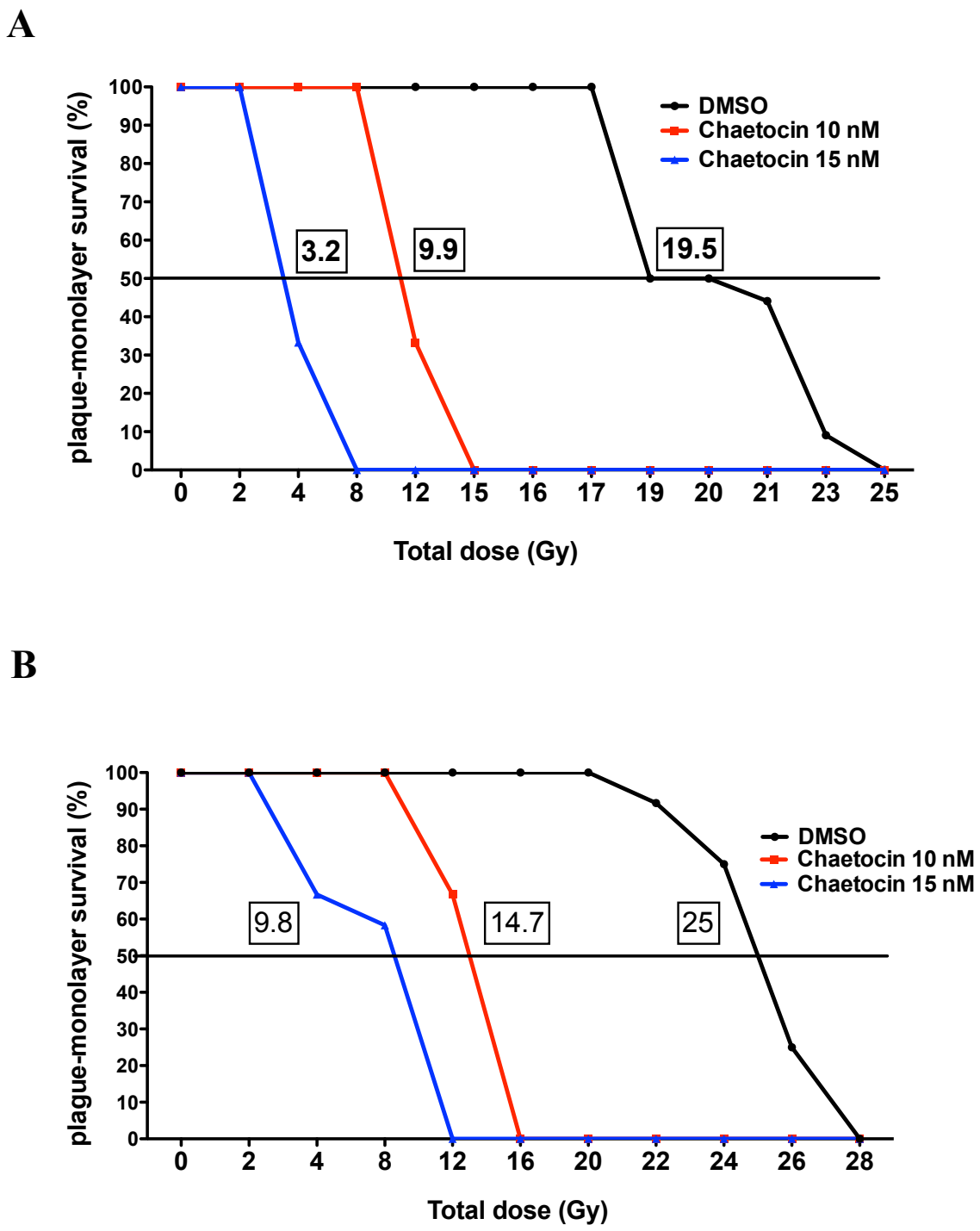

Figure 3.29: Effect of Chaetocin on tumour control dose of H1299 cells in the plague-monolayer assay. About 1500 cells in 5 µl were plated into 24 well plates and treated after adhering with Chaetocin (0, 10, 15 nM) and irradiated thereafter either with single radiation doses **(A)** and fractionated irradiation, using 2 Gy per 6 h **(B)**. At about 6 h after the fraction the medium with Chaetocin was removed and the cells were incubated for further 6 weeks. Results from one experiment are shown.

In comparison, Chaetocin also reduced the TCD50 in H460 cells from 12 Gy to 10.6, 10.2, 8.6 and 2.9 Gy after single irradiation for Chaetocin concentrations of 0, 7.5, 10.0, 15.0 and 20.0 nM, respectively (Figure 3.30A). The respective TCD50 values after fractionated

irradiation were 21.0, 14.2, 10.2, 8.6 and 8 Gy, for Chaetocin concentrations of 0, 7.5, 10.0, 15.0 and 20.0 nM, respectively (Figure 3.30B).

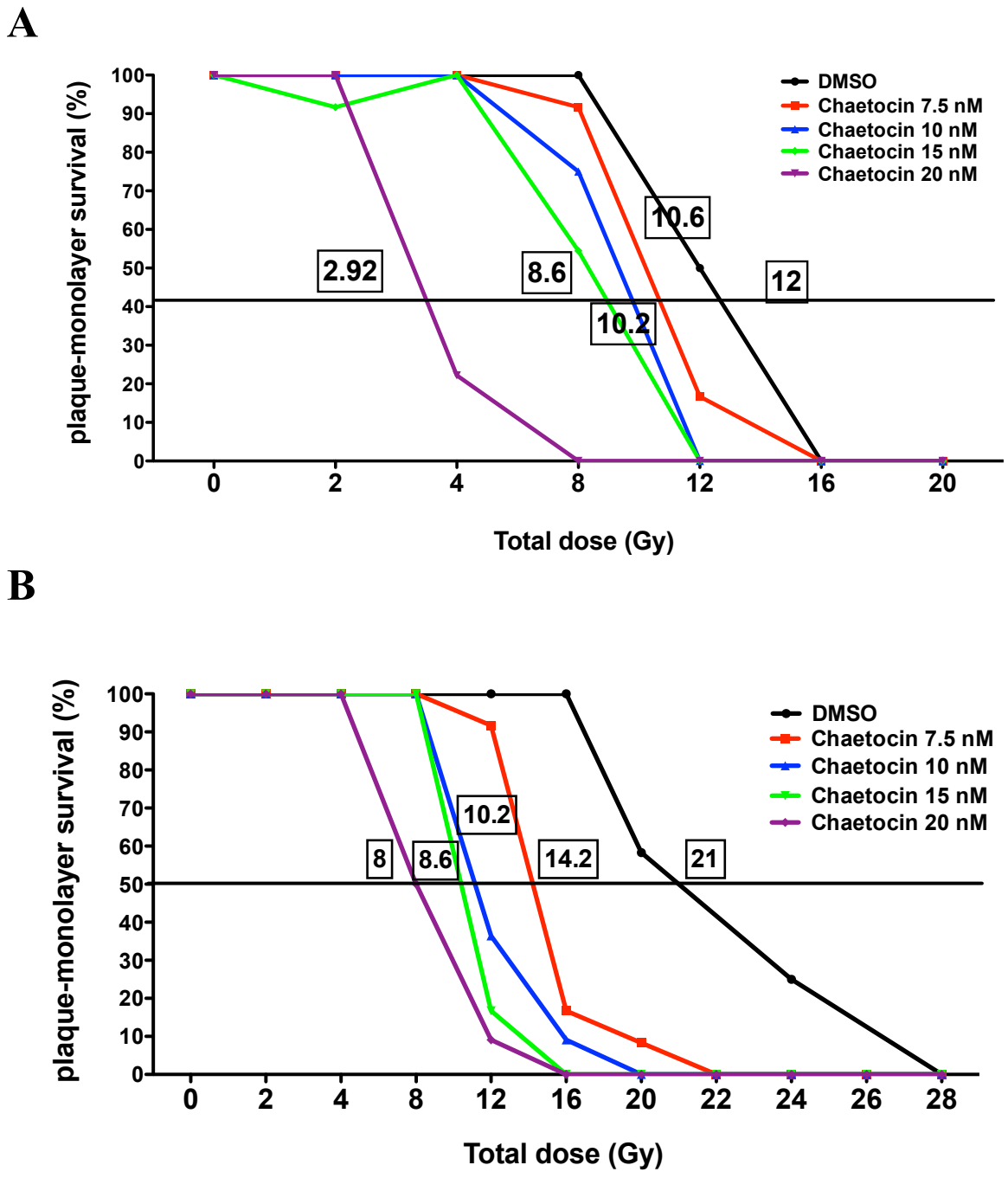

Figure 3.30: Effect of Chaetocin on tumour control dose of H460 cells in plague-monolayer survival assay. About 1500 cells in 5 µl cells were plated into 24 well plates and then were treated after adhering with Chaetocin (0, 7.5, 10, 15, 20 nM) and irradiated thereafter either in combination with single irradiation doses **(A)** and fractionated irradiation, using 2 Gy per 6 h **(B)**. At about 6 h after the last fraction the medium with Chaetocin was removed and the cells were incubated for further 6 weeks. Results from one experiment are shown.

Overall, the data show that reduced SUV39H1 deregulates DNA damage signalling with increased number of DSB associated foci during fractionated irradiation. This damage accumulation also led to an increased radiation sensitivity of the cells, which was apparent in

H1299 but not in H460 cells. In addition, preliminary data using the long term plaque-monolayer survival assay show increased radiation sensitising effect of Chaetocin at very low concentrations of <10 nM, in both cell lines. Notwithstanding, the effect of Chaetocin was more pronounced in H1299 compared to H460.

3.4 Characterisation of a Chaetocin-induced chromatin clustering phenotype

To modulate the chromatin structure, small molecules (Chaetocin, Gliotoxin, BIX1294 and UNC0638) targeting the histone methyltransferases SUV39H1 and G9a were used. Chaetocin and Gliotoxin, which belong to the chemical class of Epipolythiodioxopiperazine (ETP), was shown to inhibit both HMTs SU(VAR)3-9 and G9a (Greiner *et al*., 2005), while BIX1294 and UNC0638 inhibit only HMT G9a (Figure 3.31).

The data demonstrate global chromatin remodelling after Chaetocin treatment, which was clearly visible in fluorescent microscopy (Figure 3.32A). Illner *et al*. (2010) described this effect of Chaetocin-induced chromatin condensation (CICC) only in primary hFbs but not in tumour cells. In contrast to the results of Illner *et al*. (2010), the present data show CICC also in the NSCLC cell line H1299 as well as in primary hFbs and mFbs cells.

Chaetocin is a class of fungal metabolites knows as EPT, which is characterized by having a disulfide-bridged ring. In order to explore if hypercondenced chromatin clustering is a result of the unique chemical structure of ETPs, cells were treated with Gliotoxin, which is also a member of ETPs. In addition, BIX01294 and UNC0638, with different from ETPs chemical structures were also used. The results clearly show that condensed chromatin clustering was found only after Chaetocin and UNC0638 treatments, two structurally distinct classes of HMT inhibitors. Thus, the chemical structure seems to be not critical for the formation of condensed chromatin structure.

A

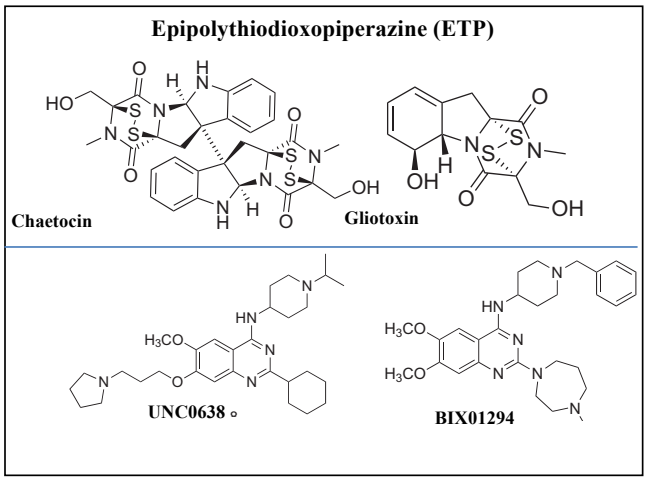

B

		Chaetocin	Gliotoxin	BIX01294	UNC0638
IC50	H460	37.14 nM	9.5 nM	1.5 µM	15 µM
	H1299	28.9 nM	28.8 nM	2.9 µM	13.3 µM
HMTs		G9a, SUV39Hs	G9a, SUV39Hs	G9a	G9a

Figure 3.31: Effect of different small-molecule HMT inhibitors on proliferation of NSCLC cell lines. A: Structure of small-molecular HMT inhibitors (modified pictures from Decarlo and Hadden, 2012); **B:** Comparison of IC50 and HMT status in NSCLC lines (H460, H1299) for the different inhibitors as measured by proliferation assay. IC50 was calculated by R program from three independent experiments are shown.

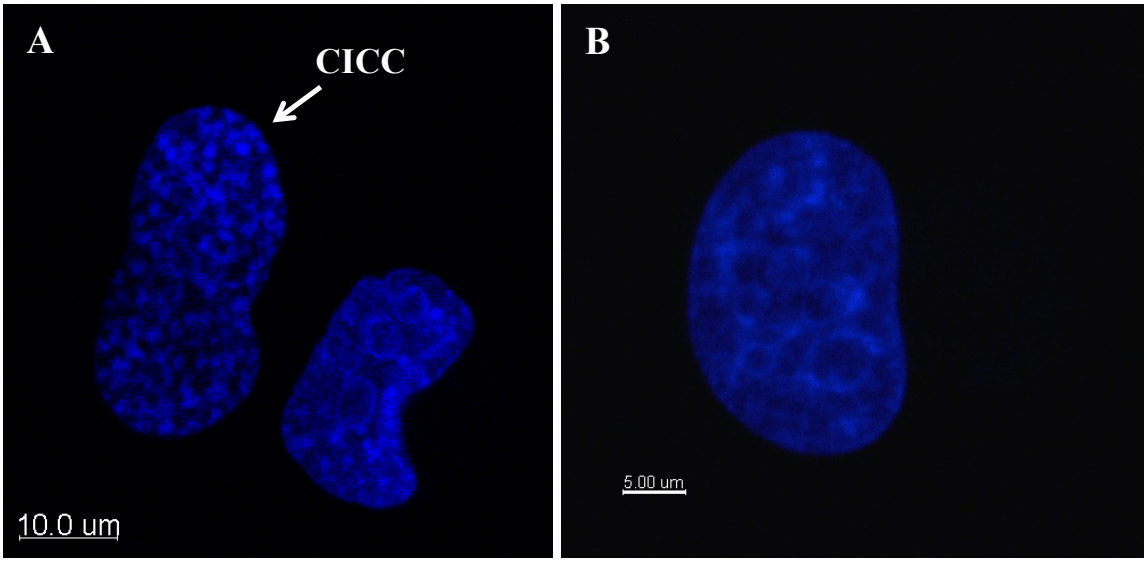

Figure 3.32: Chromatin remodelling after Chaetocin treatment in H1299. The fluorescence pictures represent nucleus after Chaetocin treatment (A) and non-treated cell nucleus (B) (blue, DAPI). Images are taken by confocal microscopy.

3.4.1 Characteristics of Chaetocin induced chromatin clustering

In order to understand the mechanism and principles of Chaetocin-induced chromatin clustering, time kinetics, effect of radiation, reversibility and its association with chromatin markers were evaluated. To investigate the time course of chromatin clustering in H1299 and in hFbs, cells were treated with Chaetocin and observed up to 40 h. The data show that the percentage of cells with Chaetocin-induced chromatin clustering (CICC) increases in a concentration- and time-dependent manner. The first chromatin clustering was detected at about 8 h after treatment with the maximum achieved at about 24 h (Figure 3.33A). Moreover, the percentage of CICC cells did not depend on IR exposure (Figure 3.33B).

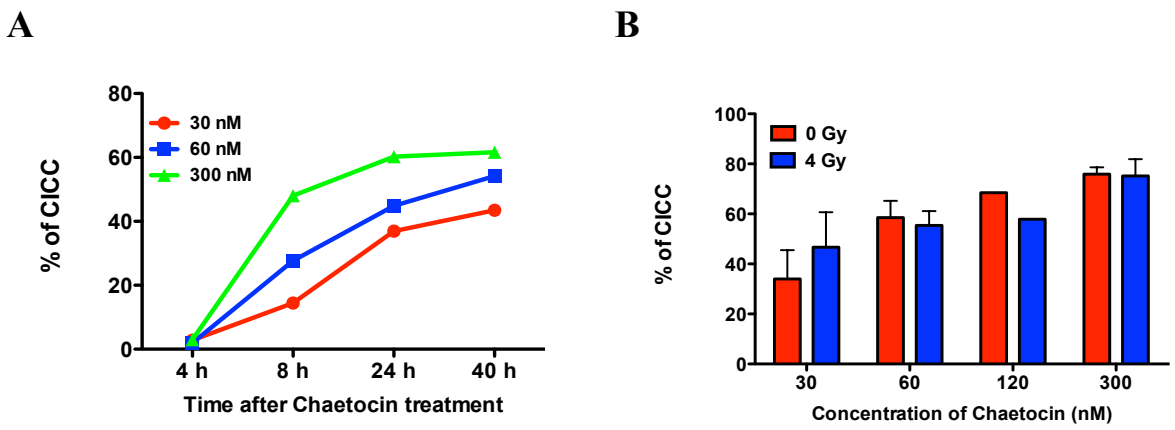

Figure 3.33: Time course of CICC phenotype in H1299 cells. A: Concentration- and time-dependent formation of CICC in H1299. The results from at least 500 scored cells per point (n=1) are shown; **B:** Effect of IR on CICC formation at 24 h after combined treatment with Chaetocin and 4 Gy. Bars represent the mean ± s.d (n = 2).

Unexpectedly, in H1299 cells transfected with siRNA targeting Suv39h1 and G9a, the percentage of CICC cells is significantly reduced after Chaetocin treatment (30 nM) (Figure 3.34). Thus, it seems that the HMTs SUV39H1 and G9a have an impact on CICC formation.

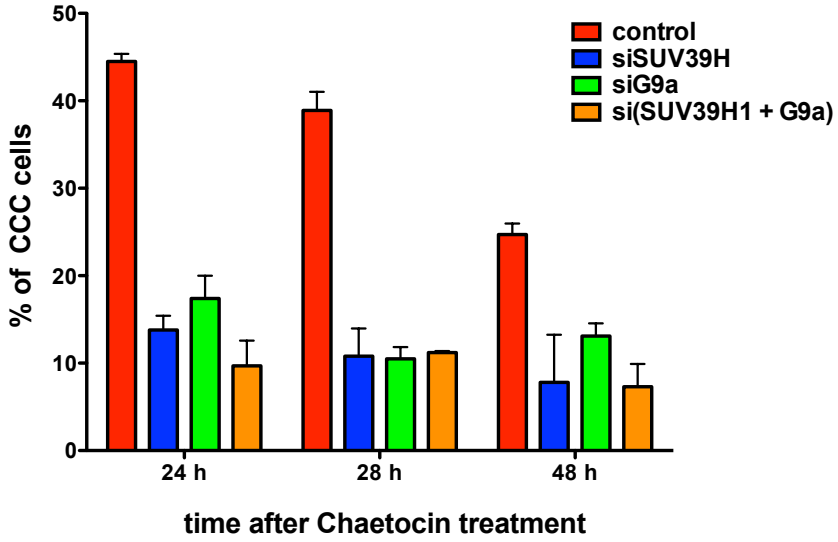

Figure 3.34: Effect of downregulation of SUV39H1 and G9a on CICC formation. Knockdown of siRNA mediated Suv39h1 and G9a decreased CICC at 48 h after Chaetocin (30 nM). The cells were fixed at 24, 28 and 48 h after Chaetocin treatment and analysed for CICC cells. Bars represent the mean ± s.d from three independent experiments.

3.4.2 Reversibility of Chaetocin-induced chromatin condensation

In order to investigate the reversibility of the chromatin effect on chromatin reorganization, Chaetocin was washed out at 24 h after treatment at that time when the maximum of CICC formation was seen. The data show that the percentage of CICC cells strongly decreases within 24 h after washout. However, in order to exclude that proliferation of non-affected cells or preferential death of CICC cells falsify the results, several control experiments were performed.

At first, to exclude that the fraction of CICC cells can be overgrown by proliferation of normal cells, i.e. non-affected cells, which do not have a visible chromatin clustering after the Chaetocin treatment, proliferation of the cells was stopped. Aphidicolin (Apc), which is a reversible inhibitor of eukaryotic DNA replication and arrests cell cycle transition of the cells at early S phase, was used for this purpose. Treatment of G1 enriched cells for 20 h with 2 μM of Apc arrested more than 80% of cells in the G1/S phase, while untreated cells went through the cell cycle (Figure 3.35A). Proliferation kinetics showed that Apc treated cells did not proliferate within 72 h of in comparison to the control groups (with and without Chaetocin treatment) (Figure 3.35B). There was no effect of Chaetocin on the cell number of Apc-treated cells, while Chaetocin significantly reduced proliferation of non-Apc treated cells. The data clearly show that the percentage of CICC cells significantly even in Apc-treated cells reduced (Figure 3.35C). In addition, hFbs, which naturally have a low proliferation capacity, were also

used to eliminate the possibility that proliferation may thin out the fraction of CICC cells (Figure 3.35D).

A

	G1 (%)	S (%)	G2 (%)
4h/0µM	84.5	6.3	9.3
4h/2µM	**83.6**	**9.9**	**6.4**
20h/0µM	46.7	53.3	0
20h/2µM	**80.9**	**11.5**	**7.6**

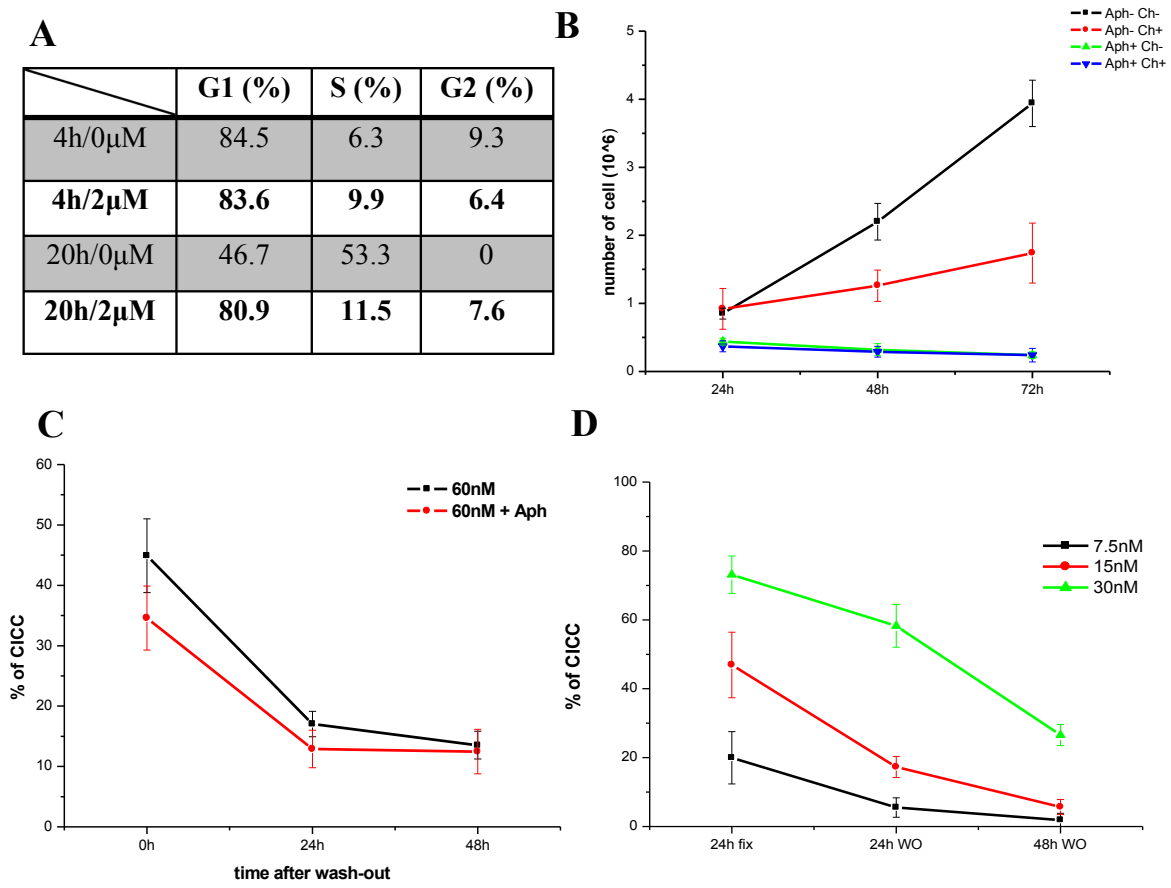

Figure 3.35: The reversibility of CICC after Aphidicolin (Apc) treatment in H1299 and HFbs. A: the cell cycle progression after 20 h Apc treatment; **B:** H1299 cells proliferation after Apc treatment with and without Apc; the reduction of CICC cells with Apc after Chaetocin washout in H1299 **(C)** and in hFbs **(D)**. Representative results from three independent experiments are shown. Bars represent the mean ± s.d.

Second, to exclude that preferential death of cells with the CICC phenotype may reduce the percentage of CICC cells live cell imaging was used. For this purpose, cells were treated with Chaetocin for 24 h and then washed out from the cell culture. Afterwards cells were stained with Hoechst 33342 and were monitored in real time up to 16 h after washout (Figure 3.36). About 33.5% ± 9.9% of the cells with CICC phenotype were reversible. For more detailed quantification (Figure 3.37), Chaetocin-treated "normal" cells without CICC as well as cells with CICC phenotype either reversible or non-reversible were divided into three groups (A, B, C): A1: "normal" cells, which survived; A2: "normal" cells, which underwent apoptotic or necrotic cell death; B1: CICC reversible cells, which survived within the observation period; B2: reversible cells, which underwent apoptotic or necrotic cell death; C1: irreversible cells, which survived; C2: irreversible cells which underwent apoptotic or necrotic cell death within the observation period. The results showed that 68.5 ± 22.5% of

"normal" cells survived (A1), while 31.5 ± 22.5% died (A2). In comparison, 82% ± 6% of CICC cells survived (B1), while 18% ± 6% were dead (B2). In contrast, 48% ± 11.6% of irreversible CICC irreversible cells survived (C1), while nearly the same fraction of irreversible cells died (C2). The Chaetocin-untreated cells during observation time did not have an apoptotic features.

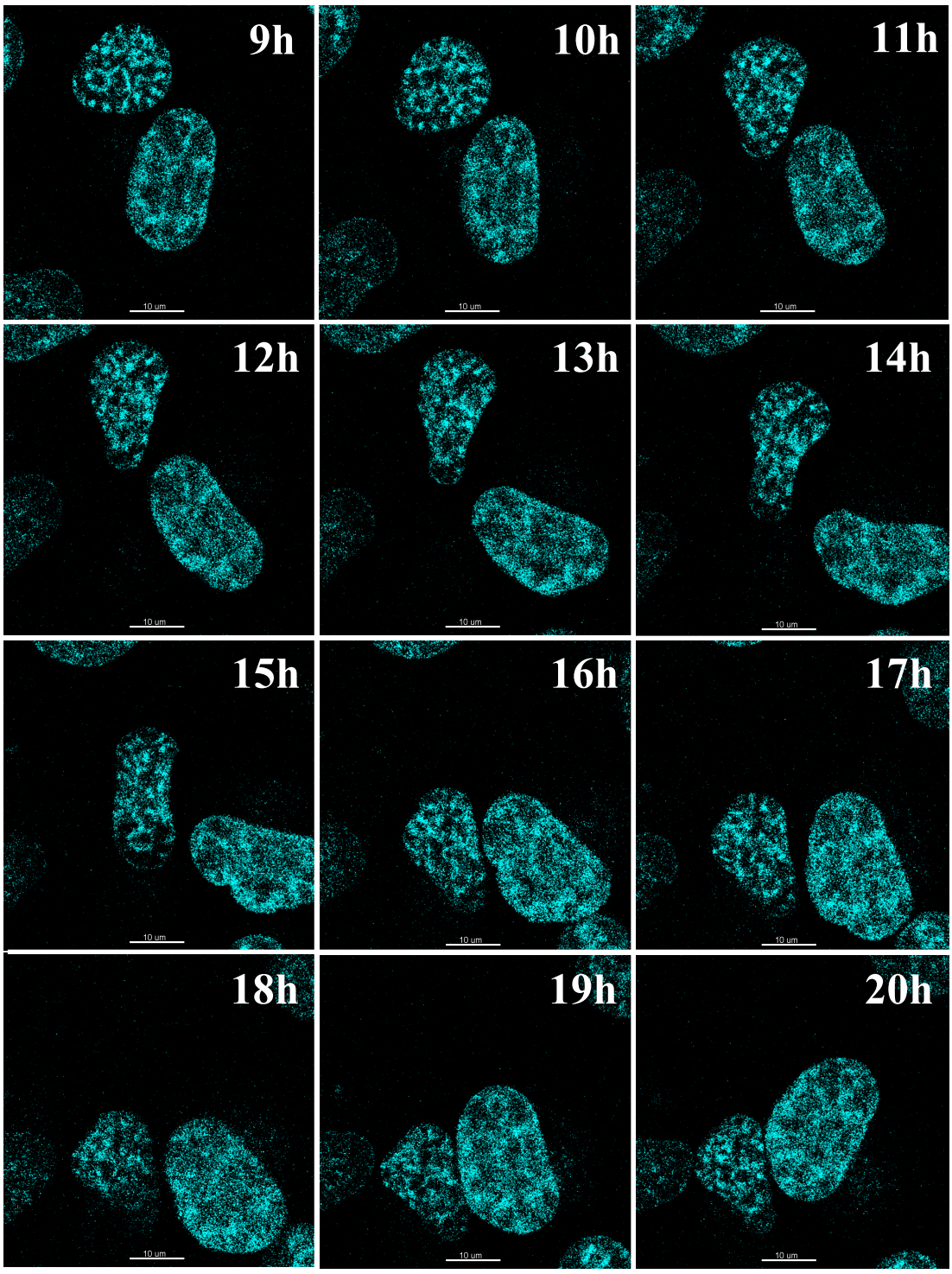

Figure 3.36: The reversibility of CICC phenotype after Chaetocin washout. The sequence of pictures shows the reversibility of CICC structure (light blue, Hoechst 33342) in H1299. Cells were observed in real time from 9 h until 20 h after Chaetocin washout. Images are taken by confocal microscopy. Scale bar = 10 µm.

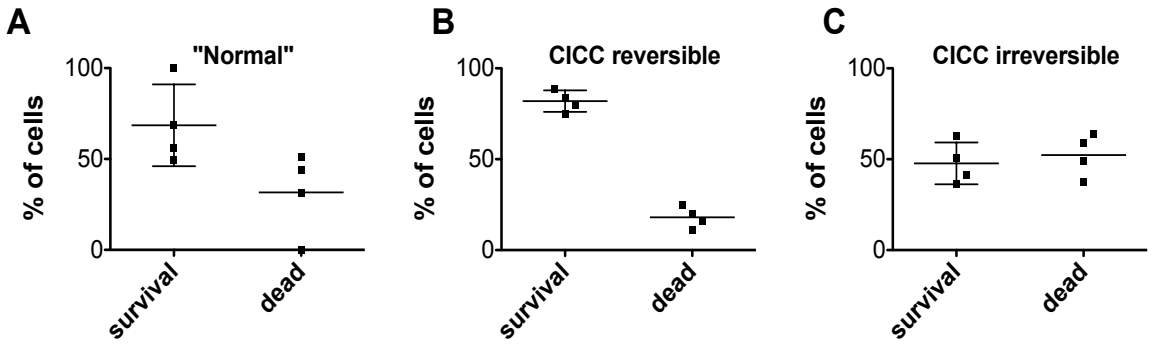

Figure 3.37: The reversibility of CICC in H1299 cell line. The cells were treated with Chaetocin (30 nM) for 24 h, thereafter the drug was washed out and the cells were observed for further 20 h. For quantification, cells were classified into 3 groups. **A:** "Normal" cell: Chaetocin-treated cells without chromatin condensation, which survived and dead cells; **B:** Cells with CICC structures, which were reversible; **C:** The observation of cells with CICC structures, which were irreversible. Data from four independent experiments with n(CICC) = 155, n(Control) = 194. The live cells imaging was performed by confocal microscopy. Representative results from four independent experiments are shown. Bars represent the mean ± s.d.

Overall, the observation shows that most of the cells with chromatin hypercondensation after Chaetocin treatment are of reversible phenotype. CICC phenotype increased with concentration and time of Chaetocin exposure reaching its maximum level at about 24 h after treatment.

3.4.3 Cell cycle dependence of CICC phenotype

Chromatin condensation is a common phenotype of cells during mitosis, when cells go to from G2 to prophase (Alberts *et al*., 2008). In order to evaluate whether Chaetocin induced chromatin condensation is related to mitotic condensation and to identify the cell cycle phase the CICC phenotype is associated with, cells were treated with Chaetocin and stained with markers for the different cell cycle phases. The cell cycle phases were analyzed by immunodetection of cyclin E, which detects cells in G1 phase. For S-phase cells, cyclin A, PCNA and EdU were used. In addition, Cyclin B1 and H3pS10, were used for G2/M phases.

The results show that CICC cells are not associated with (pre)mitotic phases (Figure 3.38) and mostly are associated with G1 cells. To confirm that CICC phenotype is associated with G1 cells, late passage (35-39) primary hFbs with low proliferative activity, i.e. with high G0/G1-fraction, were treated with Chaetocin. The results clearly show that primary hFbs in late passages can clearly adopt CICC phenotype.

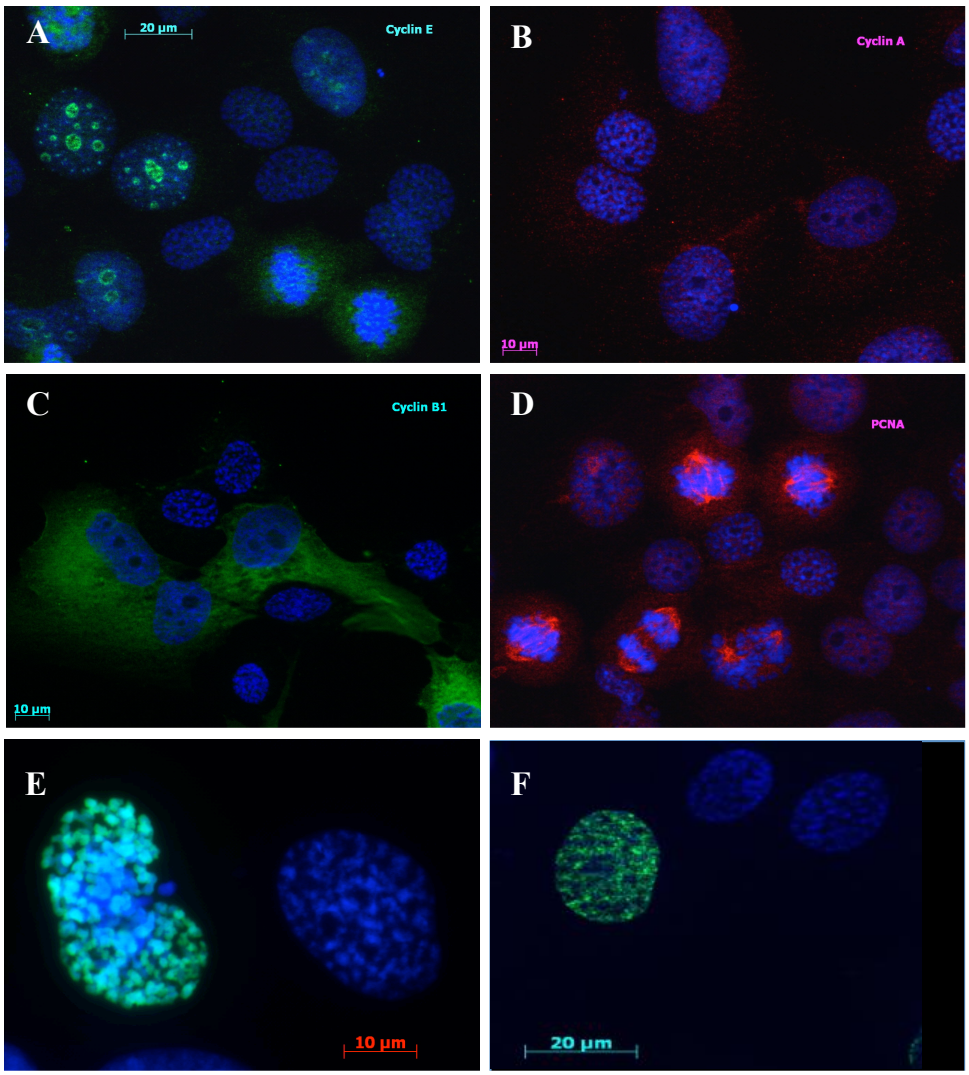

Figure 3.38: Cell cycle dependence of CICC phenotype. H1299 cells were treatment with Chaetocin for 24 h and stained for the various markers for cell cycle phases. **A:** Cyclin E (G1-phase, green), DAPI (DNA, blue); **B:** Cyclin A (S-phase, red), DAPI (DNA, blue); **C:** Cyclin B1 (G2-phase, green), DAPI (DNA, blue); **D:** PCNA (S-phase, red), DAPI (DNA, blue); **E:** H3pS10 (Mitosis, green) DAPI (DNA, blue); **F:** EdU (S-phase, green). Images are taken by fluorescent microscopy.

Overall, because CICC was not associated with cyclin A, EdU and H3S10ph, it is concluded that the CICC phenotype is mostly associated with G1-phase cells.

3.4.4 Association of CICC phenotype with heterochromatin markers

Chromatin condensation strongly correlates with domains of heterochromatin and is associated with specific histone markers, e.g. H3K9me3 and H3K27me3. In order to confirm that the CICC phenotype is enriched in heterochromatin markers cells were treated with Chaetocin, stained and analysed by immunodetection of heterochromatin associated markers H3K9me3, HP1α and H3K27me3. In addition, the euchromatin associated histone markers

H3H4me3 and H3K9ac were also used. As shown in Figure 3.40, CICC phenotype was positive for each of the heterochromatin markers, confirming that the condensed chromatin structures found after Chaetocin treatment are enriched in heterochromatic regions. Staining for euchromatin markers shows that euchromatin is less associated with CICC structures but instead the whole nucleus is evenly stained for the euchromatin marks indicating no preferential association of these markers with CICC structures (Figure 3.39).

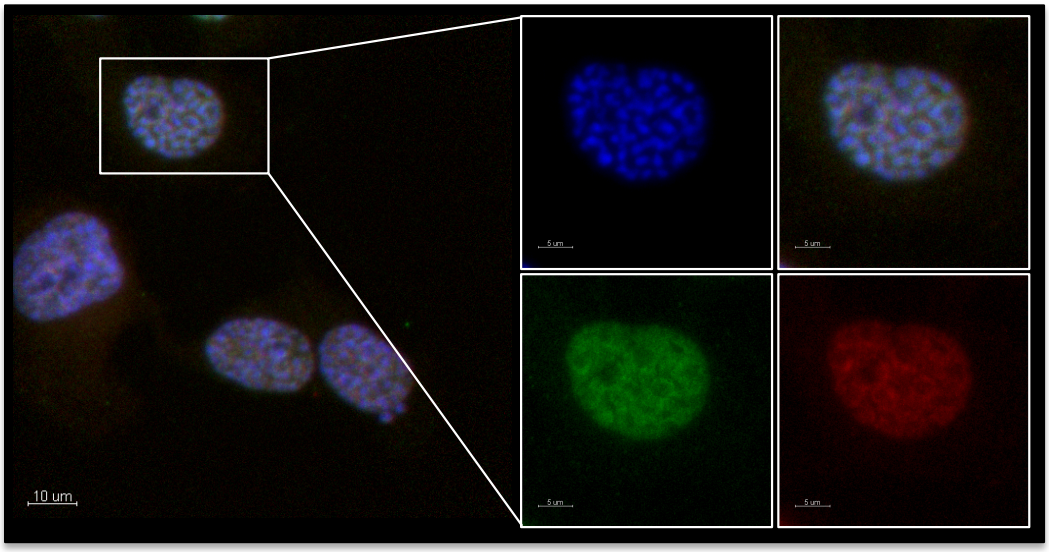

Figure 3.39: Association of euchromatin markers with CICC phenotype. H1299 cells were treated with Chaetocin for 24 h and stained for the euchromatin marker H3K4me3 (red) and H3K9ac (green). DAPI (blue) was used to stain the overall DNA. The respective overlaps are shown.

Overall, the present data show that the Chaetocin-induced chromatin clusters are enriched for heterochromatin.

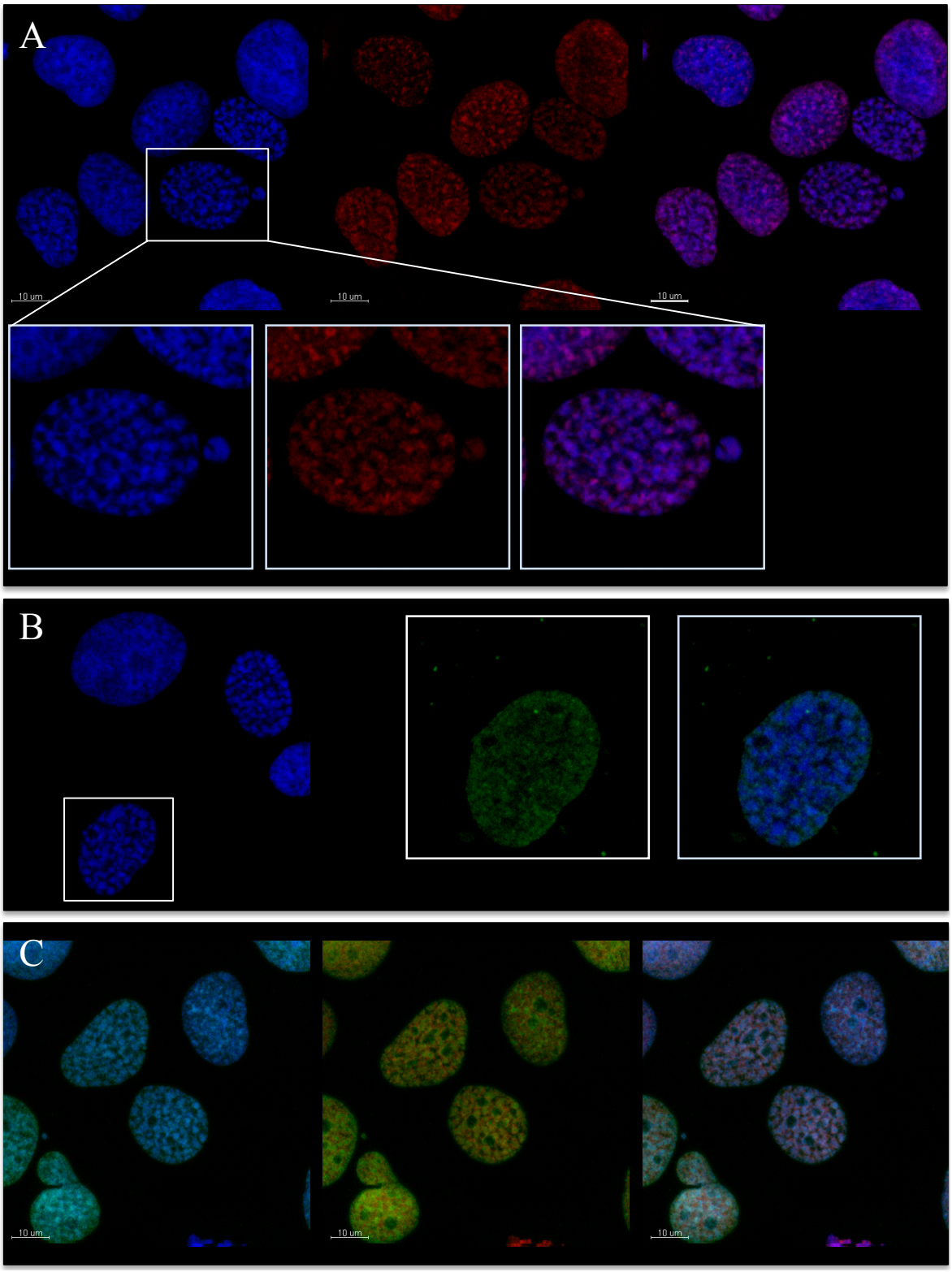

Figure 3.40: Association of heterochromatin markers and CICC. The H1299 cells were treated with Chaetocin for 24 h. **A:** H3K9me3 (DAPI, H3K9me3, overlap) stained CICC nucleus; **B:** H3K27me3 (DAPI, H3K27m3, overlap) stained CICC cell; **C:** HP1α (red rabbit, green mouse) (overlap and DAPI vs HP1α) and stained CICC nucleus. Images are taken by confocal microscopy. Scale bar = 10 µm.

3.4.5 Influence of CICC formation on IR induced 53BP1 signalling

The p53-binding protein 1 (53BP1) is an important regulator of DSB signalling and specifically localizes to damaged chromatin and protects genomic stability by signalling DSB repair (Panier and Boulton, 2014). As shown in paragraph 3.3.3, Chaetocin significantly reduced radiation-induced 53BP1 foci formation. In order to quantify this effect, radiation-induced 53BP1 and γH2AX foci were analysed separately in Chaetocin-treated cells with "normal" and CICC phenotype, respectively (Figure 3.41B, C). The data show that the reduction of 53BP1 foci in Chaetocin-treated cells mostly occurs in CICC cells, which completely lost their ability to form 53BP1 foci. In contrast, 53BP1 foci were not affected in Chaetocin-treated cells that had the "normal" phenotype. In comparison, radiation-induced γH2AX foci formation is not affected in CICC cells as well as in "normal" cells.

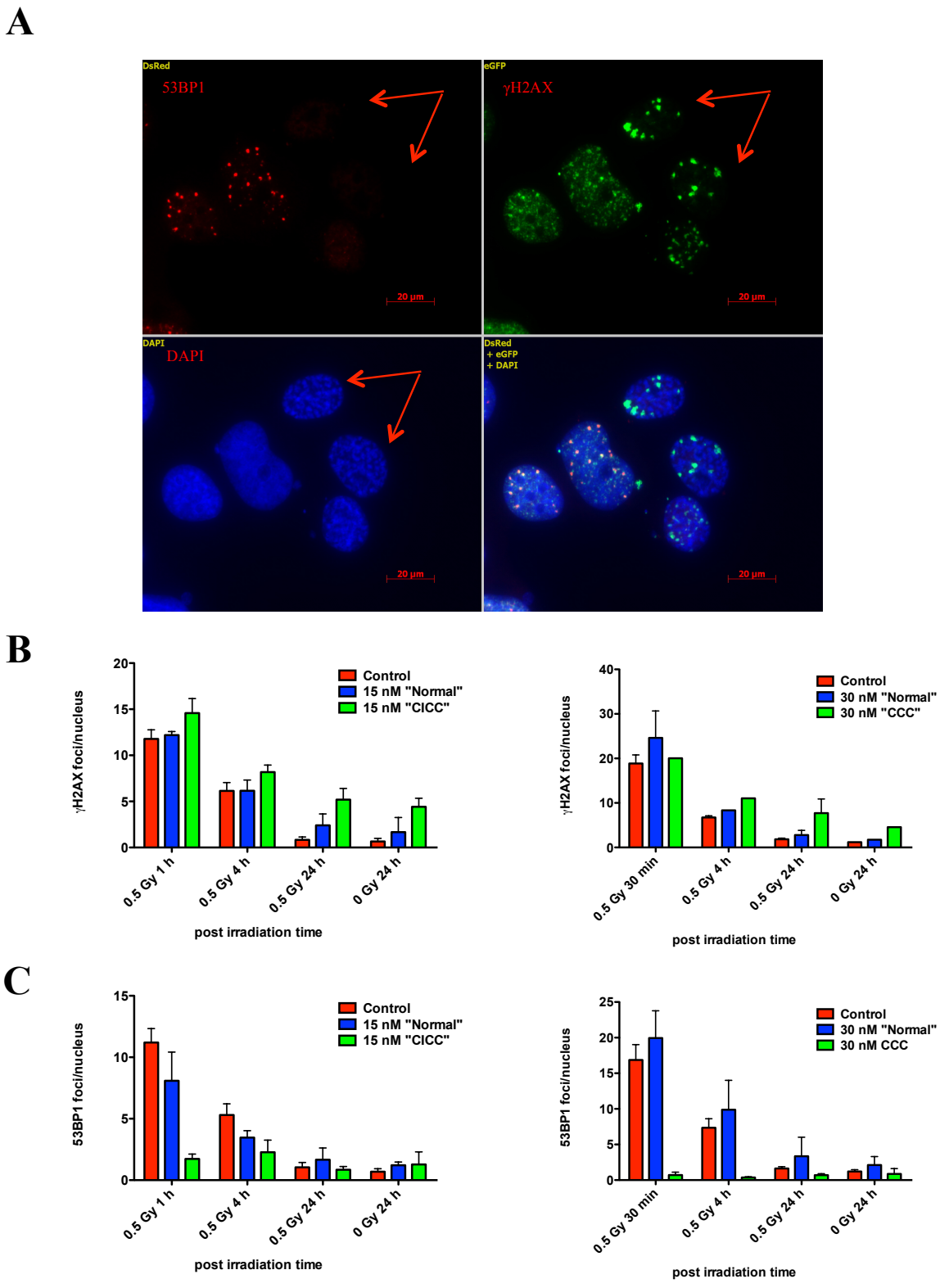

Figure 3.41: Effect of Chaetocin on 53BP1 and γH2AX foci formation in H1299 and hFbs. A: Selective inhibition of 53BP1 foci formation in H1299 cells with the CICC phenotype after Chaetocin pre-treatment (30 nM) for 24 h and fixed at 1 h after IR at 0.5 Gy (DAPI, blue; 53BP1 foci, red; γH2AX foci, green). **B:** Kinetics of γH2AX foci repair in H1299 (left) and in hFb (right) after IR at 0.5 Gy and Chaetocin treatment. "Normal" – cells without chromatin changings after Chaetocin treatment and CICC – Chaetocin induced chromatin clustering. **C:** Kinetics of 53BP1 foci repair in H1299 (left) and in hFb (right) after IR of 0.5 Gy and Chaetocin treatment. Representative results of at least two independent experiments are shown. Bars represent the mean ± s.d. Scale bar = 20 µm.

The present results show that the formation of 53BP1 foci in CICC cells is significantly abrogated. In order to investigate if this effect mainly relies on the formation of foci or if protein expression is also affected, H1299 cells were treated with Chaetocin for 24 h, irradiated with 0 Gy and 30 Gy proteins were isolated at 1 h after IR. The results from Western blotting analysis show that Chaetocin reduces not only foci formation, but also reduced 53BP1 on the protein level. For comparison, Chaetocin has no effect on the expression of other DNA repair proteins, such as Rad51 and γH2AX (Figure 3.42).

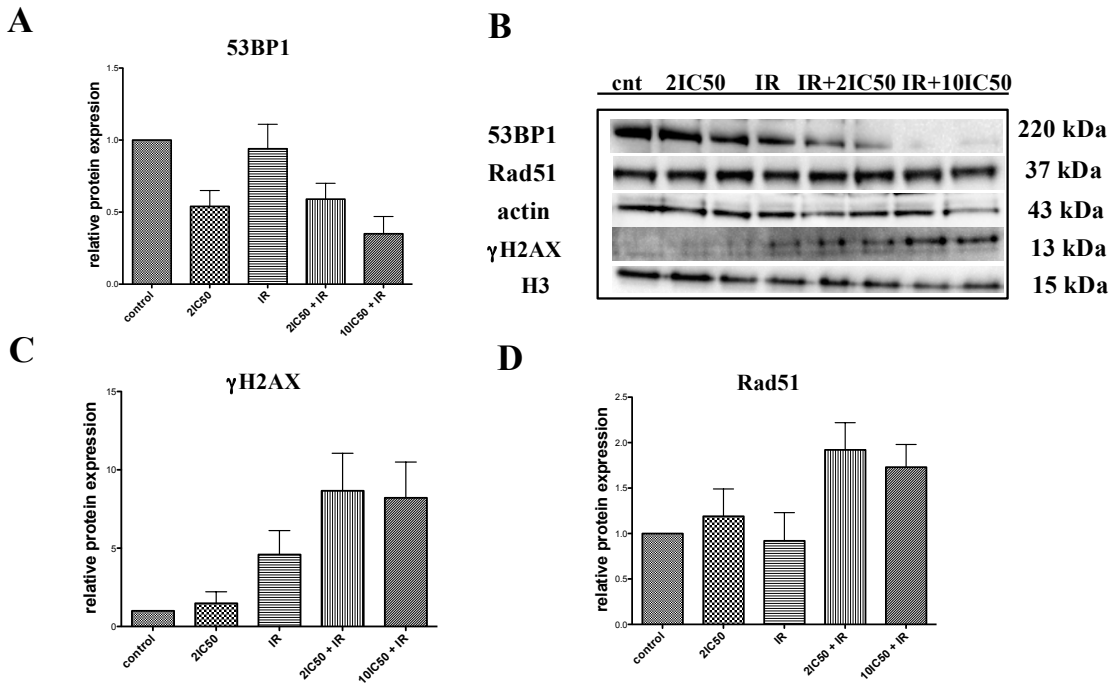

Figure 3.42: Effect of Chaetocin on DNA repair proteins expression after IR in H1299. A: The reduction of 53BP1 protein expression after Chaetocin and IR treatments by WB; **B:** a representative blot with identical results are shown; **C:** Increasing of γH2AX phosphorylation after IR; **D:** Increasing of Rad51 protein expression only with combination IR and Chaetocin treatment. Representative results from three independent experiments are shown. Bars represent the mean ± s.d.

Overall, the present results demonstrate that formation of the 53BP1 foci is strictly dependent on the chromatin phenotype of the cells, and is mostly diminished in CICC cells. The same effect was also found after UNC0638 treatment, which shows the same phenotype of CICC cells in H1299 as Chaetocin did (Figure 3.43). The effect seems to be specific to 53BP1 protein expression and foci formation because other repair signalling proteins, such as γH2AX and Rad51 were not affected.

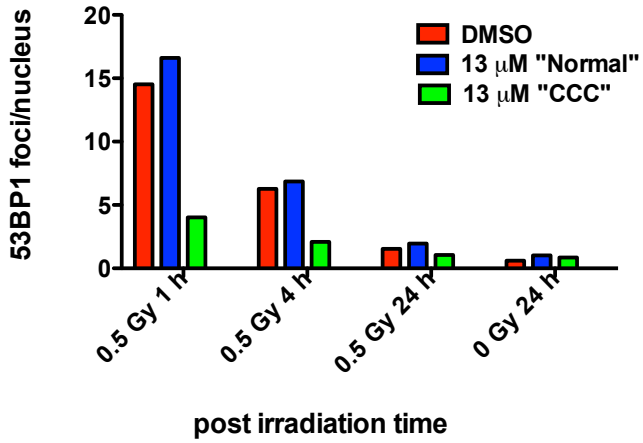

Figure 3.43: Effect of UNC0638 on 53BP1 foci formation in H1299 cells. Selective inhibition of initial 53BP1 foci formation after IR at 0.5 Gy and UNC0638 treatment. Representative results of one experiment are shown.

3.4.6 Effect of Chaetocin on pATM foci formation in CICC cells after IR

ATM is initially phosphorylated and recruited to DSBs and it retains and appears at DSBs as visible pATM foci, which however require the 53BP1 protein for foci formation (Noon and Goodarzi, 2011). Based on the results in paragraphs 3.3.3 and 3.4.5, which show that the formation of radiation-induced 53BP1 foci in CICC cells is abrogated, it was thus of interest to investigate if Chaetocin also has an influence on pATM foci formation in CICC cells. For this purpose, H1299 cells were treated with Chaetocin (30 nM) for 24 h, irradiated with 0.5 Gy and fixed at 1 h, 4 h and 24 h thereafter. The pATM foci were scored separately in “normal” and in CICC cells. The results show that Chaetocin reduces radiation-induced pATM foci in both phenotypes, CICC and "normal" cells, the effect however is more pronounced in CICC cells (Figure 3.44C). After showing the reduction in pATM foci formation we were also interested on Chaetocin effects on the expression of phosphorylated ATM (pATM) and KAP1 (pKAP1). The pKAP1 protein is of interest because ATM phosphorylates KAP1 at serine 824 during DSB repair and the reduction of pKAP1 leads to global chromatin relaxation, which is essential especially for DSB repair within heterochromatic regions (Ziv *et al.*, 2006). To investigate the protein expression of pATM and pKAP1, the cells were treated with and without Chaetocin (60 nM and 300 nM) for 24 h, irradiated with 10 Gy and then cells were harvested in 1 h after IR. The results show that Chaetocin have no effect on pATM and pKAP1 protein expression (Figure 3.44B).

In summary, the results show that Chaetocin reduces radiation-induced pATM foci formation in H1299 cells, which however does not rely on reduced expression pATM and KAP1 at the protein level.

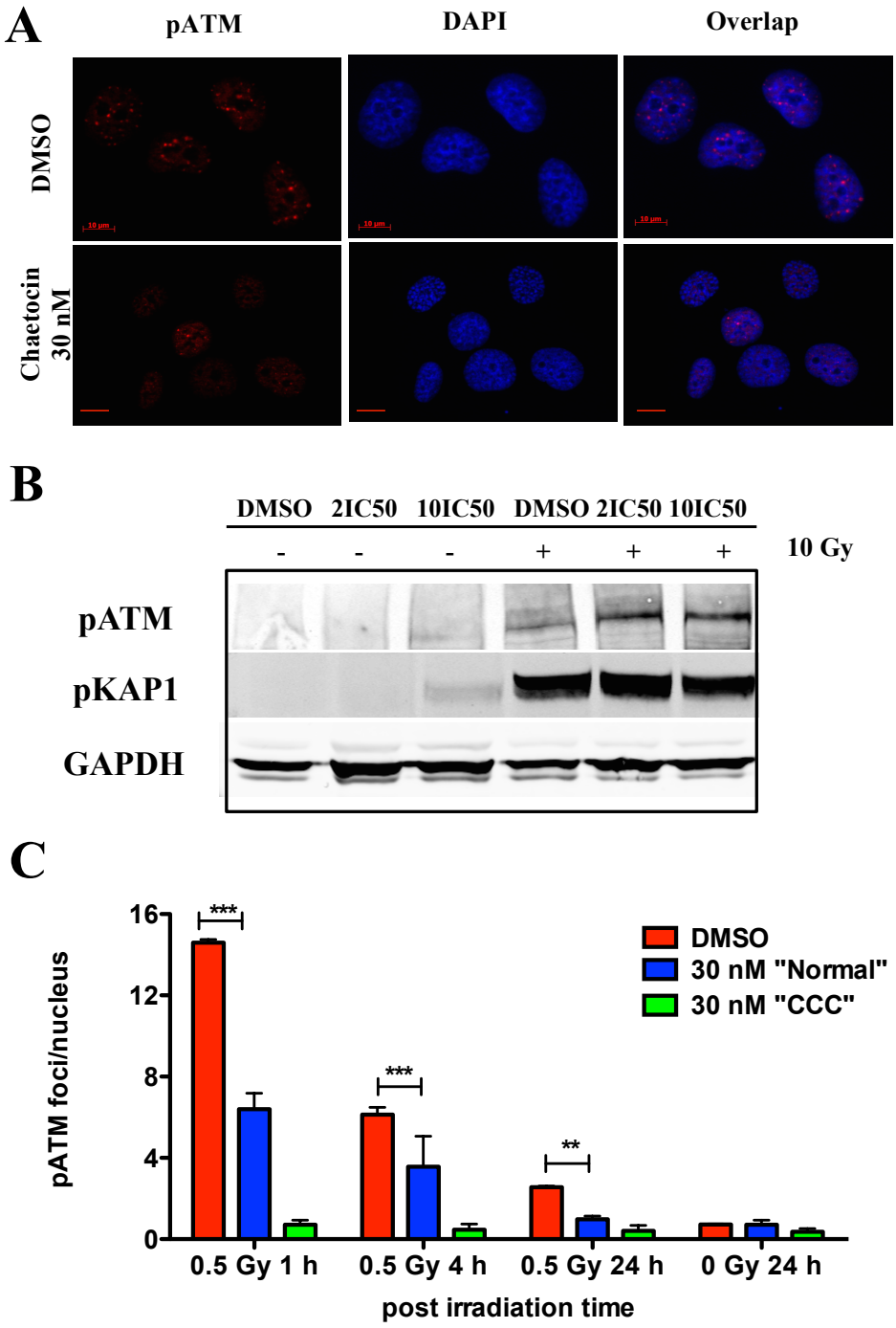

Figure 3.44: Effect Chaetocin on pATM and pKAP1 in H1299 cells. A: The immunofluorescence images of pATM foci (red) after with or without Chaetocin treatment (30 nM) in combination with radiation (0.5 Gy) in 1 h after IR; **B:** a representative blot showed the protein level of pATM and pKAP1 with and without Chaetocin treatment (0, 60, 300 nM) after IR (10 Gy) in 1 h; **C:** The quantification of the DNA repair kinetics after Chaetocin and IR treatment by visible pATM foci. "Normal" is the cell, which does not have visible morphological changes in nucleus after Chaetocin treatment. Cells were pre-treated with Chaetocin (30 nM) for 24 h, irradiated with 0.5 Gy and fixed at 1 h, 4 h, 24 h thereafter. Representative results from three independent experiments are shown. Bars represent the mean ± s.d. Statistical analysis: 2-way ANOVA analysis with Bonferroni posttest, $p < 0.01$ (**), $p < 0.001$ (***). Scale bar = 10 µm.

3.4.7 The distribution of radiation-induced DSBs in CICC

Our previously data showed that CICC structures were associated with heterochtomatin marks. Thus, we wished to investigate how radiation induced γH2AX foci were distributed in these chromatic regions. For this purpose, H1299 cells were treated with Chaetocin (60 nM) for 24 h to form the CICC structures, irradiated at 0.5, 1 Gy and then fixed in 15 min, 30 min, 1 h and 24 h post irradiation time. Our results demonstrated that after IR at 15 min the number of γH2AX foci in DAPI dense CICC region was slightly higher as compared to less intense DAPI regions (Figure 3.45). The proportion of γH2AX foci in DAPI dense CCC regions (“FOCI in”) and γH2AX foci in less DAPI dense regions (“FOCI out”) changed slightly during post irradiation time. However, the difference did not reach statistical significance in experiments.

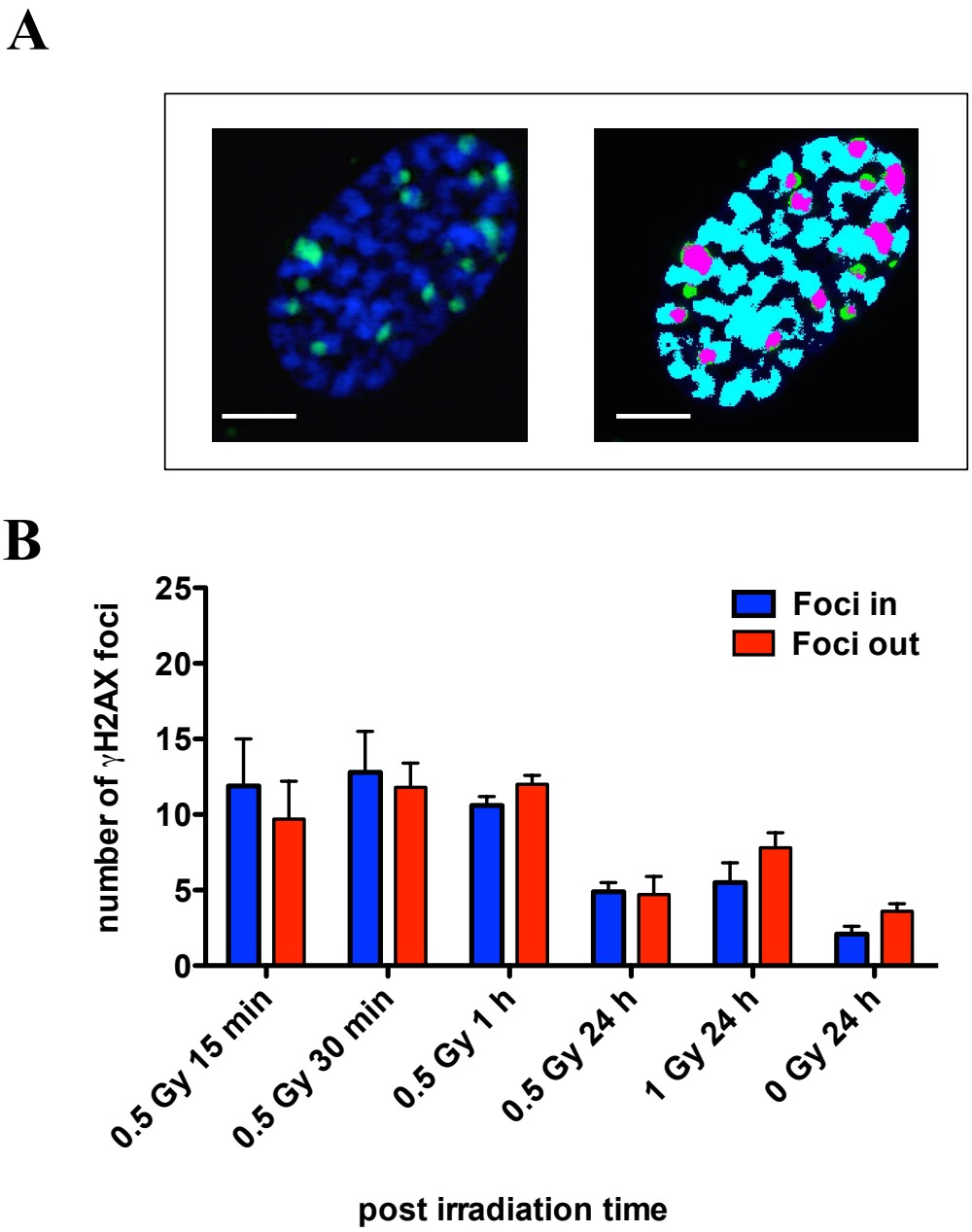

Figure 3.45: Distribution of γH2AX foci in chromatic regions after Chaetocin and IR treatment. The cells (H1299) were treated with Chaetocin (60 nM) for 24 h, then irradiated at 0.5, 1 Gy, fixed in 0.25, 0.5, 1 h, 24 h and were stained with γH2AX and DAPI. **A:** (left) the representative immunofluorescence picture of colocalization γH2AX foci (green) and DAPI (blue) and (right) the picture of colocalization (pink) γH2AX foci (green) and DAPI (blue) after Axiovision analysis. **B:** The quantification of γH2AX foci and CICC domains after IR. "FOCI in" is defined as γH2AX foci are localized with DAPI, "FOCI out" – γH2AX foci located in DAPI free region. Representative results from at least three independent experiments are shown. Bars represent the mean ± s.d.

3.4.8 Influence of ROS on cellular effects of Chaetocin

3.4.8.1 Effect of reactive oxygen species (ROS) on cell cycle, proliferation and cell death

Chaetocin is a member of ETP class, which can induce oxidative stress by activating reactive oxygen species (ROS) and thus can lead to cell death (Isham *et al*., 2007). In order to show if Chaetocin induces chromatin condensation also rely on ROS production we used various antioxidants. The superoxide dismutase Tiron, a cell-permeable superoxide scavenger (100 µM) or the antioxidant apocynin (100 µM) did not inhibit CICC induction. In contrast, N-acetyl-cysteine (NAC) an antioxidant, which is quite popular for its ability to reduce oxidative stress, fully inhibited the induction of CICC phenotype at concentration of 1 mM. However, we did not detect CCC formation after H_2O_2 (0.1%) treatment.

In order to explore the effect of NAC on downstream negative effects of Chaetocin, proliferation and activation of radiation-induced apoptosis were studied. To understand how NAC affects the cell cycle progression, cell death and cell proliferation and to determine the effective concentration to do this, cells were treated with increasing concentration of NAC (0.5, 1, 2, 5, 10 mM) for 2 h, treated with Chaetocin at 150 nM for 2 h, irradiated at 10 Gy and then incubated for 24 h. NAC treatment shows no effect on cell cycle progression with or without irradiation with 10 Gy (Figure 3.46). However, NAC reversed the cell cycle effects of Chaetocin in a concentration-dependent manner, reaching its optimum effect level at about 2 mM.

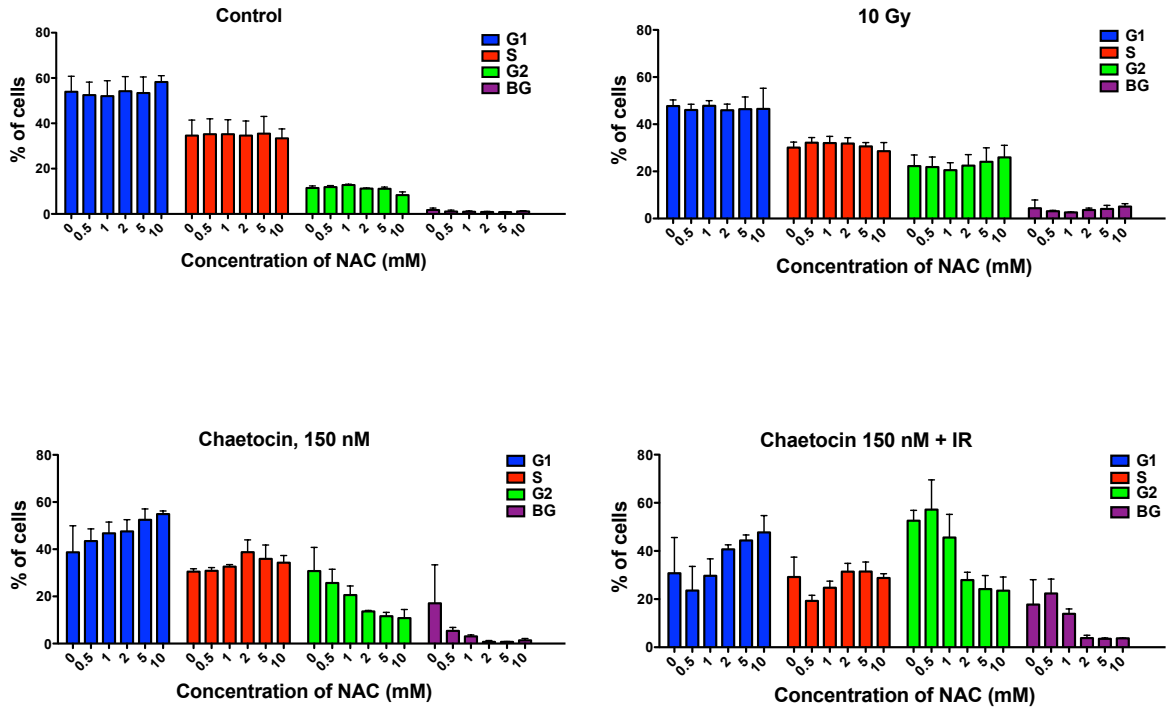

Figure 3.46: Effect of NAC on the cell cycle progression after Chaetocin treatment and IR in H1299 cell line. The cells were treated with increasing concentrations NAC (0.5, 1, 2, 5, 10 mM), after 2 h Chaetocin (150 nM) was added, in 2 h the half of the cells was irradiated at 10 Gy and incubated for 24 h. Representative results from three independent experiments are shown. Bars represent the mean ± s.d.

Additionally, we found that NAC normalized cell proliferation after Chaetocin treatment (150 nM) in a concentration-dependent manner (Figure 3.47A). Indeed, the NAC strongly reduced the percentage of dead cells after Chaetocin alone and in combination with IR (Figure 3.47B). NAC had no effect on cell death and the cell proliferation after IR only.

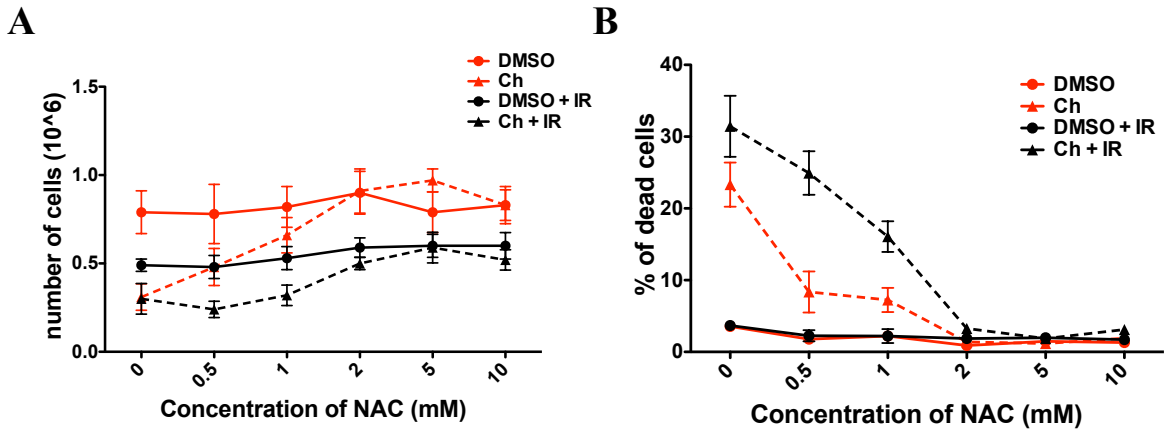

Figure 3.47: Effect of NAC on cell proliferation and cell death after Chaetocin treatment and IR in H1299. Cells were treated with increasing concentrations of NAC (0.5, 1, 2, 5, 10 mM) for 2 h, then Chaetocin "Ch" (150 nM) was added to the cell culture medium and 2 h later cells were irradiated with 0 Gy and 10 Gy and further incubated for 48 h. **A:** Cell proliferation after Chaetocin treatment; **B:** Cell death. Results from three independent experiments are shown. Bars represent mean ± SEM.

In addition, the order of treatment with Chaetocin and NAC on cell cycle progression was tested by adopting two different treatment schedules. In schedule A, cells were pre-treated for 2 h with Chaetocin (75 nM and 150 nM), then NAC (5 mM) was added to the cell culture, and after further 2 h cells were irradiated with 10 Gy and incubated for further 48 h. In schedule B, cells were pre-treated for 2 h with NAC (5 mM), then Chaetocin was added into cell culture (75 nM and 150 nM) and after further 2 h the cells were irradiated with 10 Gy and incubated for 48 h. Proliferation, cell cycle and apoptosis were determined.

The results show that in both treatment options Chaetocin resulted in cell cycle arrest in the G2 phase which increases with the concentration of Chaetocin used from 10.6 ± 3.3% to 31.8 ± 13.7% (Figure 3.48A) and from 10.5 ± 4.3% to 21.3 ± 13.1% (Figure 3.48B). In parallel to G2-phase arrest, the percentage of cells in G1 phase decreased from 59.1 ± 11.4% to 40.6 ± 14.2% for schedule A and from 58.4 ± 9.8% to 49.4 ± 14.3% for schedule B after treatment with 150 nM of Chaetocin. The same results were observed in combination with IR (10 Gy) in both treatments. In addition, an increase in the percentage of background (BG) cells, which represents fragmented dead cells, i.e. apoptotic and necrotic ones. Interestingly, that NAC normalized the cell cycle progression of Chaetocin induced deregulations in cell cycle distribution. The effect of NAC was even stronger if the cells were pre-treated with NAC before Chaetocin was added to the cell culture (treatment B).

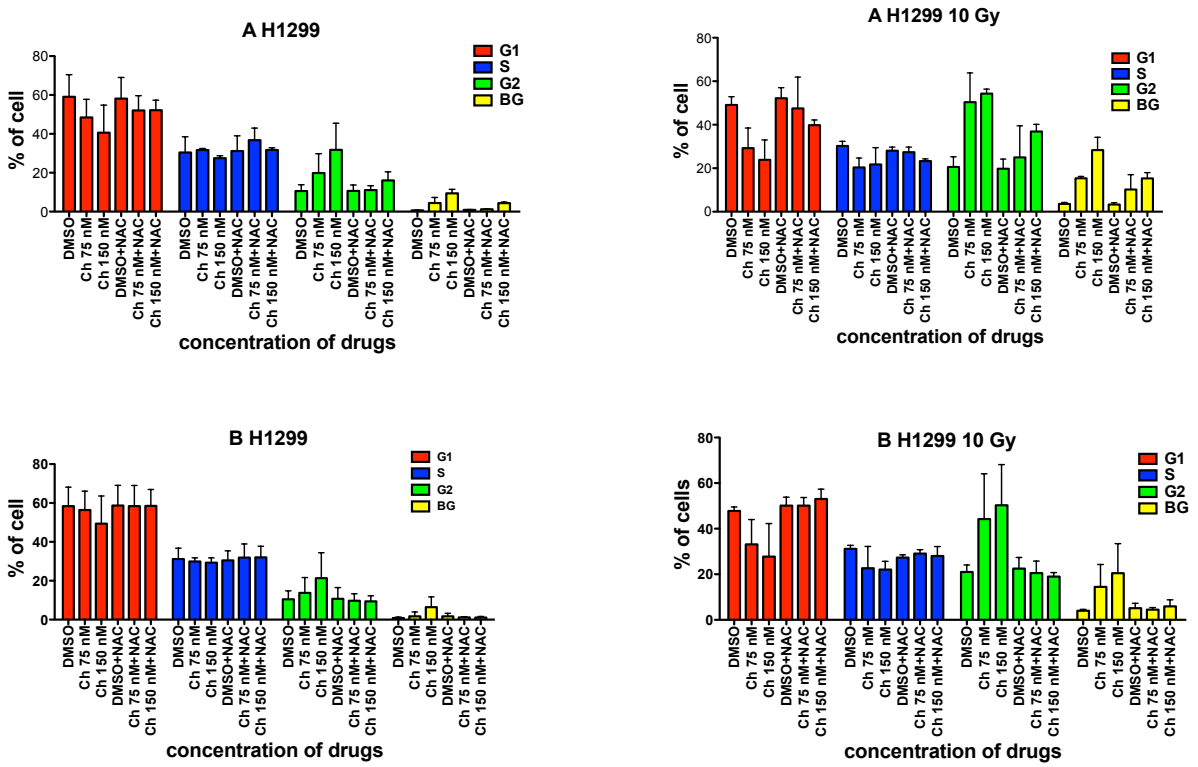

Figure 3.48: Effect of NAC on Chaetocin induced cell cycle deregulations. Treatment schedule A: Cells were treated with Chaetocin "Ch" (75 nM, 150 nM), after 2 h NAC (5 mM) was added, then 2 h later irradiated with 10 Gy and incubated for 48 h. Treatment schedule B: Cells were treated with NAC (5 mM) for 2 h, after 2 h Chaetocin (75 nM, 150 nM) was added, then in 2 h later irradiated with 10 Gy. Results from three independent experiments are shown. Bars represent mean ± s.d.

By using the different treatment schedules, the combined effect of NAC, Chaetocin and IR was tested also on the proliferation capacity of treated cells. The data show that IR and Chaetocin induce apoptotic cell death and reduce cell proliferation of H1299 (Figure 3.49) and H460 cells (Figure 3.50) in a concentration-dependent manner. Interestingly, that pre-treatment of the cells with NAC (5 mM) before IR and Chaetocin treatment significantly reduced apoptotic cell death and normalized the proliferation of cells. These results demonstrate that the ROS inhibitor NAC have a protection effect with respect to cell cycle deregulation, proliferation and apoptotic cell death induced by Chaetocin and IR.

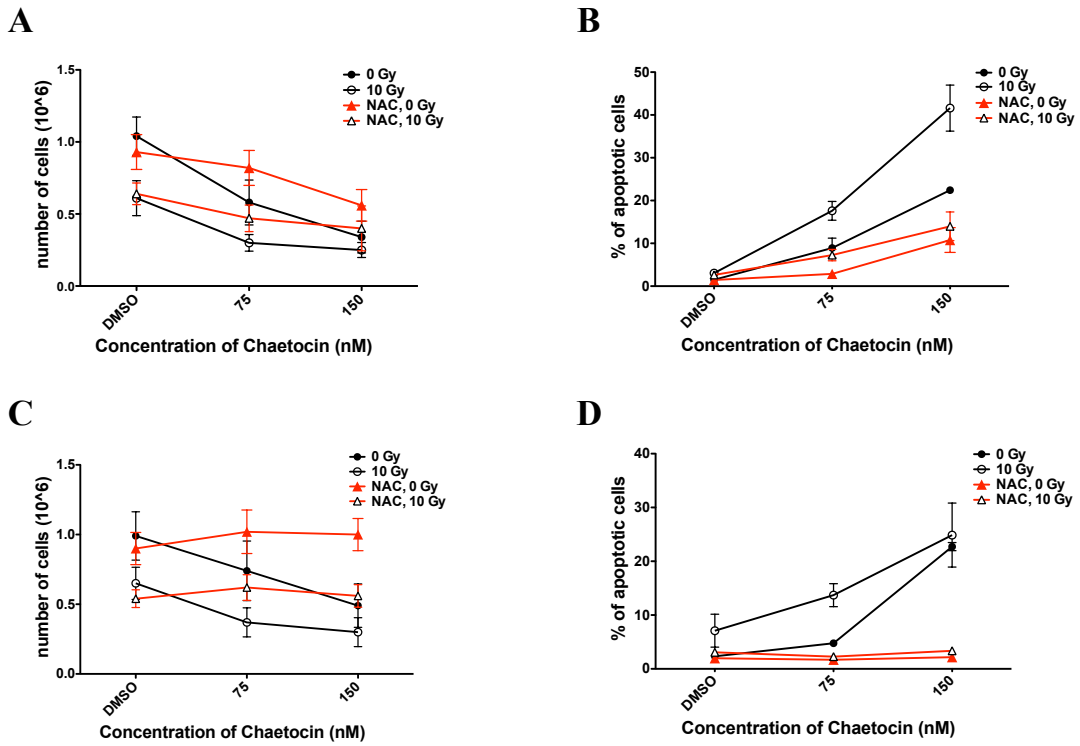

Figure 3.49: Effect of NAC on proliferation and apoptosis after combined treatment with Chaetocin and IR in H1299. Schedule A: (A, B) H1299 cells were treated with Chaetocin (75 nM, 150 nM) for 2 h, after 2 h NAC (5 mM) was added, then in 2 h the half of cells were irradiated at 10 Gy and incubated for 48 h. Method B: (C, D) H1299 cells were pre-treated with NAC (5 mM), after 2 h Chaetocin (75 nM, 150 nM) was added, then 2 h late cells were irradiated with 10 Gy. Effect on cell proliferation **(A, C)** and apoptosis **(B, D)** were measured. Results from three independent experiments are shown. Bars represent the mean ± SEM.

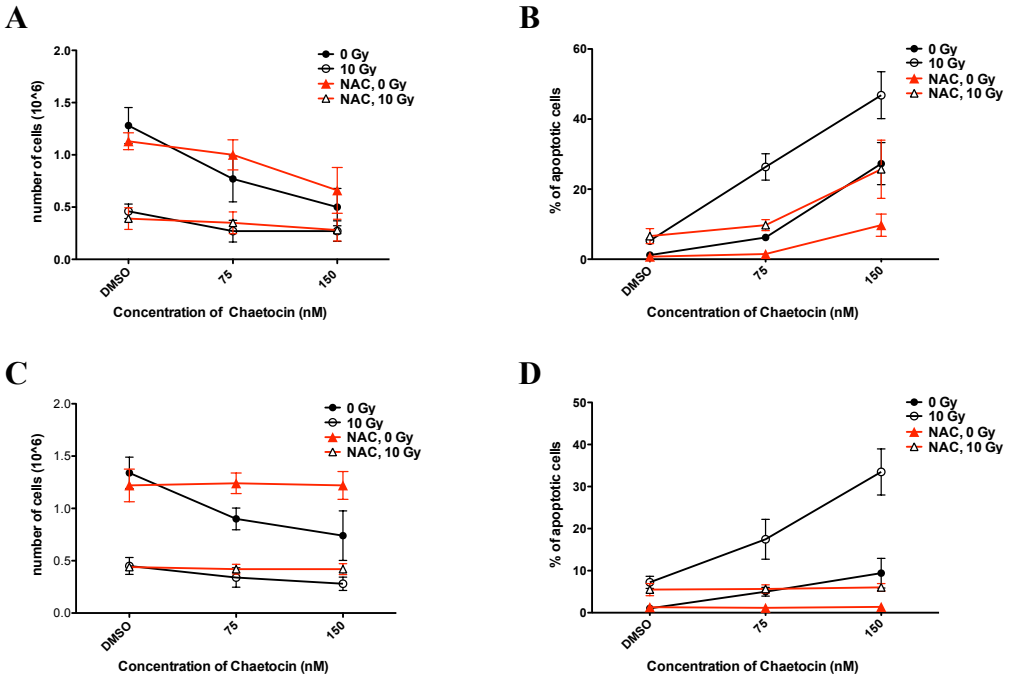

Figure 3.50: Effect of NAC on proliferation and apoptosis after combined treatment with Chaetocin and IR in H460. Schedule A: (A, B) H460 cells were treated with Chaetocin (75 nM, 150 nM) for 2 h, after 2 h NAC (5 mM) was added, then in 2 h the half of cells were irradiated at 10 Gy and incubated for 48 h. Method B: (C, D) H1299 cells were pre-treated with NAC (5 mM), after 2 h Chaetocin (75 nM, 150 nM) was added, then 2 h late cells were irradiated with 10 Gy. Effect on cell proliferation **(A, C)** and apoptosis **(B, D)** were measured. Results from three independent experiments are shown. Bars represent the mean ± SEM.

In summary, our data show that NAC, an antioxidant, fully inhibits CICC formation, reduces the number of dead cells and normalizes cell cycle progression after Chaetocin treatment alone and in combination with IR.

3.4.8.2 Effect of NAC on DNA DSBs repair after Chaetocin and IR treatments

To examine the effect of NAC on DNA repair after Chaetocin and IR treatment, H1299 cells were treated with NAC (0, 1, 2, 5 mM) and 2 h later the half of cells were treated with Chaetocin (60 nM) for 24 h, irradiated with 0.5 Gy, 4 Gy and 10 Gy and then fixed at 1 h, 4 h and 24 h thereafter. The cells were stained with γH2AX and 53BP1 antibodies and foci formation was determined. As shown in previous section of this study, Chaetocin increased the numbers of initial and residual number of foci after IR. Interestingly, that NAC significantly decreases the number of initial as well as of the residual number of foci alone and in combination with Chaetocin after IR (Figure 3.51).

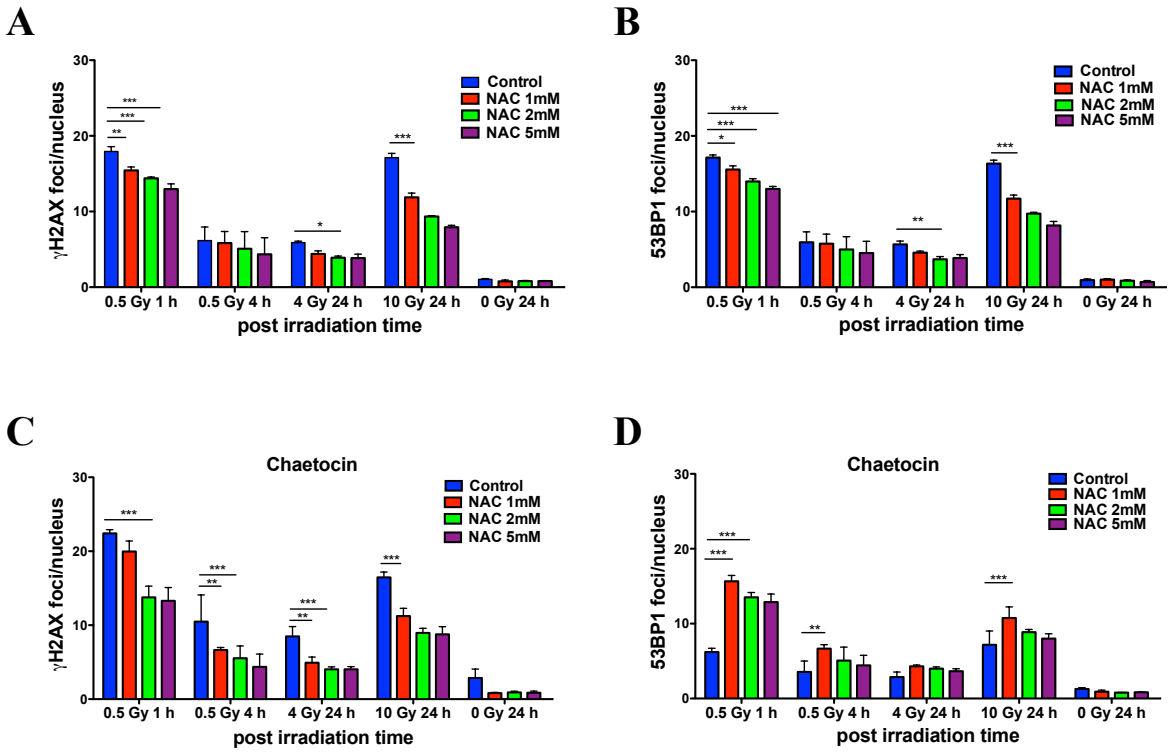

Figure 3.51: Effect of NAC on NHEJ in H1299 cell line. The cells were treated with NAC (0, 1, 2, 5mM) for 2h (A, B), then in figures C and D with Chaetocin (60 nM) for 24 nM. All cells were irradiated at 0, 0.5, 4, 10 Gy and fixed in 1 h, 4 h 24 h after IR. Number of γH2AX **(A, C)** and 53BP1 foci **(B, D)** was scored manually. Representative results from three independent experiments are shown. Bars represent the mean ± s.d. Statistical analysis: 2-way ANOVA analysis with Borferroni posttest, $p < 0.05$ (*), $p < 0.01$ (**), $p < 0.001$ (***).

From these results, we concluded that NAC is able to significantly reduce the number of initial and residual radiation γH2AX and 53BP1 foci in both Chaetocin treated and non-treated DSBs.

4. Discussion

The dynamic nature of chromatin and its modifications play a critical role in transcriptional gene regulation and thus can affect several cellular functions such as differentiation, replication, DNA damage response, activation of cell death (Deb *et al*., 2014; Dinant *et al*., 2008; Falk *et al*., 2014; Kouzarides, 2007; Misteli and Soutoglou, 2009; Mungamuri *et al*., 2012). The chromatin is divided into two distinct domains, heterochromatin and euchromatin, which are associated with silent and active gene regions, respectively. Gene expression is mostly regulated by epigenetic mechanisms, e.g. methylation, acetylation and phosphorylation of histones, as well as methylation of the DNA itself. Histone methylation regulates not only gene expression, but has also an impact on genomic instability (Putiri and Robertson, 2011).

In this respect, Pandey *et al*. (2014) considered the important role of the histone lysine methyltransfrase SUV39H1 as one of the key early events in urethane induced mouse lung tumour initiation and progression. The level of HMT SUV39H1 expression was shown to be enriched in heterochromatic regions regulating the higher-order chromatin structure (Rea *et al.*, 2000). The level of SUV39H1 expression correlates with di- or tri- methylation at lysine 9 of histone H3, which is a hallmark of silent chromatin (Noma *et al.*, 2001). Both HMTs, G9a and SUV39H1, are implicated in different types of cancers, including lung cancer (Yost, 2011). Alterations in cellular epigenetic and genetic structure, for example after IR, can lead to long term effects such as survival and genomic instability. However, the molecular mechanisms of modified chromatin structure on the DNA damage response are still unclear. In order to evaluate the effect of epigenetic modification, especially of histone methylation, we modulated the activity of the histone methyltransferase SUV39H1. Short and long term effects of SUV39H1 modulation on radiation induced DNA damage response were studied in two NSCLC cell lines (H460, H1299) and mice fibroblast cell lines (mFbs). To do this, we apply different experimental strategies: (i) genetics model of knockout of Suv39h1 in mFbs, (ii) knockdown of Suv39h1 in human NSCLC cell lines, and (iii) specific small molecule inhibitors of SUV39H1.

4.1 Genetic modulation of Suv39h1

HMT SUV39H1 has been reported as a first SET domain-containing histone lysine methyltransferase (HKMT), which generates di- and trimethylation of H3K9 (Rea *et al*., 2000). Furthermore, the HKMT G9 also generates dimethylation of H3K9 (Tachibana *et al*.,

2001). In the present study, reduced expression of H3K9me2 and H3K9me3 as well as increased expression of H3K9me1 was evident in shSuv39h1 transfected H1299 cells.

Previous studies showed that Suv39h genes regulate viability as well as pre-and postnatal development of mice (Peters *et al*., 2001). It is involved in cell migration in breast and colorectal cancer cells (Yokoyama et al., 2013) with reduced cell proliferation after downregulation of SUV39H1 (Wang *et al*., 2013). An increase in the number of hepacellular carcinoma cells in G0/G1 phase after Suv39h1 knockdown can explain this reduced proliferation (Chiba *et al*., 2014). Moreover, the human embryonic kidney cells (293T) lacking Suv39h1 show increased radiation sensitivity (Ayrapetov *et al*., 2014). In addition, deficiency of HMT G9a ($G9a^{-/-}$) in mice leads to embryonic lethality, with a significant increase in apoptosis (Tachibana *et al*., 2002).

In the present work, we focused on the role of HMT SUV39H1 in radiation resistance of NSCLC and mice fibroblasts. On the hypothesis that the radiation sensitivity can be modulated by an altered methylation status of histones, we wanted to investigate the role of HMT SUV39H1 in cellular response to DNA damage induced by IR. The results confirm the findings from a previous study (Jeong *et al*., 2009), which showed that the human H1299 cell line is significantly more resistant to ionizing radiation compared to H460. In this respect, it has been shown that the number of hypermethylated genes in radioresistant H1299 cells was by a factor of two higher compared to that of the radiosensitive H460 cells (Kim *et al.,* 2010; Shames *et al*., 2006).

Indeed, deregulation of epigenetic control through histone methylations as well as DNA and histone modification is an important issue for the radiation resistance of cancer cells (Kim *et al*., 2002). We also found that Suv39h1 influences radiation sensitivity of mFbs, because knockout Suv39h1 significantly decreased clonogenic survival. However, no significant effect of Suv39h1 knockdown on the radiation sensitivity was observed in human NSCLC cell lines, although a trend to more radiation sensitivity at higher doses was evident in H1299 cells. The most likely explanation for the different effect of HMT SUV39H1 on radiation sensitivity in knockout and knockdown cells may be that the level of downregulation by about 50% is not sufficient to reduce the radiosensitization in H460 and H1299 cells.

In order to explore the molecular mechanism of increased radiation sensitivity after downregulation of Suv39h1, activation of DNA response mechanisms were focused on. Studies suggest that epigenetic abnormalities indeed can influence the DNA damage response of the cells (Putiri and Robertson, 2011). A number of histone modifications are known to be

involved in DNA damage response (Friedl *et al.*, 2012; Karagiannis *et al*., 2007; Kinner *et al.*, 2008; Maroschik *et al.*, 2014; Masumoto *et al*., 2005). However, the role of these modifications in DNA repair is not fully understood.

DSB repair initiates dynamic changes in histone modifications, including the phosphorylation of H2AX on serine 139 and thus the formation of γH2AX foci, which is a hallmark of NHEJ. In mammalian cells nonhomologous end joining (NHEJ) repair is the predominant DNA repair pathway, which is active in all phases of the cell cycle (Rothkamm et al., 2003). In addition, dynamic changes in H3K9 modification in euchromatin is one of the earliest events within 5 min required for processing and remodelling of the damaged chromatin template. It was shown that HMT SUV39H1 rapidly recruits to DSBs, where it directs H3K9 methylation on large chromatin domains adjacent to the DSB (Ayrapetov *et al*., 2014). Zheng *et al*. (2014) reported about the importance of SUV39H1 in DNA repair, with sustained expression of SUV39H1 being shown to delay the repair of heterochromatic DNA after IR. The induction of γH2AX in heterochromatin was also shown to be significantly lower compared to euchromatin (Cowell *et al*., 2007; Karagiannis *et al*., 2007; Sak *et al*., 2015). In addition, depletion of SUV39H1 was shown to reduce H3K9me3 level and restored DNA repair capacity (Liu *et al*., 2013). Furthermore, SUV39H1 is involved in heterochromatin relaxation and genome instability in response to DNA damage in cancer cells (Wang *et al*., 2013). Our results from immunofluorescence analysis show that loss of HMT SUV39H1 regulates DNA damage repair mostly by NHEJ repair mechanism. The number of initial 53BP1 foci was significantly reduced in mFbs with knockout Suv39h1 as well as in knockdown H1299 compared with the respective wild type cells. In addition, the number of residual foci was significantly decreased in SUV39H1-reduced H1299 cells. However, the number of residual foci was significantly increased and DNA repair was slower in mFbs with knockout of Suv39h1 compared to the wt cells.

Unrepaired DNA damage after IR can lead to cell death, which was the case in D5 mFb with reduction of clonogenic survival after IR. Interestingly, we observed that clonogenic survival after IR is slightly lower in SUV39H1 knockdown H1299 cells. These findings correlate with results from pulsed–field gel electrophoresis (PFGE). The data from PFGE show that Suv39h1-knockout increases DNA DSBs in D5 mFbs compared with wild type (W8) cells. In addition, difference in DNA repair kinetics was also observed with slower DNA repair in D5 compared with W8. Furthermore, residual damage was also higher in D5 compared to W8. Overall, these results are supported by the findings of Goodarzi *et al*. (2008), who found that DNA repair was mildly slower in the Suv39H1/2$^{-/-}$ MEFs compared

with wt cells. Downregulation of HMT SUV39H1 in response to IR results in loss of heterochromatin, which may result in altered gene expression or genomic instability in primary hFbs (Sidler *et al*., 2014).

Homologous recombination (HR) was also discussed to depend on chromatin structure. In addition, the findings of Ayrapetov *et al*. (2014) suggest that although NHEJ activity was not significantly altered by loss of Suv39h1 in U2OS cells, the HR-mediated repair was significantly reduced. This led us to investigate the function of HR pathway repair in Suv39h1 deficient cells or after treatment with chemical inhibitors. Our results showed that the number of initial Rad51 foci was significantly reduced in SUV39H1 downregulated H1299 cells compared with wt cells and also slightly reduced in knockout D5 mFbs.

Taking together, our results confirm that SUV39H1 plays an important role in cell survival after IR through modulation of DNA damage response and the in mFbs, but with a mirror effect on survival of NSCLC tumour cell lines.

4.2 Chromatin modulation by small molecule inhibitors

We were also interested in the modification of chromatin structure modulated by different small molecule inhibitors and how this affects NHEJ and HR repair mechanisms and other cellular responses. It is known that the HMTs SUV39H1 and G9a are methylation writers on lysine and are altered in many types of human cancers, including lung cancer (Pandey *et al*., 2014). We used Chaetocin as a SUV39H1 and G9a inhibitor and Triptolide as a SUV39H1 inhibitor (Zhao *et al*., 2010) to modify chromatin structure and to investigate the effect of HMTs on DNA repair pathways in NSCLC H460 and H1299 cells. We obtained a significant effect on cell proliferation with an IC50 of 29 nM and 37 nM for Chaetocin and of 2.9 nM and 1.5 nM for Triptolide in H1299 and H460, respectively. However, at these low concentrations, Chaetocin (<300 nM) and Triptolide (<30 nM) do not induce any changes in methylation status of H3K9me3, H3K9me2 or H3K9me1.

In addition, the effect of small molecules on DNA repair mechanisms was evaluated in NSCLC cells. Here we could show that Triptolide influences NHEJ and HR repair pathways in H1299 with significantly higher 53BP1 foci, as a measure for NHEJ and significantly decreases the number of initial Rad51 foci, as a measure for HR. In comparison, Chueh *et al*. (2013) showed that Thiptolide induced higher levels of DNA damage in human malignant melanoma cells which is thought to be mediated by reduction of DNA repair genes (BRCA1, DNA-PKcs, ATM, ATR and MGMT). From these data it is concluded, that most of the DSBs induced in H1299 were rejoined by slow kinetics.

Chaetocin, which inhibits both HMTs SUV39H1 and G9a, increased the number of initial radiation induced 53BP1 foci at low doses (<60 nM) after short drug pre-treatment in H1299. Chaetocin impaired DNA DSB repair resulting in increased number of residual 53BP1 foci in both H460 and H1299 cell lines. Additionally, the effect of Chaetocin on DNA DSB repair in H1299 after a long Chaetocin pre-treatment (24 h) and combined with IR was similar to short drug pre-treatment (4 h), as measured by γH2AX foci. Longer pre-treatment with Chaetocin also resulted in significantly higher number of initial and residual Rad51 foci in H1299. Most plausible explanation for this effect could be rapid Chaetocin uptake in cells. It has been reported by Isham *et al*. (2007) that Chaetocin is rapidly accumulated in cancer cells, i.e. intracellular concentration of Chaetocin reached 10-fold higher level within 1 to 2 min and up to 1000-fold after 24 h. Overall, the present data show that Chaetocin modifies DNA repair with slower kinetics and increased residual damage. Also, it can affect chromatin structure and thereby impair DNA damage signalling of tumour cell lines.

4.3 The cellular effects of Chaetocin

Since Hauser *et al*. (1970) elucidated the unique chemical structure of Chaetocin, therapeutic cancer research focused on the biological functions of Chaetocin as a potential therapeutic agent. It is a natural product produced by *Chaetomium* fungal species, which belongs to the epipolythiodioxopiperazine (ETP) class of fungal toxin (Gardiner *et al*., 2005) and is characterized by the presence of an internal disulphide bridge. Cherblanc *et al*. (2013a) reported that Chaetocin is a non-specific inhibitor of histone lysine methyltransferases. However, several recent studies considered that Chaetocin specifically inhibits the HMTs G9a and SUV39H1 (Cherblan *et al.*, 2013; Greiner *et al*., 2005; Maleszewska *et al*., 2014). If Chaetocin specifically inhibit the HMT SUV39H1, then knockdown Suv39h1 and Chaetocin treatment should have similar effects. Here we show that knockdown of Suv39h1 can reduce H3K9me3 methylation, but Chaetocin treatment at low concentrations used in the present study (<300 nM) did not result in significant changes of H3K9me3. However, Chaetocin inhibits cell proliferation in H1299 and H460 with IC50 values of 29 nM and 37 nM, respectively. On the other hand, Chaetocin induces CICC changes, which was not detected after SUV39H1 knockdown. Therefore, it seems that Chaetocin exerts other effects compared to that of suppressing SUV39H1 expression. It was shown that Chaetocin has an antimyeloma effect via induction of oxidative stress (Isham *et al.*, 2007) and decreases cell migration in breast cancer possibly by inhibition of trimethylation of lysine 9 (H3K9me3) (Yokoyama *et al*., 2013). Chaetocin also inhibits HMTs through protein – ETP adduct formation, that

involves chromatin remodelling (Illner *et al*., 2010) and selective gene expression. Chiba *et al.* (2014) clearly demonstrated that Chaetocin treatment (>50 nM) reduced SUV39H1 and H3K9me3 levels in hepatocellular carcinoma cells. The same effect was observed after treatment with a high (>500 nM) concentration of Chaetocin in human leukaemia cell lines (Chaib *et al*., 2012).

With respect to cell inactivation, the present data show that low concentrations of Chaetocin (<40 nM) do not induce apoptotic cell death within 72 h after drug treatment in the NSCLC cell lines used in this study. However, it seems that the toxicity of Chaetocin depends on cell type. Isham *et al*. (2007) reported that Chaetocin at concentration of 200 nM induces a higher level of apoptosis (90%) in 24 h in myeloma cells (OCI-MY5). Teng *et al*. (2010) reported that Chaetocin at higher concentrations of 0.3 μM and 30 μM induces apoptosis in human leukaemia HL-60 cells through the caspase-8/caspase-3 activation pathway. Another study has shown that Chaetocin treatment (100 nM) of U937 human leukaemia cells induced more than 60% apoptotic cells after 24 h (Tran *et al*., 2013).

Activation of cell cycle checkpoints can be the mechanism for reduced proliferation after Chaetocin treatment. Our findings demonstrate that Chaetocin increases the fraction of the cells in G2 phase and decreases the fraction of cells in G1 in H460 and H1299 cell lines. Chaetocin at high concentration of about 500 nM was shown to induce cell cycle arrest in S phase after 24 h (Chaib *et al*., 2012).

Recently it was reported (Sepsa *et al*., 2015) that Chaetocin treatment reduces the ability of T98G glioblastoma cells to form colonies. However, our results demonstrate no significant radiosensitizing effect of Chaetocin at these low concentrations as measured by clonogenic assay. However, in long term mini-monolayer growth assay, which enable to follow the proliferation of the cells for several weeks, Chaetocin at low concentration of 10 nM was shown to reduce the radiation dose, which is necessary to control 50% of the plague-monolayer culture (TCD50), from 20 Gy to 10 Gy. In addition, we also found a significant radiosensitizing effect of Chaetocin at low concentration of Chaetocin (30 nM) after fractionated IR (3x 2 Gy in 24 h) in NSCLC H1299 ($p < 0.05$). This finding correlates with significant increase in the number of γH2AX foci after fractionated IR as compared to cells without Chaetocin treatment ($p < 0.001$). Overall, the data show that Chaetocin can radiosensitize tumour cells depending on the treatment and experimental conditions and influences DNA repair, cell cycle, and apoptotic response of the cells.

Previous studies showed that Chaetocin induces the production of ROS, resulting in oxidative damage of cells (Chaib *et al*., 2012; Isham *et al*., 2012; Teng *et al*., 2010). It was

also shown that N-acetyl-L-cysteine (NAC), a well-known inhibitor of radical oxygen species (ROS), co-treatment abrogates Chaetocin-induced toxicity (Isham *et al*., 2007). According to these findings, we hypothesized that NAC treatment may also abrogate the Chaetocin effects seen in the NSCLC cells. Thus, the NSCLC cell lines were treated with NAC before and after Chaetocin treatment to reduce the effect of oxidative stress. Here we showed that NAC significantly reduced (i) the initial as well as the residual number of DSBs, (ii) normalized the reduction of cell proliferation after Chaetocin treatment, (iii) decreased Chaetocin modulated cell cycle delay in G2/M and (iv) reduced Chatocin-induced apoptosis with and without IR. The effect of NAC was higher if NAC was added to the cell culture before Chaetocin treatment.

4.3.1 Chaetocin as a potential chromatin remodelling agent

Previous studies reported that chromatin changes play an important role during transcription (Li *et al*., 2007), replication (Groth *et al*., 2007) and DNA repair (Misteli and Soutoglou, 2009). In the present study we focused on chromatin remodelling processes with respect to the cellular response to DNA damage. Chromatin remodelling is necessary for main features of the DNA damage repair mechanisms. Moreover, chromatin structure influences the response to DNA damage. Chromatin undergoes rapid local and global decondensation after ionizing irradiation (Unal *et al*., 2004; Ziv *et al*. 2006), thus enhancing the access of repair proteins to sites of DNA damage. Local perturbation in chromatin structure and DNA damage-induced histone modifications after IR provide docking sites for DNA damage-associated proteins in the vicinity of DNA DSBs. DSBs in heterochromatic regions are characterized by lower initial induction (Sak *et al*., 2015) and slower repair kinetics than those in euchromatic regions (Goodarzi *et al*., 2008).

In the present work, we were able to modulate the global nuclear chromatin assembly by Chaetocin. For the first time we showed that Chaetocin induces visible reorganisation not only in human fibroblast nuclei (Illner *et al.*, 2010) and mouse fibroblasts, but also in human tumour cells. Up to now, the formation of senescence associated heterochromatic foci was described only in fibroblasts (Narita *et al*., 2003). Our data from the time course experiments demonstrated that the induction of CICC phenotype became visible as early as 4 h after treatment with Chaetocin and reached its maximum in 24 h. The percentage of CICC increased in a concentration-dependent manner with an asymptotic level at about 80% at the highest concentration of 300 nM Chaetocin. IR has no effect on CICC formation. We suggest that Chaetocin modulates chromatin structures by concentrating heterochromatic regions or

the whole chromosomal domains (Illner *et al*., 2010).

We analysed the nature of the chromatin remodelling process and demonstrated that CICC is associated with heterochromatin marks (H3K9me3, HP1α) and is negative for euchromatin marks (H3K4me3, H3K9as). Remarkably, that the CICC nuclei are phenotypically similar to condensing chromosomes in late prophase or in mitotic phase. However, CICC was not found to be associated with an intensive expression of Cyclin A and the phosphorylation of H3S10, which characterizes cells in S phase and mitotic phases, respectively. CICC cells were negative for EdU staining, as a measurement for replication. To confirm that CICC phenotype mostly originates from G1 phase, we used late passages of primary hFbs with low S phase and mitotic activity. CICC were clearly visible and detectable with the same kinetics as shown in tumour cells with a maximum at about 24 h.

We demonstrated that the induction of CICC formation by low doses (29 nM) of Chaetocin is a reversible process in human H1299 cells. Same results were observed in tumour cells with Aphidicolin cotreatment as well as in late passage primary hFbs, which having low proliferative capacity. However, Illner *et al*. (2010) reported that the induction of CICC phenotypes became an irreversible process in primary hFbs.

Chaetocin was shown to inactivate proteins via reaction with thiol groups and generate ROS by redox cycling (Chaib *et al*., 2012; Gardiner *et al*., 2005; Isham *et al*., 2007). Illner *et al*. (2010) suggested that the formation of CICC phenotype could be protected in a thiol-dependent manner. However the effect of thiols on CICC formation was not related to ROS scavenging. These studies imposed us to investigate the formation of CICC structure trough oxidation stress. There is no CCC formation 24 h after treatment with 0.1% H_2O_2. As expected, treatment with NAC, as an ROS scavenger, fully inhibited the induction of CICC phenotype in H1299 cells. However NAC is not a specific ROS inhibitor (Halasi *et al*., 2013). Thus, we used other more specific ROS inhibitors such as Tiron (100 μM) and Apocynin (100 μM), which were reported to be the specific for NADPH oxidases (An *et al*., 2007). They do not have an effect on CICC induction.

Chaetocin belongs to ETPs class of fungal metabolites and was shown to inhibit HMTs SUV39H1 and G9a. Thus, it was of interesting to know whether the chemical structure of Chaetocin has an impact on CICC induction or if it has an inhibition effect on HMTs. In order to test this possibility, various small molecules were tested to investigate the effect of Chaetocin on the CICC formation. Gliotoxin, as the structurally simplest member of ETPs and also an inhibitor of the HMTs SUV39h1 and G9a (Takahashi *et al*., 2012), does not induce chromatin condensation. In contrast, UNC0638, which belongs to a different chemical

class, selectively inhibits HMT G9a (Vedadi *et al*., 2012) and induces CICC. However BIX0194, another selective inhibitor of HMT G9a (Kubicek *et al*., 2007), does not induce chromatin condensation. Interestingly, transfection of H1299 cells with specific siRNA targeting both Suv39h1 and/or G9a decreased the formation of CICC.

Thus, the effect of Chaetocin on chromatin condensation seems to be partly related to functional HMTs SUV39H1 or G9a.

4.3.2 Chaetocin inhibits radiation-induced 53BP1 and ATM foci in CICC cells

Nonhomologous end joining (NHEJ) and homologous recombination (HR) are now well-characterized repair pathways. However, it is still unclear how exactly DNA DSBs in different chromatin regions – heterochtomain (HC) and euchromatin (EC) – are repaired. It was already reported that heterochromatic regions are highly compacted and this might be a barrier for DNA repair (Goodarzi *et al*., 2010). The repair of DSB in HC needs relaxation of chromatin to increase the accessibility of repair proteins to the site of damage. In addition, a local decondensation of HC at the sites of damage promotes the movement of DSBs to the HC periphery where repair may proceed (Goodarzi and Jeggo, 2012; Jakob *et al*., 2011).

To investigate the repair kinetics of DSBs in different chromatin regions we used CICC cells as a model system for heterochromatin. This allowed us to study DSBs repair signalling in condensed chromatin clusters after Chaetocin treatment. For this endpoint, we explore the formation of γH2AX and 53BP1 foci as a measured for NHEJ. Surprisingly, the formation of 53BP1 foci was dramatically reduced in CICC cells. In addition, 53BP1 foci reduction is correlated with protein reduction at the protein level after Chaetocin treatment. Interestingly, that γH2AX foci formation was not significantly affected after Chaetocin treatment. Also, the distribution of γH2AX foci in CICC cells after IR showed that colocalization of initial and residual γH2AX foci in DAPI free regions and in condensed chromatin domains was the same.

It is shown that 53BP1 promotes repair by NHEJ (Bunting *et al*., 2010). A current model of 53BP1 action in HC involves its ability to promote the phosphorylation of KAP1 (KRAB-assosiated protein 1) by ATM kinase, which is needed for repair in HC (Goodarzi *et al*., 2008; Jakob *et al*., 2011). Indeed, 53BP1 concentrates pATM at DSBs (Noon and Goodarzi, 2011). As expected, we observed that lack of 53BP1 also leads to disappearance of pATM foci in CICC cells. We did not, however, detect any alterations on the pATM and pKAP1 at the protein level after IR in CICC cells. Frohns *et al*. (2014) has recently reported

that adult retina cells, which generally have a high chromatin density, fail to form 53BP1 and pATM foci after IR. These data suggest that heterochtomatic structure negatively affects 53BP1 and pATM foci formation. The level of other proteins involved in DNA repair, such as pATP, pKAP1, Rad51 were not compromised after Chaetocin treatment. This finding may imply a preferential effect of CICC on 53BP1. In support of this model, supercondensed chromatin is an interesting model to study repair of DSBs in HC regions.

The most likely explanation of 53PB1 foci reduction in CICC cells was practically reported by Gonzalez-Suarez and Gonzalo (2010). They indicated that loss of lamin A, a member of the type V intermediate filament family and part of nucleoplasmic network, associates tightly with chromatin (Goldman, 1992) and leads to destabilization of 53BP1 in mFbs, thus providing inappropriate signalling or repair of DNA damage. As we demonstrated here, Chaetocin remodelled the chromatin structure by induction of CICC, which could destroy or affect the function of lamin A and C and thereby reduce the level of 53BP1. Thus, dysfunction of lamin A can also lead to decreased 53BP1 protein level.

5. Summary

In this study we investigated the influence of histone methylation on chromatin structure and its effect on radiation response. In this respect the different DNA repair (NHEJ, HR), cell cycle checkpoints, proliferation, apoptosis and clonogenic survival in different experimental models were evaluated. Initially, the influence of histone methyltransferase SUV39H1 on radiation response has been studied using genetic model systems. Mouse fibroblasts with genetically knockout Suv39h1 show significant lower clonogenic survival, which can be attributed to reduced DSB repair capacity of these cells. The results from repair foci analyses show an increase in the fraction of non-repaired damage, i.e. residual 53BP1 foci as a measure for NHEJ in the mouse model. In addition, decreased number of initial Rad51 foci as a measure for HR was evident. Furthermore, experiments with pulsed-field gel electrophoresis (PFGE) confirmed the reduced repair capacity, i.e. with higher initial fraction of DNA DSB and slower DNA repair kinetics in mFbs with knockout Suv39h1.

In a second approach we used genetically downregulated Suv39h1 model, using siRNA or shRNA in human lung cancer cells. In these experiments SUV39H1 expression could be downregulated up to about 50% of the initial level. The results show that the effect of HMT SUV39H1 downregulation on clonogenical survival was less marked as compared to the mouse knockout model. In addition, there was an obvious difference in the repair signalling in both systems with a significant reduced number of residual γH2AX in knockdown Suv39h1 NSCLC in contrast to an increased number of residual repair foci in knockout mFbs. In addition, results from PFGE experiments show no difference in the initial DSBs, but slightly faster repair kinetics in knockdown NSCLC cells in comparison to an increase of initial DSB induction and slower repair in knockout mFbs.

In a third approach, the chromatin structure was modulated in the NSCLC cell lines, H460 and H1299 by the small-molecule Chaetocin, which targets the HMT SUV39H1. The respective half maximal inhibitory concentration (IC50) for each cell lines was determined by using proliferation assays. In the clonogenic assay Chaetocin did not significantly radiosensitize the cells. Only an addictive effect could be shown. However, we also performed tumour control experiments in the plaque-monolayer assay. The radiation dose necessary to control 50% of a plague-monolayer culture after treatment with low Chaetocin concentrations significantly reduced from about 20 Gy to 10 Gy.

In addition, the effect of Chaetocin on the NHEJ and HR repair mechanism and other cellular responses was evaluated. The effect of Chaetocin on NHEJ and HRR was investigated by 53BP1 and Rad51 foci assay, respectively. Our results show that Chaetocin

significantly increases the number of initial and residual 53BP1 foci in NSCLC after short Chaetocin pre-treatment. The same effect was observed for γH2AX foci and Rad51 after long Chaetocin pre-treatment.

Most interestingly, Chaetocin was found to remodel the nuclear chromatin structure by forming Chaetocin-induced chromatin condensation/clustering (CICC) in primary hFbs, transformed mFbs and in the tumour cell line H1299, but not in H460. The CICC structure was shown to be reversible after drug washout. IR does not influence the formation of CICC. In addition, we confirmed that CICC are mainly associated with heterochromatin marks (H3K9me3 and HP1α). Interestingly, if cells were treated with N-acetyl-L-cysteine (NAC), a well-known inhibitor of radical oxygen species (ROS), before Chaetocin addition, CICC formation was completely abolished. NAC also decreased Chaetocin-induced cell cycle delay in G2/M as well as Chaetocin-induced apoptosis. The results further show that formation of CICC and radiation induced 53BP1 foci and pATM foci formation are mutually exclusive. This was not the case for γH2AX or Rad51 foci. Reduction of 53BP1 foci in CICC forming cells mainly relies on reduction of 53BP1 protein expression, as measured by western blot analysis.

Overall, the present study provided data on the effect of downregulation the expression of the HMT SUV39H1 for the activation of DNA repair signalling, cell cycle checkpoints and cell death mechanisms in mouse and human fibroblast and human cancer cell lines after IR. However, additional questions with respect to the molecular interaction of HMTs, DNA repair signalling and radiation sensitivity remain open, which have to be addressed in further studies. Notwithstanding, because chromatin modifying genes are frequently mutated in human tumours, in especially in lung tumours (Govindan *et al*., 2012; Imielinski *et al.*, 2012), it is an innovative field for understanding the role of chromatin structure for radio- and chemotherapy. Therefore, research is ongoing in this lab to find targets for selective sensitization of tumour cells by additional chromatin modifications.

References

Alberts, B., Johnson, A., Lewis, J., Raff, M., Roberts, K., & Walter, P. (2008). The Cell Cycle. In M. Anderson & S. Granum (Eds.), *Molecular Biology of the Cell* (5th ed., pp. 1053–1114). New York.

Allis, D. C., Jenuwein, T., & Reinberg, D. (2006). Overview and Concepts. In D. C. Allis, T. Jenuwein, & D. Reinberg (Eds.), *EPIGENETICS* (3th ed., pp. 23–69). New York.

An, S. J., Boyd, R., Zhu, M., Chapman, A., Pimentel, D. R., & Wang, H. Di. (2007). NADPH oxidase mediates angiotensin II-induced endothelin-1 expression in vascular adventitial fibroblasts. *Cardiovascular Research*, *75*(4), 702–709. http://doi.org/10.1016/j.cardiores.2007.02.015

Ariyoshi, K., Suzuki, K., Goto, M., Watanabe, M., & Kodama, S. (2007). Increased chromosome instability and accumulation of DNA double-strand breaks in Werner syndrome cells. *Journal of Radiation Research*, *48*(3), 219–231. http://doi.org/10.1269/jrr.07017

Ayrapetov, M. K., Gursoy-Yuzugullu, O., Xu, C., Xu, Y., & Price, B. D. (2014). DNA double-strand breaks promote methylation of histone H3 on lysine 9 and transient formation of repressive chromatin. *Proceedings of the National Academy of Sciences of the United States of America*, *111*(25), 9169–74. http://doi.org/10.1073/pnas.1403565111

Balgkouranidou, I., Liloglou, T., & Lianidou, E. S. (2013). Lung cancer epigenetics: emerging biomarkers. *Biomarkers in Medicine*, *7*(1), 49–58. http://doi.org/10.2217/bmm.12.111

Barh, D., Jain, N., Tiwari, S., Field, J. K., Padin-Iruegas, E., Ruibal, A., … Liloglou, T. (2013). A novel in silico reverse-transcriptomics-based identification and blood-based validation of a panel of sub-type specific biomarkers in lung cancer. *BMC Genomics*, *14 Suppl 6*(Suppl 6), S5. http://doi.org/10.1186/1471-2164-14-S6-S5

Barski, A., Cuddapah, S., Cui, K., Roh, T. Y., Schones, D. E., Wang, Z., … Zhao, K. (2007). High-Resolution Profiling of Histone Methylations in the Human Genome. *Cell*, *129*(4), 823–837. http://doi.org/10.1016/j.cell.2007.05.009

Baylin, S. B., & Jones, P. A. (2006). Epigenrtic Determinatnts of Cancer. In D. C. Allis, T. Jenuwein, & D. Reinberg (Eds.), *EPIGENETICS* (3th ed., pp. 457–477). New York: Inglis, John.

Bekker-Jensen, S., Lukas, C., Kitagawa, R., Melander, F., Kastan, M. B., Bartek, J., & Lukas, J. (2006). Spatial organization of the mammalian genome surveillance machinery in response to DNA strand breaks. *The Journal of Cell Biology*, *173*(2), 195–206. http://doi.org/10.1083/jcb.200510130

Bunting, S. F., Callén, E., Wong, N., Chen, H., Polato, F., Gunn, A., … Stark, J. M. (2010). 53BP1 inhibits homologous recombination in Brca-1-deficient cells by Blocking resection of DNA breaks. *Cell*, *141*(2), 243–254. http://doi.org/10.1016/j.cell.2010.03.012.53BP1

Caldecott, K. W. (2001). Mammalian DNA single-strand break repair: An X-ra(y)ted affair. *BioEssays*, *23*(5), 447–455. http://doi.org/10.1002/bies.1063

Cann, K. L., & Dellaire, G. (2011). Heterochromatin and the DNA damage response: the need to relax. *Biochemistry and Cell Biology = Biochimie et Biologie Cellulaire*, *89*(1), 45–60. http://doi.org/10.1139/O10-113

Chaib, H., Nebbioso, a, Prebet, T., Castellano, R., Garbit, S., Restouin, a, … Collette, Y. (2012). Anti-leukemia activity of chaetocin via death receptor-dependent apoptosis and dual modulation of the histone methyl-transferase SUV39H1. *Leukemia*, *26*(4), 662–674. http://doi.org/10.1038/leu.2011.271

Chen, M. W., Hua, K. T., Kao, H. J., Chi, C. C., Wei, L. H., Johansson, G., … Kuo, M. L. (2010). H3K9 histone methyltransferase G9a promotes lung cancer invasion and metastasis by silencing the cell adhesion molecule Ep-CAM. *Cancer Research*, *70*(20), 7830–7840. http://doi.org/10.1158/0008-5472.CAN-10-0833

Cherblanc, F. L., Chapman, K. L., Brown, R., & Fuchter, M. J. (2013). Chaetocin is a nonspecific inhibitor of histone lysine methyltransferases. *Nature Chemical Biology*, *9*(3), 136–7. http://doi.org/10.1038/nchembio.1187

Cherblanc, F. L., Chapman, K. L., Reid, J., Borg, A. J., Sundriyal, S., Alcazar-Fuoli, L., … Fuchter, M. J. (2013). On the histone lysine methyltransferase activity of fungal metabolite chaetocin. *Journal of Medicinal Chemistry*, *56*(21), 8616–8625. http://doi.org/10.1021/jm401063r

Chiba, T., Saito, T., Yuki, K., Zen, Y., Koide, S., Kanogawa, N., … Yokosuka, O. (2014). Histone lysine methyltransferase SUV39H1 is a potent target for epigenetic therapy of hepatocellular carcinoma. *International Journal of Cancer*, *23*, 1–10. http://doi.org/10.1002/ijc.28985

Chiolo, I., Minoda, A., Colmenares, S. U., Polyzos, A., Costes, S. V., & Karpen, G. H. (2011). Double-strand breaks in heterochromatin move outside of a dynamic HP1a domain to complete recombinational repair. *Cell*, *144*(5), 732–744. http://doi.org/10.1016/j.cell.2011.02.012

Christmann, M., Tomicic, M. T., Roos, W. P., & Kaina, B. (2003). Mechanisms of human DNA repair: An update. *Toxicology*, *193*(1-2), 3–34. http://doi.org/10.1016/S0300-483X(03)00287-7

Chueh, F. S., Chen, Y. L., Hsu, S. C., Yang, J. S., Hsueh, S. C., Ji, B. C., … Chung, J. G. (2013). Triptolide induced DNA damage in A375.S2 human malignant melanoma cells is mediated via reduction of DNA repair genes. *Oncol Rep*, *29*(2), 613–618. http://doi.org/10.3892/or.2012.2170

Cowell, I. G., Sunter, N. J., Singh, P. B., Austin, C. a., Durkacz, B. W., & Tilby, M. J. (2007). gH2AX foci form preferentially in euchromatin after ionising-radiation. *PLoS ONE*, *2*(10), 1–8. http://doi.org/10.1371/journal.pone.0001057

Czvitkovich, S., Sauer, S., Peters, a H., Deiner, E., Wolf, a, Laible, G., … Jenuwein, T. (2001). Over-expression of the SUV39H1 histone methyltransferase induces altered proliferation and differentiation in transgenic mice. *Mechanisms of Development*, *107*(1-2), 141–153. http://doi.org/10.1016/S0925-4773(01)00464-6

Daskalos, A., Logotheti, S., Markopoulou, S., Xinarianos, G., Gosney, J. R., Kastania, A. N., … Liloglou, T. (2011). Global DNA hypomethylation-induced ΔNp73 transcriptional activation in non-small cell lung cancer. *Cancer Letters*, *300*(1), 79–86. http://doi.org/10.1016/j.canlet.2010.09.009

Deb, M., Kar, S., Sengupta, D., Shilpi, A., Parbin, S., Rath, S. K., … Patra, S. K. (2014). Chromatin dynamics: H3K4 methylation and H3 variant replacement during development and in cancer. *Cellular and Molecular Life Sciences*. http://doi.org/10.1007/s00018-014-1605-4

Decarlo, D., & Hadden, M. K. (2012). Oncoepigenomics: Making histone lysine methylation count. *European Journal of Medicinal Chemistry*, *56*, 179–194. http://doi.org/10.1016/j.ejmech.2012.08.010

Dibiase, S. J., Zeng, Z., Chen, R., Hyslop, T., Curran, W. J., & Iliakis, G. (2000). DNA-dependent Protein Kinase Stimulates an Independently DNA-dependent Protein Kinase Stimulates an Independently Active ,. *Cancer Research*, *60*(1), 1245–1253.

Dinant, C., Houtsmuller, A. B., & Vermeulen, W. (2008). Chromatin structure and DNA damage repair. *Epigenetics & Chromatin*, *1*(1), 9. http://doi.org/10.1186/1756-8935-1-9

Elgin, S. C. ., & Reuter, G. (2006). Position-Effect Variegation, Heterochromatin Formation, and Gene Silencing in Drosophila. In D. C. Allis, T. Jenuwein, & D. Reinberg (Eds.), *EPIGENETICS* (3th ed., pp. 81–100). New York: Inglis, John.

Falk, M., Lukasova, E., Gabrielova, B., Ondrej, V., & Kozubek, S. (2007). Chromatin dynamics during DSB repair. *Biochimica et Biophysica Acta - Molecular Cell Research*, *1773*(10), 1534–1545. http://doi.org/10.1016/j.bbamcr.2007.07.002

Falk, M., Lukasova, E., & Kozubek, S. (2010). Higher-order chromatin structure in DSB induction, repair and misrepair. *Mutation Research - Reviews in Mutation Research*, *704*(1-3), 88–100. http://doi.org/10.1016/j.mrrev.2010.01.013

Falk, M., Lukášová, E., & Kozubek, S. (2008). Chromatin structure influences the sensitivity of DNA to γ-radiation. *Biochimica et Biophysica Acta - Molecular Cell Research*, *1783*(12), 2398–2414. http://doi.org/10.1016/j.bbamcr.2008.07.010

Falk, M., Lukášová, E., Štefančíková, L., Baranová, E., Falková, I., Ježková, L., … Kozubek, S. (2014). Heterochromatinization associated with cell differentiation as a model to study DNA double strand break induction and repair in the context of higher-order chromatin structure. *Applied Radiation and Isotopes*, *83*, 177–185. http://doi.org/10.1016/j.apradiso.2013.01.029

Fernandez-Capetillo, O., Lee, A., Nussenzweig, M., & Nussenzweig, A. (2004). H2AX: the histone guardian of the genome. *DNA Repair*, *3*(8-9), 959–967.

Fontanière, S., Tost, J., Wierinckx, a., Lachuer, J., Lu, J., Hussein, N., … Zhang, C. X. (2006). Gene expression profiling in insulinomas of Men1 β-cell mutant mice reveals early genetic and epigenetic events involved in pancreatic β-cell tumorigenesis. *Endocrine-Related Cancer*, *13*(4), 1223–1236. http://doi.org/10.1677/erc.1.01294

Fradet-Turcotte, A., Canny, M. D., Escribano-Díaz, C., Orthwein, A., Leung, C. C. Y., Huang, H., … Durocher, D. (2013). 53BP1 is a reader of the DNA-damage-induced H2A Lys 15 ubiquitin mark. *Nature*, *499*(7456), 50–4. http://doi.org/10.1038/nature12318

Friedl, A. a., Mazurek, B., & Seiler, D. M. (2012). Radiation-induced alterations in histone modification patterns and their potential impact on short-term radiation effects. *Frontiers in Oncology*, *2*(September), 1–10. http://doi.org/10.3389/fonc.2012.00117

Frohns, A., Frohns, F., Naumann, S. C., Layer, P. G., & Löbrich, M. (2014). Inefficient double-strand break repair in murine rod photoreceptors with inverted heterochromatin organization. *Current Biology*, *24*(10), 1080–1090. http://doi.org/10.1016/j.cub.2014.03.061

Gardiner, D. M., Waring, P., & Howlett, B. J. (2005). The epipolythiodioxopiperazine (ETP) class of fungal toxins: Distribution, mode of action, functions and biosynthesis. *Microbiology*, *151*(4), 1021–1032. http://doi.org/10.1099/mic.0.27847-0

Goldman, A. E. (1992). Pathway of incorporation of microinjected lamin A into the nuclear envelope. *The Journal of Cell Biology*, *119*(4), 725–735. http://doi.org/10.1083/jcb.119.4.725

Gonzalez-Suarez, I., & Gonzalo, S. (2010). Nurturing the genome: A-type lamins preserve genomic stability. *Nucleus*, *1*(2), 129–135. http://doi.org/10.4161/nucl.1.2.10797

Goodarzi, A. a., & Jeggo, P. a. (2012). The heterochromatic barrier to DNA double strand break repair: How to get the entry visa. *International Journal of Molecular Sciences*, *13*(9), 11844–11860. http://doi.org/10.3390/ijms130911844

Goodarzi, A. a., Jeggo, P., & Lobrich, M. (2010). The influence of heterochromatin on DNA double strand break repair: Getting the strong, silent type to relax. *DNA Repair*, *9*(12), 1273–1282. http://doi.org/10.1016/j.dnarep.2010.09.013

Goodarzi, A. a., Noon, A. T., Deckbar, D., Ziv, Y., Shiloh, Y., Löbrich, M., & Jeggo, P. a. (2008). ATM Signaling Facilitates Repair of DNA Double-Strand Breaks Associated with Heterochromatin. *Molecular Cell*, *31*(2), 167–177. http://doi.org/10.1016/j.molcel.2008.05.017

Govindan, R., Ding, L., Griffith, M., Subramanian, J., Dees, N. D., Kanchi, K. L., … Wilson, R. K. (2012). Genomic landscape of non-small cell lung cancer in smokers and never-smokers. *Cell*, *150*(6), 1121–1134. http://doi.org/10.1016/j.cell.2012.08.024

Greiner, D., Bonaldi, T., Eskeland, R., Roemer, E., & Imhof, A. (2005). Identification of a specific inhibitor of the histone methyltransferase SU(VAR)3-9. *Nature Chemical Biology*, *1*(3), 143–145. http://doi.org/10.1038/nchembio721

Grewal, S. I. S., & Moazed, D. (2003). Heterochromatin and epigenetic control of gene expression. *Science (New York, N.Y.)*, *301*(5634), 798–802. http://doi.org/10.1126/science.1086887

Groth, A., Rocha, W., Verreault, A., & Almouzni, G. (2007). Chromatin Challenges during DNA Replication and Repair. *Cell*, *128*(4), 721–733. http://doi.org/10.1016/j.cell.2007.01.030

Halasi, M., Wang, M., Chavan, T. S., Gaponenko, V., & Hay, N. (2013). ROS inhibitor N-acetyl-L-cysteine the activity of proteasome inhibitors. *Biochem J.*, *29*(6), 997–1003. http://doi.org/10.1016/j.biotechadv.2011.08.021.Secreted

Hall, E. J., D.PHIL, D.Sc, & F.A.C.R. (1993). The Physics and Chemistry of Radiation Absorption. In J. D. Ryan (Ed.), *Radiobiology for the Radiologist* (4th ed., pp. 1–13). New York: J.B. Lippimcott Company.

Hauser, D., Weber, H., & Sigg, H. (1970). Isolation and configuration of Chaetocin. *Helvetica Chimica Acta.*, *53*(5), 1061–73.

Helman, E., Naxerova, K., & Kohane, I. S. (2012). DNA hypermethylation in lung cancer is targeted at differentiation-associated genes. *Oncogene*, *31*(9), 1181–1188. http://doi.org/10.1038/onc.2011.307

Hsu, T. C. (1975). A possible function of constitutive heterochromatin: the bodyguard hypothesis. *Genetics*, *79*(Sup), 137–150.

Hunt, C. R., Ramnarain, D., Horikoshi, N., Iyengar, P., Pandita, R. K., Shay, J. W., & Pandita, T. K. (2013). Histone modifications and DNA double-strand break repair after exposure to ionizing radiations. *Radiation Research*, *179*(4), 383–92. http://doi.org/10.1667/RR3308.2

Iliakis, G. (2009). Backup pathways of NHEJ in cells of higher eukaryotes: Cell cycle dependence. *Radiotherapy and Oncology*, *92*(3), 310–315. http://doi.org/10.1016/j.radonc.2009.06.024

Iliakis, G., Wu, W., Wang, M., Terzoudi, G. I., & Pantelias, G. E. (2007). Backup Pathways of Nonhomologous End Joining May Have a Dominant Role in the Formation of Chromosome Aberrations. *Chromosomal Alterations*, 67–85. http://doi.org/10.1007/978-3-540-71414-9

Illner, D., Zinner, R., Handtke, V., Rouquette, J., Strickfaden, H., Lanctôt, C., … Cremer, M. (2010). Remodeling of nuclear architecture by the thiodioxoxpiperazine metabolite chaetocin. *Experimental Cell Research*, *316*(10), 1662–1680. http://doi.org/10.1016/j.yexcr.2010.03.008

Imielinski, M., Berger, A. H., Hammerman, P. S., Hernandez, B., Pugh, T. J., Hodis, E., … Meyerson, M. (2012). Mapping the hallmarks of lung adenocarcinoma with massively parallel sequencing. *Cell*, *150*(6), 1107–1120. http://doi.org/10.1016/j.cell.2012.08.029

Isham, C. R., Tibodeau, J. D., Bossou, a R., Merchan, J. R., & Bible, K. C. (2012). The anticancer effects of chaetocin are independent of programmed cell death and hypoxia, and are associated with inhibition of endothelial cell proliferation. *British Journal of Cancer*, *106*(2), 314–23. http://doi.org/10.1038/bjc.2011.522

Isham, C. R., Tibodeau, J. D., Jin, W., Xu, R., Timm, M. M., & Bible, K. C. (2007). Chaetocin: A promising new antimyeloma agent with in vitro and in vivo activity mediated via imposition of oxidative stress. *Blood*, *109*(6), 2579–2588. http://doi.org/10.1182/blood-2006-07-027326

Jackson, S. P. (2002). Sensing and repairing DNA double-strand breaks. *Carcinogenesis*, *23*(5), 687–696. http://doi.org/10.1093/carcin/23.5.687

Jakob, B., Splinter, J., Conrad, S., Voss, K. O., Zink, D., Durante, M., … Taucher-Scholz, G. (2011). DNA double-strand breaks in heterochromatin elicit fast repair protein recruitment, histone H2AX phosphorylation and relocation to euchromatin. *Nucleic Acids Research*, *39*(15), 6489–6499. http://doi.org/10.1093/nar/gkr230

Jeggo, P. a., Geuting, V., & Löbrich, M. (2011). The role of homologous recombination in radiation-induced double-strand break repair. *Radiotherapy and Oncology*, *101*(1), 7–12. http://doi.org/10.1016/j.radonc.2011.06.019

Jeong, S.-H., Wu, H.-G., & Park, W.-Y. (2009). LIN28B confers radio-resistance through the posttranscriptional control of KRAS. *Experimental & Molecular Medicine*, *41*(12), 912–918. http://doi.org/10.3858/emm.2009.41.12.097

Karagiannis, T. C., Harikrishnan, K. N., & El-Osta, a. (2007). Disparity of histone deacetylase inhibition on repair of radiation-induced DNA damage on euchromatin and constitutive heterochromatin compartments. *Oncogene*, *26*(27), 3963–3971. http://doi.org/10.1038/sj.onc.1210554

Kim, E.-H., Park, a-K., Dong, S. M., Ahn, J.-H., & Park, W.-Y. (2010). Global analysis of CpG methylation reveals epigenetic control of the radiosensitivity in lung cancer cell lines. *Oncogene*, *29*(33), 4725–4731. http://doi.org/10.1038/onc.2010.223

Kim, W., Vo, Q., Shrivastav, M., Lataxes, T., & Brown, K. (2002). Aberrant methylation of the ATM promoter correlates with increased radiosensitivity in a human colorectal tumor cell line. *Oncogene*, (October 2001), 3864–3871. http://doi.org/10.1038/sj/onc/1205485

Kinner, A., Wu, W., Staudt, C., & Iliakis, G. (2008). Gamma-H2AX in recognition and signaling of DNA double-strand breaks in the context of chromatin. *Nucleic Acids Research*, *36*(17), 5678–94. http://doi.org/10.1093/nar/gkn550

Kouzarides, T. (2007). Chromatin Modifications and Their Function. *Cell*, *128*(4), 693–705. http://doi.org/10.1016/j.cell.2007.02.005

Kouzarides, T., & Berger, S. L. (2006). Chromatin Modifications and Their Mechanism of Action. In C. D. Allis, T. Jenuwein, & D. Reinberg (Eds.), *EPIGENETICS* (3rd ed., pp. 191–210). New York: Inglis, John.

Kubicek, S., O'Sullivan, R. J., August, E. M., Hickey, E. R., Zhang, Q., Teodoro, M. L., … Jenuwein, T. (2007). Reversal of H3K9me2 by a Small-Molecule Inhibitor for the G9a Histone Methyltransferase. *Molecular Cell*, *25*(3), 473–481. http://doi.org/10.1016/j.molcel.2007.01.017

Lachner, M., O'Sullivan, R. J., & Jenuwein, T. (2003). An epigenetic road map for histone lysine methylation. *Journal of Cell Science*, *116*(Pt 11), 2117–2124. http://doi.org/10.1242/jcs.00493

Lavelle, C., & Foray, N. (2014). Chromatin structure and radiation-induced DNA damage: from structural biology to radiobiology. *The International Journal of Biochemistry & Cell Biology*, *49*, 84–97. http://doi.org/10.1016/j.biocel.2014.01.012

Leatherbarrow, E. L., Harper, J. V, Cucinotta, F. A., & Neill, P. O. (2006). Induction and quantification of g -H2AX foci following low and high LET-irradiation. *Int. J. Radiat. Biol.*, *82*(2), 111–118. http://doi.org/10.1080/09553000600599783

Li, B., Carey, M., & Workman, J. L. (2007). The Role of Chromatin during Transcription. *Cell*, *128*(4), 707–719. http://doi.org/10.1016/j.cell.2007.01.015

Lips, J., & Kaina, B. (2001). DNA double-strand breaks trigger apoptosis in p53-deficient fibroblasts. *Carcinogenesis*, *22*(4), 579–585. http://doi.org/10.1093/carcin/22.4.579

Liu, B., Wang, Z., Zhang, L., Ghosh, S., Zheng, H., & Zhou, Z. (2013). Depleting the methyltransferase Suv39h1 improves DNA repair and extends lifespan in a progeria mouse model. *Nature Communications*, *4*(May 2012), 2–12. http://doi.org/10.1038/ncomms2885

Liu, S. V, Fabbri, M., Gitlitz, B. J., & Laird-Offringa, I. A. (2013). Epigenetic therapy in lung cancer. *Frontiers in Oncology*, *3*(May), 135. http://doi.org/10.3389/fonc.2013.00135

Löbrich, M., Rief, N., Kühne, M., Heckmann, M., Fleckenstein, J., Rübe, C., & Uder, M. (2005). In vivo formation and repair of DNA double-strand breaks after computed tomography examinations. *Proceedings of the National Academy of Sciences of the United States of America*, *102*(25), 8984–8989. http://doi.org/10.1073/pnas.0501895102

Lorat, Y., Schanz, S., Schuler, N., Wennemuth, G., Rübe, C., & Rübe, C. E. (2012). Beyond repair foci: DNA double-strand break repair in euchromatic and heterochromatic compartments analyzed by transmission electron microscopy. *PLoS ONE*, *7*(5). http://doi.org/10.1371/journal.pone.0038165

Lou, Z., Minter-Dykhouse, K., Franco, S., Gostissa, M., Rivera, M. a., Celeste, A., … Chen, J. (2006). MDC1 maintains genomic stability by participating in the amplification of ATM-dependent DNA damage signals. *Molecular Cell*, *21*(2), 187–200. http://doi.org/10.1016/j.molcel.2005.11.025

Maes, K., Menu, E., Van Valckenborgh, E., Van Riet, I., Vanderkerken, K., & de Bruyne, E. (2013). Epigenetic modulating agents as a new therapeutic approach in multiple myeloma. *Cancers*, *5*(2), 430–461. http://doi.org/10.3390/cancers5020430

Maleszewska, M., Steranka, A., & Kaminska, B. (2014). The effects of selected inhibitors of histone modifying enzyme on C6 glioma cells. *Pharmacological Reports*, *66*(1), 107–113. http://doi.org/10.1016/j.pharep.2013.08.011

Maroschik, B., Gürtler, A., Krämer, A., Rößler, U., Gomolka, M., Hornhardt, S., … Friedl, A. a. (2014). Radiation-induced alterations of histone post-translational modification levels in lymphoblastoid cell lines. *Radiation Oncology (London, England)*, *9*, 15. http://doi.org/10.1186/1748-717X-9-15

Masumoto, H., Hawke, D., Kobayashi, R., & Verreault, A. (2005). A role for cell-cycle-regulated histone H3 lysine 56 acetylation in the DNA damage response. *Nature*, *436*(7048), 294–298. http://doi.org/10.1038/nature03714

Mehta, A., Dobersch, S., Romero-Olmedo, A. J., & Barreto, G. (2015). Epigenetics in lung cancer diagnosis and therapy. *Cancer and Metastasis Reviews*. http://doi.org/10.1007/s10555-015-9563-3

Mills, K. D., Ferguson, D. O., & Alt, F. W. (2003). The role of DNA breaks in genomic instability and tumorigenesis. *Immunological Reviews*, *194*, 77–95. http://doi.org/10.1034/j.1600-065X.2003.00060.x

Misteli, T., & Soutoglou, E. (2009). The Emerging role of nuclear architecture in DNA repair and genome maintenance. *Nature Reviews Molecular Cell Biology*, *10*(4), 243–254. http://doi.org/10.1038/nrm2651.The

Mladenov, E., & Iliakis, G. (2011). Induction and repair of DNA double strand breaks: The increasing spectrum of non-homologous end joining pathways. *Mutation Research - Fundamental and Molecular Mechanisms of Mutagenesis*, *711*(1-2), 61–72. http://doi.org/10.1016/j.mrfmmm.2011.02.005

Mungamuri, S. K., Benson, E. K., Wang, S., Gu, W., Lee, S. W., & Aaronson, S. a. (2012). P53-Mediated Heterochromatin Reorganization Regulates Its Cell Fate Decisions. *Nature Structural & Molecular Biology*, *19*(5), 478–484. http://doi.org/10.1038/nsmb.2271

Murray, J. M., Stiff, T., & Jeggo, P. a. (2012). DNA double-strand break repair within heterochromatic regions, 173–178. http://doi.org/10.1042/BST20110631

Nagy, Z., & Soutoglou, E. (2009). DNA repair: easy to visualize, difficult to elucidate. *Trends in Cell Biology*, *19*(11), 617–629. http://doi.org/10.1016/j.tcb.2009.08.010

Narita, M., Nũnez, S., Heard, E., Narita, M., Lin, A. W., Hearn, S. a., … Lowe, S. W. (2003). Rb-mediated heterochromatin formation and silencing of E2F target genes during cellular senescence. *Cell*, *113*(6), 703–716. http://doi.org/10.1016/S0092-8674(03)00401-X

Noma K, Allis, C. D., & Grewal, S. I. (2001). Transitions in distinct histone H3 methylation patterns at the heterochromatin domain boundaries. *Science (New York, N.Y.)*, *293*(5532), 1150–1155. http://doi.org/10.1126/science.1064150

Noon, A. T., & Goodarzi, A. a. (2011). 53BP1-mediated DNA double strand break repair: Insert bad pun here. *DNA Repair*, *10*(10), 1071–1076. http://doi.org/10.1016/j.dnarep.2011.07.012

Pachaiyappan, B., & Woster, P. M. (2014). Design of small molecule epigenetic modulators. *Bioorganic and Medicinal Chemistry Letters*, *24*(1), 21–32. http://doi.org/10.1016/j.bmcl.2013.11.001

Pandey, M., Sahay, S., Tiwari, P., Upadhyay, D. S., Sultana, S., & Gupta, K. P. (2014). Involvement of EZH2, SUV39H1, G9a and associated molecules in pathogenesis of urethane induced mouse lung tumors: Potential targets for cancer control. *Toxicology and Applied Pharmacology*, *280*(2), 296–304. http://doi.org/10.1016/j.taap.2014.08.015

Panier, S., & Boulton, S. J. (2014). Double-strand break repair: 53BP1 comes into focus. *Nature Reviews. Molecular Cell Biology*, *15*(1), 7–18. http://doi.org/10.1038/nrm3719

Panier, S., & Durocher, D. (2013). Push back to respond better: regulatory inhibition of the DNA double-strand break response. *Nature Reviews. Molecular Cell Biology*, *14*(10), 661–72. http://doi.org/10.1038/nrm3659

Paull, T. T., Rogakou, E. P., Yamazaki, V., Kirchgessner, C. U., Gellert, M., & Bonner, W. M. (2000). A critical role for histone H2AX in recruitment of repair factors to nuclear foci after DNA damage. *Current Biology*, *10*(15), 886–895. http://doi.org/10.1016/S0960-9822(00)00610-2

Peters, A. H. F. M., O'Carroll, D., Scherthan, H., Mechtler, K., Sauer, S., Schöfer, C., … Jenuwein, T. (2001). Loss of the Suv39h histone methyltransferases impairs mammalian heterochromatin and genome stability. *Cell*, *107*(3), 323–337. http://doi.org/10.1016/S0092-8674(01)00542-6

Putiri, E. L., & Robertson, K. D. (2011). Epigenetic mechanisms and genome stability. *Clinical Epigenetics*, *2*(2), 299–314. http://doi.org/10.1007/s13148-010-0017-z

Qiu, G.-H. (2015). Protection of the genome and central protein-coding sequences by non-coding DNA against DNA damage from radiation. *Mutation Research/Reviews in Mutation Research*, *764*, 108–117. http://doi.org/10.1016/j.mrrev.2015.04.001

Rea, S., Eisenhaber, F., O'Carroll, D., Strahl, B. D., Sun, Z. W., Schmid, M., … Jenuwein, T. (2000). Regulation of chromatin structure by site-specific histone H3 methyltransferases. *Nature*, *406*(6796), 593–599. http://doi.org/10.1038/35020506

Rice, J. C., Briggs, S. D., Ueberheide, B., Barber, C. M., Shabanowitz, J., Hunt, D. F., … Allis, C. D. (2003). Histone Methyltransferases Direct Different Degrees of Methylation to Define Distinct Chromatin Domains. *Molecular Cell*, *12*(6), 1591–1598. http://doi.org/10.1016/S1097-2765(03)00479-9

Robert Koch Institute. (2014). *Cancer in Germany 2009/2010*. (Robert Koch Institute & the Association of Population-based Cancer Registrie, Eds.) (9th ed.). Berlin.

Rothkamm, K., Krüger, I., Thompson, L. H., Kru, I., & Lo, M. (2003). Pathways of DNA Double-Strand Break Repair during the Mammalian Cell Cycle Pathways of DNA Double-Strand Break Repair during the Mammalian Cell Cycle. *Molecular and Cellular Biology*, *23*(16), 5706–5715. http://doi.org/10.1128/MCB.23.16.5706

Rothkamm, K., & Löbrich, M. (2003). Evidence for a lack of DNA double-strand break repair in human cells exposed to very low x-ray doses. *Proceedings of the National Academy of Sciences of the United States of America*, *100*(9), 5057–5062. http://doi.org/10.1073/pnas.0830918100

Sak, A., Kübler, D., Bannik, K., Groneberg, M., & Stuschke, M. (2015). Dependence of radiation-induced H2AX phosphorylation on histone methylation: Evidence from the chromatin immunoprecipitation assay. *International Journal of Radiation Biology*, *91*(4), 346–353. http://doi.org/10.3109/09553002.2015.997895

Sak, A., Stuschke, M., Groneberg, M., Kübler, D., Pöttgen, C., & Eberhardt, W. E. E. (2012). Inhibiting the aurora B kinase potently suppresses repopulation during fractionated irradiation of human lung cancer cell lines. *International Journal of Radiation Oncology Biology Physics*, *84*(2), 492–499. http://doi.org/10.1016/j.ijrobp.2011.12.021

Sepsa, A., Levidou, G., Gargalionis, A., Adamopoulos, C., Spyropoulou, A., Dalagiorgou, G., … Korkolopoulou, P. (2015). Emerging Role of Linker Histone Variant H1x as a Biomarker with Prognostic Value in Astrocytic Gliomas. A Multivariate Analysis including Trimethylation of H3K9 and H4K20. *Plos One*, *10*(1), e0115101. http://doi.org/10.1371/journal.pone.0115101

Shames, D. S., Girard, L., Gao, B., Sato, M., Lewis, C. M., Shivapurkar, N., … Minna, J. D. (2006). A genome-wide screen for promoter methylation in lung cancer identifies novel methylation markers for multiple malignancies. *PLoS Medicine*, *3*(12), 2244–2263. http://doi.org/10.1371/journal.pmed.0030486

Sidler, C., Li, D., Wang, B., Kovalchuk, I., & Kovalchuk, O. (2014). SUV39H1 downregulation induces deheterochromatinization of satellite regions and senescence after exposure to ionizing radiation. *Frontiers in Genetics*, *5*(November), 1–15. http://doi.org/10.3389/fgene.2014.00411

Singh, S. K., Wu, W., Zhang, L., Klammer, H., Wang, M., & Iliakis, G. (2011). Widespread dependence of backup NHEJ on growth state: Ramifications for the use of DNA-PK inhibitors. *International Journal of Radiation Oncology Biology Physics*, *79*(2), 540–548. http://doi.org/10.1016/j.ijrobp.2010.08.018

Spyropoulou, A., Gargalionis, A., Dalagiorgou, G., Adamopoulos, C., Papavassiliou, K. a., Lea, R. W., … Papavassiliou, A. G. (2014). Role of histone lysine methyltransferases SUV39H1 and SETDB1 in gliomagenesis: Modulation of cell proliferation, migration, and colony formation. *NeuroMolecular Medicine*, *16*(1), 70–82. http://doi.org/10.1007/s12017-013-8254-x

Tachibana, M., Sugimoto, K., Fukushima, T., & Shinkai, Y. (2001). SET Domain-containing Protein, G9a, is a Novel Lysine-preferring Mammalian Histone Methyltransferase with Hyperactivity and Specific Selectivity to Lysines 9 and 27 of Histone H3. *Journal of Biological Chemistry*, *276*(27), 25309–25317. http://doi.org/10.1074/jbc.M101914200

Tachibana, M., Sugimoto, K., Nozaki, M., Ueda, J., Ohta, T., Ohki, M., … Shinkai, Y. (2002). G9a histone methyltransferase plays a dominant role in euchromatic histone H3 lysine 9 methylation and is essential for early embryogenesis. *Genes and Development*, *16*(14), 1779–1791. http://doi.org/10.1101/gad.989402

Takahashi, A., Kubo, M., Ma, H., Nakagawa, A., Yoshida, Y., Isono, M., … Nakano, T. (2014). Nonhomologous End-Joining Repair Plays a More Important Role than Homologous Recombination Repair in Defining Radiosensitivity after Exposure to High-LET Radiation. *Radiation Research*, *182*(3), 338–344. http://doi.org/10.1667/RR13782.1

Takahashi, M., Takemoto, Y., Shimazu, T., Kawasaki, H., Tachibana, M., Shinkai, Y., … Yoshida, M. (2012). Inhibition of histone H3K9 methyltransferases by gliotoxin and related epipolythiodioxopiperazines. *The Journal of Antibiotics*, *65*(5), 263–265. http://doi.org/10.1038/ja.2012.6

Teng, Y., Iuchi, K., Iwasa, E., Fujishiro, S., Hamashima, Y., Dodo, K., & Sodeoka, M. (2010). Unnatural enantiomer of chaetocin shows strong apoptosis-inducing activity through caspase-8/caspase-3 activation. *Bioorganic and Medicinal Chemistry Letters*, *20*(17), 5085–5088. http://doi.org/10.1016/j.bmcl.2010.07.032

Tichý, A., Vávrová, J., Pejchal, J., & Rezácová, M. (2010). Ataxia-telangiectasia mutated kinase (ATM) as a central regulator of radiation-induced DNA damage response. *Acta Medica (Hradec Kralove) / Universitas Carolina, Facultas Medica Hradec Kralove*, *53*(1), 13–17.

Tran, H. T. T., Kim, H. N., Lee, I. K., Nguyen-Pham, T. N., Ahn, J. S., Kim, Y. K., … Kim, H. J. (2013). Improved therapeutic effect against leukemia by a combination of the histone methyltransferase inhibitor chaetocin and the histone deacetylase inhibitor trichostatin A. *Journal of Korean Medical Science*, *28*(2), 237–246. http://doi.org/10.3346/jkms.2013.28.2.237

Ünal, E., Arbel-Eden, A., Sattler, U., Shroff, R., Lichten, M., Haber, J. E., & Koshland, D. (2004). DNA damage response pathway uses histone modification to assemble a double-strand break-specific cohesin domain. *Molecular Cell*, *16*(6), 991–1002. http://doi.org/10.1016/j.molcel.2004.11.027

Vedadi, M., Barsyte-lovejoy, D., Liu, F., Rival-gervier, S., Allali-hassani, A., Labrie, V., … Jin, J. (2012). A chemical probe selectively inhibits G9a and GLP methyltransferase and genanylgeranyltransferase I with antitumor activity against brest cancer in vivo. *Nature Chemical Biology*, *7*(8), 566–574. http://doi.org/10.1038/nchembio.599.A

Vigushin, D. M., Mirsaidi, N., Brooke, G., Sun, C., Pace, P., Inman, L., … Coombes, R. C. (2004). Gliotoxin is a dual inhibitor of farnesyltransferase and geranylgeranyltransferase I with antitumor activity against breast cancer in vivo. *Medical Oncology (Northwood, London, England)*, *21*(1), 21–30. http://doi.org/10.1385/MO:21:1:21

Wang, D., Zhou, J., Liu, X., Lu, D., Shen, C., Du, Y., … Zhu, W.-G. (2013). Methylation of SUV39H1 by SET7/9 results in heterochromatin relaxation and genome instability. *Proceedings of the National Academy of Sciences of the United States of America*, *110*(14), 5516–21. http://doi.org/10.1073/pnas.1216596110

Wang, H., Rosidi, B., Perrault, R., Wang, M., Zhang, L., Windhofer, F., & Iliakis, G. (2005). DNA Ligase III as a Candidate Component of Backup Pathways of Nonhomologous End Joining DNA Ligase III as a Candidate Component of Backup Pathways of Nonhomologous End Joining, (10), 4020–4030.

Wang, M., Wu, W., Wu, W., Rosidi, B., Zhang, L., Wang, H., & Iliakis, G. (2006). PARP-1 and Ku compete for repair of DNA double strand breaks by distinct NHEJ pathways. *Nucleic Acids Research*, *34*(21), 6170–6182. http://doi.org/10.1093/nar/gkl840

Xu, Y., & Price, B. D. (2011). Chromatin dynamics and the repair of DNA double strand breaks. *Cell Cycle*, *10*(2), 261–267. http://doi.org/10.4161/cc.10.2.14543

Yokoyama, Y., Hieda, M., Nishioka, Y., Matsumoto, A., Higashi, S., Kimura, H., … Matsuura, N. (2013). Cancer-associated upregulation of histone H3 lysine 9 trimethylation promotes cell motility in vitro and drives tumor formation in vivo. *Cancer Science*, *104*(7), 889–895. http://doi.org/10.1111/cas.12166

Yost, J. M. (2011). Targets in Epigenetics: Inhibiting the Methyl Writers of the Histone Code. *Current Chemical Genomics*, *5*(1), 72–84. http://doi.org/10.2174/1875397301005010072

Zhang, Y., Máté, G., Müller, P., Hillebrandt, S., & Krufczik, M. (2015). Radiation Induced Chromatin Conformation Changes Analysed by Fluorescent Localization Microscopy, Statistical Physics, and Graph Theory. *PLoS ONE*, *10*(6), 1–23. http://doi.org/10.11588/data/10031.Funding

Zhao, F., Chen, Y., Li, R., Liu, Y., Wen, L., & Zhang, C. (2010). Triptolide alters histone H3K9 and H3K27 methylation state and induces G0/G1 arrest and caspase-dependent apoptosis in multiple myeloma in vitro. *Toxicology*, *267*(1-3), 70–79. http://doi.org/10.1016/j.tox.2009.10.023

Zheng, H., Chen, L., Pledger, W. J., Fang, J., & Chen, J. (2014). p53 promotes repair of heterochromatin DNA by regulating JMJD2b and SUV39H1 expression. *Oncogene*, *33*(6), 734–44. http://doi.org/10.1038/onc.2013.6

Ziv, Y., Bielopolski, D., Galanty, Y., Lukas, C., Taya, Y., Schultz, D. C., … Shiloh, Y. (2006). Chromatin relaxation in response to DNA double-strand breaks is modulated by a novel ATM- and KAP-1 dependent pathway. *Nature Cell Biology*, *8*(8), 870–876. http://doi.org/10.1038/ncb1446

Acknowledgements

First of all, I am very grateful to my supervisor Prof. Dr. Martin Stuschke, for giving me the opportunity to work on my PhD thesis at the Department of Radiotherapy in University hospital Essen. Also I would like to thank Dr. Ali Sak for all the support during the last years, whether scientifically or personally, as well as for the critical reading of this thesis and the valuable suggestions on structure and interpretation.

Special thanks go to the "Deutsche Forschungsgemeinschaft" for the financial support of my thesis and for allowing me to be a member of the DFG graduate training program 1739 "Molecular determinants of the cellular radiation response and their potential for response modulation". To all the participants of the GRK1739, graduate students, PIs and coordinators, thank you for teaching and advising, and all the helpful suggestions and critical comments during the meetings.

I wish to express profound gratitude to Prof. Dr. George Iliakis for agreeing to be the second reviewer for this thesis and for giving me the opportunity to work his lab and also Dr. Fanghua Li, Dr. Emil Mladenov and Vladimir Nikolov for providing me support and facilities to perform this research work.

I am also very grateful to Prof. Dr. Shirley Knauer for agreeing to be my mentor during my research work and her support and valuable discussions.

I would like to thank Dr. Michael Rosemann for the critical proofreading of this thesis and valuable suggestions.

I would like to thank all members of my lab and especially Michael Gronerberg for his continued support throughout the years not only on scientific but also on personal matters. Also, my special thank to Natalia Pyzhova for the proofreading of this thesis and her support since student's time at University of "Dubna".

Finally but profoundly, heartily thanks to my family and friends for their love, support for my success during the whole period of my studies.

Curriculum Vitae

The curriculum vitae is not included in the online version for reasons of data protection.

The curriculum vitae is not included in the online version for reasons of data protection.

Erklärungen

Erklärung:

Hiermit erkläre ich, gem. § 6 Abs. (2) g) der Promotionsordnung der Fakultät für Biologie zur Erlangung der Dr.rer.nat., dass ich das Arbeitsgebiet, dem das Thema "Short and long term radiation effects after ionizing radiation and its dependence on chromatin modification and repair inhibition in human lung cell lines" zuzuordnen ist, in Forschung und Lehre vertrete und den Antrag von Kristina Bannik befürworte und die Betreuung auch im Falle eines Weggangs, wenn nicht wichtige Gründe dem entgegenstehen, weiterführen werde.

Essen, den _____

Prof. Dr. Martin Stuschke

Erklärung:

Hiermit erkläre ich, gem. § 7 Abs. (2) d) + f) der Promotionsordnung der Fakultät für Biologie zur Erlangung des Dr.rer.nat., dass ich die vorliegende Dissertation selbstständig verfasst und mich keiner anderen als der angegebenen Hilfsmittel bedient, bei der Abfassung der Dissertation nur die angegeben Hilfsmittel benutzt und alle wörtlich oder inhaltlich übernommenen Stellen als solche gekennzeichnet habe.

Essen, den _____

Kristina Bannik

Erklärung:

Hiermit erkläre ich, gem. § 7 Abs. (2) e) + g) der Promotionsordnung der Fakultät für Biologie zur Erlangung des Dr. rer. nat., dass ich keine anderen Promotionen bzw. Promotionsversuche in der Vergangenheit durchgeführt habe und dass diese Arbeit von keiner anderen Fakultät/Fachbereich abgelehnt worden ist.

Essen, den _____

Kristina Bannik